

# **Monitoring Strategies**

for Chatter Detection In a Drilling Process

Amor Ben Salah Messaoud

Doctoral Thesis  
submitted in partial fulfillment  
the requirements for the Degree of  
“Doktor der Naturwissenschaften”  
in the Department of Statistics  
University of Dortmund

Dortmund, November 2006

Prüfungskommission:

Prof. Dr. Joachim Kunert (Vorsitzender)	Universität Dortmund
Prof. Dr. Claus Weihs (Gutachter)	Universität Dortmund
Prof. Dr. Franz Hering (Gutachter)	Universität Dortmund
Prof. Dr. Mohamed Limam (Gutachter)	University of Tunis
Dr. Uwe Ligges (Beisitzer)	Universität Dortmund

Tag der mündlichen Prüfung: 21. Dezember 2006

Copyright © 2006 by Amor Messaoud  
All rights reserved

# DEDICATION

To the memory of my father  
and  
to my mother for her unconditional love, sacrifices  
and support

This page intentionally left blank



# Contents

<b>Acknowledgements</b>	<b>v</b>
<b>1 Introduction</b>	<b>1</b>
1.1 Motivation . . . . .	1
1.2 Introduction to Statistical Process Control (SPC) . . . . .	2
1.3 Overview of the Thesis . . . . .	4
<b>I A Nonparametric Control Chart for Multivariate Data</b>	<b>7</b>
<b>2 The Rank Based Multivariate EWMA Control Chart</b>	<b>9</b>
2.1 Data Depth . . . . .	9
2.2 The Proposed $r$ MEWMA Control Chart . . . . .	12
2.3 Asymptotic Average Run Length of the In-Control Process . . . . .	13
2.4 Illustrative Example . . . . .	15
<b>3 Simulation Results</b>	<b>19</b>
3.1 Effect of the Reference Sample Size on $r$ MEWMA Control Charts Performance . . . . .	19
3.1.1 Simulation Study . . . . .	20
3.1.2 Simulation Results . . . . .	20
3.2 Effect of the Geometrical Nature of Simplicial Depth on the Performance of $r$ MEWMA Control Charts . . . . .	29
3.2.1 Lower Bounds to $Q_t^m$ . . . . .	30
3.2.2 Illustrative Example . . . . .	34

<b>4</b>	<b>Performance Comparisons</b>	<b>37</b>
4.1	The Parametric Multivariate EWMA Control Chart . . . . .	37
4.2	Simulation Study . . . . .	39
4.3	Simulation Results . . . . .	41
4.3.1	Comparison of Performances of Mahalanobis $r$ MEWMA and $p$ MEWMA Control Charts . . . . .	41
4.3.2	Performance of Mahalanobis and Simplicial $r$ MEWMA Control Charts . . . . .	46
4.4	Discussion and Conclusion . . . . .	46
<b>II</b>	<b>Monitoring the BTA Deep-Hole Drilling Process</b>	<b>49</b>
<b>5</b>	<b>The BTA Deep-Hole Drilling Process</b>	<b>51</b>
5.1	The Drilling Process . . . . .	51
5.1.1	The Drilling Machine . . . . .	51
5.1.2	The Drilling Tool and Principle of the Process . . . . .	52
5.2	Process Disturbances . . . . .	54
5.3	Experimental Investigation . . . . .	55
5.3.1	A Drilling Depth Dependency of Chatter Frequency . . . . .	59
5.3.2	Mechanical Interpretation . . . . .	61
<b>6</b>	<b>Time Varying Process Dynamics</b>	<b>63</b>
6.1	Introduction to Dynamical Systems Theory: The van der Pol Equation . . . . .	63
6.2	Modelling the Drilling Torque by a Stochastic Differential Equation . . . . .	65
6.3	Modelling the Amplitudes of Relevant Frequencies . . . . .	66
6.3.1	Time Series Analysis . . . . .	66
6.3.2	Autoregressive Approximation . . . . .	67
6.3.3	Empirical Results: Diagnostic Checks of the Residuals . . . . .	68
6.4	Conclusion . . . . .	70
<b>7</b>	<b>Nonlinear Time Series Modelling of the the Drilling Process</b>	<b>71</b>
7.1	Basic Definitions . . . . .	71
7.2	Amplitude-dependent Exponential Autoregressive Time Series Models . . . . .	72
7.3	Estimation of the ExpAr Models . . . . .	75
7.3.1	Maximum Likelihood Estimate . . . . .	75
7.3.2	Real-time Estimate . . . . .	76
7.4	Modelling the Drilling Torque Using ExpAr Time Series Models: Experimental Results . . . . .	77

7.4.1	Diagnostic Checks . . . . .	78
7.4.2	Description of the Time Varying Dynamics . . . . .	78
7.5	ExpAr( $p$ ) Time Series Models Based Control Charts . . . . .	81
7.6	Conclusion . . . . .	83
<b>8</b>	<b>Experimental Results</b>	<b>85</b>
8.1	Experimental Settings . . . . .	85
8.2	Transition from Stable Drilling to Chatter Vibration . . . . .	87
8.3	Monitoring Strategies . . . . .	88
8.3.1	Residual $r$ MEWMA Control Charts . . . . .	88
8.3.2	ExpAr(40) Time Series Based $r$ UEWMA Control Charts . . . . .	88
8.3.3	Choice of the Control Charts Parameters . . . . .	89
8.3.4	Experimental Results . . . . .	89
8.4	The Masking Problem . . . . .	96
<b>9</b>	<b>Summary and Future Work</b>	<b>103</b>
9.1	Summary . . . . .	103
9.2	Future Work . . . . .	104
9.2.1	Multiple Frequency Modelling . . . . .	104
9.2.2	Integration of Process Monitoring and Adjustment . . . . .	105
<b>A</b>	<b>Tables on the Performance of <math>r</math>MEWMA and <math>p</math>MEWMA Control Charts</b>	<b>107</b>
<b>B</b>	<b>Plots of the Amplitudes of Frequencies 234, 703 and 1183 Hz</b>	<b>123</b>
<b>C</b>	<b>Tables on the Time Series Analysis of the Amplitudes of the Relevant Frequencies</b>	<b>127</b>
	<b>Bibliography</b>	<b>141</b>

This page intentionally left blank





## Acknowledgements

First of all I am thankful for the financial support that I received from the Graduate School of Production Engineering and Logistics of the University of Dortmund and the Collaborative Research Centre “Reduction of Complexity in Multivariate Data Structures” (SFB 475) of the German Research Council (Deutsche Forschungsgemeinschaft, DFG).

I would like to thank Prof. Claus Weihs. This thesis would have never been finished without his support and guidance. I really enjoyed working with him. I also would like to thank Prof. Franz Hering. He contributed a lot to this work by providing me with many useful suggestions and comments. I learned a lot from him and my debt to him is enormous. Special thanks to Prof. Mohamed Limam for his guidance and encouragement throughout the course of this work. I have benefited enormously from his moral support. I am also grateful to the members of my dissertation committee for their useful suggestions for improvements.

I am indebted to Dr. Winfried Theis for his great support during the first years of my work. My thanks go to Dr. Uwe Ligges for his help on **R** and **L<sup>A</sup>T<sub>E</sub>X** and maintaining my computer. Another thanks go to Dr. Oliver Webber who helped me to understand the deep-hole drilling process.

I also wish to thank Mrs. Edelgard Kürbis, Mrs. Sabine Bell, Mrs. Meni Syrou and Mrs. Gundula Plaep for their administrative support. My deep gratitude to all the staff members of the Department of Statistics of the University of Dortmund for their assistance throughout the course of this work.

I would like to thank all my colleagues at the Department of Statistics and the Graduate School of Production Engineering and Logistics of the University of Dortmund for their support.

Finally and most importantly, I would like to thank my mother for all the sacrifices she made to ensure that I obtain the best education possible. Her unconditional love,

generous support and prayers at all times provided me a constant source of inspiration. My mother has always given me guidance and teaching that no university could match. I also thank my brother for his constant encouragement and support.

*Dortmund, Germany*  
*November 2006*

*Amor Messaoud*

# Introduction

This thesis is part of the project “Analysis and Modelling of the Deep-Hole Drilling Process with Methods of Statistics and Neuronal Networks” in the Collaborative Research Centre 475 “Reduction of Complexity for Multivariate Data Structures” of the German Research Council (Deutsche Forschungsgemeinschaft, DFG). The goal of this project is to model the process in order to prevent dynamic disturbances, chatter vibration and spiralling, to identify the cause(s) of these disturbances, and to choose optimal production parameters for faster and more secure production with high quality.

## 1.1 Motivation

Usually, the BTA (Boring and Trepanning Association) deep-hole drilling process is used during the last production phases of expensive workpieces. For example, axial bores in turbines or compressor shafts are made with this process. Thus, it is necessary that a process monitoring system is devised to detect disturbances during the process operation. The aim of this PhD thesis is to develop such real-time monitoring strategies for the early and reliable detection of chatter vibration and changes in the process by using statistical process control (SPC) techniques. Such strategies are needed in order to allow engineers to know when and how to adjust the process.

SPC is a collection of problem solving tools useful in achieving process stability through the reduction of variability. The major tools in SPC are control charts. These charts have been shown to be useful in monitoring many industrial processes. For the drilling process, many assumptions used by SPC are no longer valid. This is due to the time varying dynamics of the process and the nature of the collected data, “data-rich” environments in industry. Therefore, we will focus on the development of adequate SPC

procedures by understanding and modelling the time varying dynamics of the process using times series techniques.

## 1.2 Introduction to Statistical Process Control (SPC)

Reducing variation in manufacturing processes is desirable to reduce cost and improve product performance and quality. To achieve this objective SPC is used. SPC consists of methods and techniques for understanding and monitoring a production process. That is, to determine whether the process is stable over time and capable of producing high quality products. Montgomery (2001) mentioned that no two units of product produced by a manufacturing process are identical. Some variation is inevitable. Then improving quality will be obtained if the aim is to reduce variation around the target. That is, quality is inversely proportional to variability.

The approach towards reduction of variability is based on the idea that the phenomena causing variation in process outcomes can be classified in two groups:

- Common or chance causes of variation are considered to be due to the inherent nature of the process and cannot be altered without changing the process itself.
- Assignable or special causes are unusual shocks or other disruptions to the process. These causes can and should be removed.

One purpose of control charting, the featured tool of SPC, is to distinguish between these two sources of process variation. In other words, control charts are used to detect the presence of assignable causes of variation by checking the desired stable state of the process. Reduction of variation is thus achieved via rapid detection and elimination of such special causes. A process is said to be in a state of statistical control if it operates under common causes of variation and the probability distribution representing the quality characteristic is constant over time. If there are some changes over time in this distribution, the process is said to be out-of-control. Woodall (2000) mentioned that this traditional definition of statistical control has been generalized over the years to include cases for which an underlying statistical model of the quality characteristic is stable over time. These useful generalizations include, for example, regression, variance components and time series models.

### The Shewhart $\bar{X}$ Control Chart

A typical Shewhart  $\bar{X}$  control chart is given in Figure 1.1. Samples of size  $n$  are taken at equally spaced intervals. The control statistic  $\bar{X}$  is calculated from the sampled data. The control chart is based on the idea that if the process is in state of statistical control, then the outcomes are predictable. That is, based on previous observations, it is possible

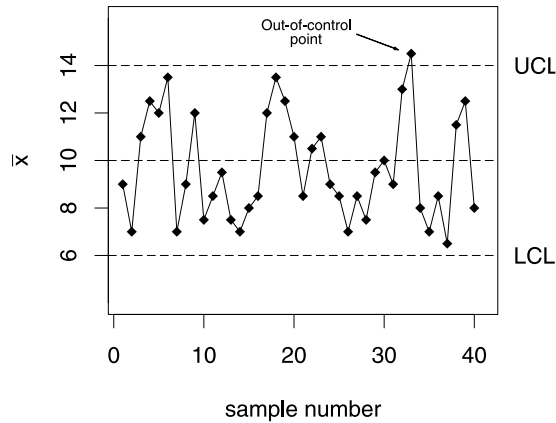


**Figure 1.1:** An illustration of a Shewhart control chart (UCL: Upper control limit and LCL: Lower control limit)

for a given set of control limits to determine the probability that future observations fall within these control limits. An out-of-control signal is given by the chart as soon as  $\bar{X}$  calculated from a sample falls outside the upper and lower control limits, labelled UCL and LCL, respectively. Other rules are also used for signaling an out-of-control situation based on “non-random” patterns of the chart. Shewhart  $\bar{X}$  control charts use only the current observation or sample to monitor the process. Other control charts, such as cumulative sum (CUSUM) and exponentially weighted moving average (EWMA) charts, accumulate information across successive observations. That is, they not only use the current sample statistic, but incorporate the information that can be gained from the previous sample statistics in some fashion. For further details, see Montgomery (2001).

### Monitoring Autocorrelated and Nonnormal Data

An important assumption in the application of statistical control charts is that the observations generated by the monitored process are independent. However, this assumption is often violated in many industrial processes and the observations are frequently autocorrelated. This may be due, for example, to the measurement system and the dynamics of the process. The autocorrelation has a large impact on the performance of control charts developed under the independence assumption. Its typical effect is to increase the number of false alarms compared with an independent process.

Some SPC methodologies have been developed in recent years in order to monitor autocorrelated data. One approach is to use residual control charts. They are suggested by several authors. For example, see Alwan and Roberts (1988) and Montgomery and Mastrangelo (1991). This procedure requires a model of the autocorrelative structure

of the data which can be achieved by fitting an appropriate time series model to the observations. The idea behind residual control charts is if the time series model fits the data well, the residuals will be approximately independent. Then, traditional control charts designed to monitor independent observations can be applied to the residuals.

Another basic assumption, used in the development of many control charts, is that the underlying distribution of the process is normal. The statistical properties of these charts are exact only if this assumption is satisfied. In practice, it is well known that this assumption rarely holds. Therefore, distribution-free or nonparametric control charts are used. For further details, see Chakraborti *et al.* (2001).

### **Control Chart Performance Measures**

The statistical design of a control chart refers to choices of its parameters. It ensures the chart performance meets certain statistical criteria. These criteria are often based on aspects of the run length distribution of the control chart. The run length (RL) of a control chart is a random variable that represents the number of plotted statistics until a signal occurs. The most common measure of control chart performance is the expected value of the run length; i.e. the average run length (ARL). The ARL should be large when the process is statistically in-control (in-control ARL) and small when a shift has occurred (out-of-control ARL). However, conclusions based on in-control and out-of-control ARL alone can be misleading. Knowledge of the in-control and out-of-control RL distributions would provide a comprehensive understanding of the in-control and out-of-control control chart performances. For example, the lower percentiles of the in-control and out-of-control RL distributions give information about the early false alarm rates and the ability to quickly detect an out-of-control condition of a control chart.

## **1.3 Overview of the Thesis**

The thesis is divided into two main parts. The first part is devoted to the development of a new distribution-free control chart for multivariate data, the study of its properties and comparison of its performance against alternative procedures. In Chapter 2, the principles used to construct the new control chart are given and its statistical design is proposed. Simulations are conducted in Chapters 3 and 4 in order to assess its applicability and to compare its performance against alternative procedures, respectively.

The second part of the thesis is devoted to the introduction and modelling of the drilling process and experimental investigation of the performance of the proposed monitoring strategies. In Chapter 5, the BTA deep-hole drilling process is introduced. Previous work to understand and to predict the temporal development of the process is reviewed in Chapter 6. Based on it, a modelling approach of the sampled data is proposed in order to setup the monitoring procedures. In Chapter 7, nonlinear time series

modelling is used to describe the time varying dynamics of the process. It provides the basis of nonlinear time series based control charts. In Chapter 8, the empirical performance of the proposed monitoring strategies is studied using several data sets.

Finally, some thoughts and discussion for possible future research issues are given in Chapter 9.

This page intentionally left blank



## **Part I**

# **A Nonparametric Control Chart for Multivariate Data**

This page intentionally left blank

# The Rank Based Multivariate EWMA Control Chart

In this chapter, we propose a new rank based multivariate EWMA (*rMEWMA*) control chart. It is a generalization, using the data depth notion, of the nonparametric EWMA control chart for individual observations proposed by Hackl and Ledolter (1992). In section 2.1, we review the data depth notion. The proposed control chart is introduced in section 2.2. Its asymptotic in-control average run length is approximated in section 2.3. Finally, an illustrative example is given in section 2.4.

## 2.1 Data Depth

Data depth measures how deep (or central) a given point  $\mathbf{X} \in \mathbb{R}^d$  is with respect to (w.r.t.) a probability distribution  $F$  or w.r.t. a given data cloud  $S = \{\mathbf{Y}_1, \dots, \mathbf{Y}_m\}$ . There are several measurements for the depth of the observations, such as Mahalanobis depth, the simplicial depth, half-space depth, and the majority depth of Singh, see Liu *et al.* (1999). In this work, the Mahalanobis and simplicial depths are considered.

### The Mahalanobis Depth

The Mahalanobis depth of a given point  $\mathbf{X} \in \mathbb{R}^d$  w.r.t.  $F$  is defined by

$$MD(F, \mathbf{X}) = \frac{1}{1 + (\mathbf{X} - \mu_F)' \Sigma_F^{-1} (\mathbf{X} - \mu_F)},$$

where  $\mu_F$  and  $\Sigma_F$  are the mean vector and covariance matrix of  $F$ , respectively. The sample version of  $MD$  is obtained by replacing  $\mu_F$  and  $\Sigma_F$  with their sample estimates.

## The Simplicial Depth

The simplicial depth was introduced by Liu (1990) and revised by Burr *et al.* (2004).

### Definition 2.1.1 Simplicial depth (Liu, 1990)

Given a probability distribution  $F$  in  $\mathbb{R}^d$ , the simplicial depth of  $\mathbf{X}$  w.r.t.  $F$  is the probability that  $\mathbf{X}$  belongs to a random closed simplex in  $\mathbb{R}^d$ , that is

$$SD_{Liu}(F, \mathbf{X}) = P_F\{\mathbf{X} \in s[\mathbf{Y}_1, \dots, \mathbf{Y}_{d+1}]\},$$

where  $s[\mathbf{Y}_1, \dots, \mathbf{Y}_{d+1}]$  is a  $d$ -dimensional closed simplex whose vertices are random observations  $\{\mathbf{Y}_1, \dots, \mathbf{Y}_{d+1}\}$  from  $F$ .

### Definition 2.1.2 Simplicial depth for the sample version (Liu, 1990)

The simplicial depth of a point  $\mathbf{X}$  w.r.t. a data set  $S = \{\mathbf{Y}_1, \dots, \mathbf{Y}_m\}$  is the fraction of closed simplices formed by  $d+1$  points of  $S$  containing  $\mathbf{X}$

$$SD_{Liu}(S, \mathbf{X}) = \left( \binom{m}{d+1} \right)^{-1} \sum_{1 \leq i_1 < \dots < i_{d+1} \leq m} I(\mathbf{X} \in s[\mathbf{Y}_{i_1}, \dots, \mathbf{Y}_{i_{d+1}}]), \quad (2.1)$$

where  $I(\cdot)$  is the indicator function.

Note that a simplex in  $\mathbb{R}^d$  is the boundary of the region defined by  $d+1$  vertices in general position. It represents the simplest polytope in any dimension. In one dimension, a simplex is simply a line segment. In 2 and 3 dimensions, it is a triangle and a tetrahedron, respectively.

Liu (1990) investigated the basic properties of the simplicial depth. The author showed that if  $F$  is absolutely continuous, then as  $m \rightarrow \infty$ ,  $SD_{Liu}(S, \mathbf{X})$  converges uniformly and strongly to  $SD_{Liu}(F, \mathbf{X})$  and that  $SD_{Liu}(F, \mathbf{X})$  is affine invariant.

Several problems arise in the finite case of simplicial depth under Liu's definition. Burr *et al.* (2004) proposed a revised definition of simplicial depth.

### Definition 2.1.3 Revised simplicial depth (Burr *et al.*, 2004)

Given a data set  $S = \{\mathbf{Y}_1, \dots, \mathbf{Y}_m\}$ , the simplicial depth of a point  $\mathbf{X}$  is the average of the fraction of closed simplices containing  $\mathbf{X}$  and the fraction of open simplices containing  $\mathbf{X}$ , that is

$$SD_{BRS}(S, \mathbf{X}) = \frac{1}{2} \left( \binom{m}{d+1} \right)^{-1} \sum_{1 \leq i_1 < \dots < i_{d+1} \leq m} \left[ I(\mathbf{X} \in s[\mathbf{Y}_{i_1}, \dots, \mathbf{Y}_{i_{d+1}}]) + I(\mathbf{X} \in \text{int}(s[\mathbf{Y}_{i_1}, \dots, \mathbf{Y}_{i_{d+1}}])) \right], \quad (2.2)$$

where  $\text{int}(s[\mathbf{Y}_{i_1}, \dots, \mathbf{Y}_{i_{d+1}}])$  refers to the open relative interior of  $s[\mathbf{Y}_1, \dots, \mathbf{Y}_{d+1}]$ . Equivalently, this could be formulated as,  $SD_{BRS}(S, \mathbf{X}) = \rho(S, \mathbf{X}) + (1/2)\sigma(S, \mathbf{X})$ , where

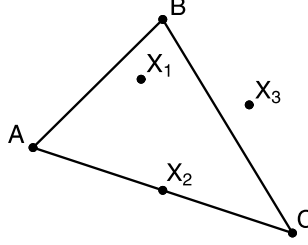


**Figure 2.1:** Computation of the simplicial depth in  $\mathbb{R}^2$

$\rho(S, \mathbf{X})$  is the number of simplices with data points as vertices which contain  $\mathbf{X}$  in their open interior, and  $\sigma(S, \mathbf{X})$  is the number of simplices with data points as vertices which contain  $\mathbf{X}$  in their boundary.

Figure 2.1 shows the computation of the simplicial depth in  $\mathbb{R}^2$ . Using the definition of Liu, the simplicial depths of  $\mathbf{X}_1$  and  $\mathbf{X}_2$  w.r.t.  $S = \{\mathbf{A}, \mathbf{B}, \mathbf{C}\}$  are equal to 1. The simplicial depth of  $\mathbf{X}_3$  w.r.t.  $S$  is equal to 0. Using the revised definition, the simplicial depths of  $\mathbf{X}_1$ ,  $\mathbf{X}_2$  and  $\mathbf{X}_3$  w.r.t.  $S$  are equal to 1, 0.5 and 0, respectively.

In the following, the revised simplicial depth is used and we will omit the word revised from it.

## Simplicial Depth Algorithms

In this section, algorithms to compute the simplicial depth of a point or a position in  $\mathbb{R}^d$  are reviewed. For the simplicial depth computation in  $\mathbb{R}^2$ , Rousseeuw and Ruts (1996) proposed an efficient algorithm to compute the simplicial depth of a point using Liu's definition. It has a time complexity  $O(n \log n)$ , where  $n$  is the size of the reference sample. Burr *et al.* (2004) proposed certain modifications to this algorithm in order to compute the revised simplicial depth. When the point or position is in  $\mathbb{R}^3$ , Cheng and Ouyang (2001) proposed an  $O(n^3)$  time algorithm. They generalized it to  $\mathbb{R}^4$  with a time complexity  $O(n^4)$ . These two algorithms are based on Liu's definition. Burr *et al.* (2004) showed that these algorithms remain valid under the revised definition with some adjustments. For  $\mathbb{R}^d$  ( $d \geq 5$ ), there are no known algorithms faster than the straightforward method. That is to generate all the simplices  $s[\mathbf{Y}_{i_1}, \dots, \mathbf{Y}_{i_{d+1}}]$  and then to count the number of containments. A point  $\mathbf{X}$  is in the simplex  $s[\mathbf{Y}_{i_1}, \dots, \mathbf{Y}_{i_{d+1}}]$  if  $\mathbf{X}$  can be expressed as a convex combination of  $\mathbf{Y}_{i_1}, \dots, \mathbf{Y}_{i_{d+1}}$ . As there are  $O(n^{d+1})$  simplices, it takes  $O(n^{d+1})$  time in the real RAM model of computation. This algorithm is extremely computationally intensive which constitutes an obstacle for the use of simplicial depth in practice.

## 2.2 The Proposed $r$ MEWMA Control Chart

Let  $\mathbf{X}_t = (x_{1,t}, \dots, x_{d,t})'$  denote the  $d \times 1$  vector of quality characteristic measurements taken from a process at the  $t^{\text{th}}$  time point where  $x_{j,t}$ ,  $j = 1, \dots, d$ , is the observation on variate  $j$  at time  $t$ . Assume that the successive  $\mathbf{X}_t$  are independent and identically distributed random vectors. Assume that  $m > 1$  independent random observations  $\{\mathbf{X}_1, \dots, \mathbf{X}_m\}$  from an in-control process are available. That is, the  $r$ MEWMA monitoring procedure starts at time  $t = m$ .

Let  $RS = \{\mathbf{X}_{t-m+1}, \dots, \mathbf{X}_t\}$  denote a reference sample comprised of the  $m$  most recent observations taken from the process at time  $t \geq m$ . It is used to decide whether or not the process is still in control at time  $t$ . The main idea of the proposed  $r$ MEWMA control chart is to represent each multivariate observation of the reference sample by its corresponding data depth. Thus, the depths  $D(RS, \mathbf{X}_i)$ ,  $i = t - m + 1, \dots, t$ , are calculated w.r.t.  $RS$ .

Now, the same principles proposed by Hackl and Ledolter (1992) are used to construct the  $r$ MEWMA control chart. Let  $Q_t^*$  denote the sequential rank of  $D(RS, \mathbf{X}_t)$  among  $D(RS, \mathbf{X}_{t-m+1}), \dots, D(RS, \mathbf{X}_t)$ . It is given by

$$Q_t^* = 1 + \sum_{i=t-m+1}^t I\left(D(RS, \mathbf{X}_t) > D(RS, \mathbf{X}_i)\right), \quad (2.3)$$

where  $I(\cdot)$  is the indicator function. It is assumed that tied data depth measures are not observed. Thus,  $Q_t^*$  is uniformly distributed on the  $m$  points  $\{1, 2, \dots, m\}$ . The standardized sequential rank  $Q_t^m$  is given by

$$Q_t^m = \frac{2}{m} \left( Q_t^* - \frac{m+1}{2} \right). \quad (2.4)$$

It is uniformly distributed on the  $m$  points

$$\left\{ \frac{1}{m} - 1, \frac{3}{m} - 1, \dots, 1 - \frac{1}{m} \right\},$$

with mean  $\mu_{Q_t^m} = 0$  and variance  $\sigma_{Q_t^m} = \frac{m^2-1}{3m^2}$ . For more details, see Hackl and Ledolter (1992).

The control statistic  $T_t$  is the EWMA of standardized sequential ranks. It is computed as follows

$$T_t = \min \left\{ B, (1 - \lambda)T_{t-1} + \lambda Q_t^m \right\}, \quad (2.5)$$

$t = 1, 2, \dots$ , where  $0 < \lambda \leq 1$  is a smoothing parameter,  $B > 0$  is a reflecting boundary and  $T_0 = u$  is a starting value. The process is considered in-control as long as  $T_t \geq h$ , where  $h < 0$  is a lower control limit ( $h \leq u \leq B$ ). Note that the lower-sided EWMA is considered because the statistic  $Q_t^m$  is higher “the better”. In section 2.4, an illustrative example is given to introduce the implementation of the  $r$ MEWMA control chart.

A reflecting boundary is included to prevent the  $r$ MEWMA control statistic from drifting to one side indefinitely. It is known that EWMA schemes can suffer from an “inertia problem” when there is a process change some time after beginning of monitoring. That is, an EWMA control statistic can have wandered away from a center line in a direction opposite to that of a shift that occurs some time after the start of monitoring. In this unhappy circumstance, an EWMA scheme can take long time to signal.

Hackl and Ledolter (1992) considered a continuous quality criterion. This continuity assumption assures that ties are not observed. However, in practice when measurements or other numerical observations are taken, it is often that two or more observations are tied. For example, ties may be due to the nature of the phenomenon modelled or rounding of continuous variables. In this work, the simplicial depth is a discrete measure and ties may occur. Especially, there always exist at least  $(d + 1)$  extreme points that share the minimum simplicial depth of  $\frac{d+1}{2m}$ , see Stoumbos and Jones (2000). The most common approach to this problem is to assign to each observation in a tied set the midrank, that is, the average of the ranks reserved for the observations in the tied set, see Gibbons and Chakraborti (1992).

## 2.3 Asymptotic Average Run Length of the In-Control Process

The statistical design of the  $r$ MEWMA control chart refers to choices of combinations of  $\lambda$ ,  $h$ ,  $B$  and  $m$ . It ensures the chart performance meets certain statistical criteria. As mentioned in section 1.2, these criteria are often based on aspects of the run length distribution of the control chart.

In this work, we used the integral equation to approximate the in-control ARL, see Crowder (1987). Let  $L(u)$  be the ARL of the lower-sided  $r$ MEWMA control chart given that  $T_0 = u$ . It can be shown that the integral equation for  $L(u)$  is given by

$$L(u) = 1 + L(B)\Pr\left(q \geq \frac{B - (1 - \lambda)u}{\lambda}\right) + \int_h^B L\left((1 - \lambda)u + \lambda q\right)dF(q),$$

where  $F(q)$  is the cumulative distribution of  $q = Q_t^m$ . We assumed that ties are not observed. Therefore,  $Q_t^m$  are uniformly distributed on the  $m$  points  $\{1/m - 1, 3/m - 1, \dots, 1 - 1/m\}$ ,

For moderate and large  $m$  the discrete distribution of  $Q_t^m$  is approximated by a continuous uniform distribution, which leads to

$$L(u) = 1 + L(B)\Pr\left(q \geq \frac{B - (1 - \lambda)u}{\lambda}\right) + \int_h^B L\left((1 - \lambda)u + \lambda q\right)f(q)dq, \quad (2.6)$$

where  $f(q)$  is the probability density of the uniform distribution. The solutions to the integral equation (2.6) can be obtained by replacing the equation with a system of linear

**Table 2.1:** In-control ARL values of the  $r$ MEWMA control chart with reflecting boundary  $B = -h$ 

$h$	$\lambda = 0.05$	$\lambda = 0.1$	$\lambda = 0.2$	$\lambda = 0.3$
-0.10	-	-	-	-
-0.15	137.2	-	-	-
-0.20	382.7	-	-	-
-0.25	+	127.3	-	-
-0.30	+	286.4	-	-
-0.35	+	766.1	-	-
-0.40	+	+	123.5	-
-0.45	+	+	249.4	-
-0.50	+	+	580.3	103.2
-0.55	+	+	+	197.9
-0.60	+	+	+	437.5
-0.65	+	+	+	+

“-” In-control ARL less than 100,

“+” In-control ARL greater than 1000.

equations using the collocation method and solving the system of equations, see Messaoud *et al.* (2004). As recommended by Calzada and Scariano (2003), the collocation method is used because the continuous uniform distribution does not have the entire real line as numerical support.

In the previous approximation, we ignored the slight dependence among successive ranks  $Q_t^m$ . Therefore, the result in (2.6) applies only approximately, as there are small correlations among successive ranks. For moderate and large values of  $m$  the correlations are quite small, see Hackl and Ledolter (1992). Table 2.1 shows the in-control ARL of the  $r$ MEWMA control charts with different smoothing parameters  $\lambda$  and control limits  $h$ . It assumed that the  $r$ MEWMA statistic starts at 0, that is  $T_0 = 0$ . Table 2.1 shows a decrease in the ARL with increasing  $\lambda$  for fixed control limit  $h$ . As mentioned by Hackl and Ledolter (1992), this is explained by the fact that  $\sigma_{T_t}^2$  increases with  $\lambda$  so that the probability of crossing the control limit  $h$  becomes larger.

A simulation study is carried in order to validate the ARL approximation. We generate independent random vectors  $\{\mathbf{X}_t\}$  from a bivariate normal distribution with zero mean vector and identity covariance matrix. Note that due to the nonparametric nature of the monitoring strategy, the normality is not required and any other distribution could be used. The simulation strategy is described in section 3.1.1. Note that only the Mahalanobis depth is considered. In fact, the simulations of the proposed monitoring strategy based on simplicial depth are extremely time consuming for reference samples larger than 200 observations.

Figure 2.2 shows the simulated in-control ARL ( $ARL_0$ ) values of the  $r$ MEWMA control charts with  $\lambda = 0.05, 0.1, 0.2$  and  $0.3$ . Note that 10000 replications are used.



Figure 2.2 shows that for large values of  $m$ , the  $ARL_0$  values of the  $rMEWMA$  control charts approach their asymptotic values. Moreover, the four  $rMEWMA$  control charts achieve their asymptotic  $ARL_0$  performances when a *relatively* small reference samples are used. However, it is shown in section 3.1.2 that the use of these reference samples is not optimal with respect to the out-of-control performance of the  $rMEWMA$  control charts.

## 2.4 Illustrative Example

In this section, an illustrative example is given to introduce the implementation of the  $rMEWMA$  control charts. Table 2.2 shows 20 observations simulated from a bivariate normal distribution with mean vector  $\boldsymbol{\mu} = (0, 0)'$  and the identity matrix as variance covariance matrix. The  $rMEWMA$  control chart based on simplicial depth with  $\lambda = 0.2$ ,  $h = -0.435$  and  $B = -h$  is considered. Its asymptotic in-control ARL is equal to 200. A small reference sample of size  $m = 10$  is considered in order to facilitate this illustration. Note that the simplicial depth is computed using the revised definition.

The monitoring procedure starts at time  $t = 10$ . That is after the first 10 observations are obtained and the reference sample is formed, i.e.,  $RS = \{\mathbf{X}_1, \dots, \mathbf{X}_{10}\}$ . The simplicial depth of  $\mathbf{X}_{10}$  w.r.t.  $RS$ ,  $SD(RS, \mathbf{X}_{10})$ , is equal to 0.250. Its sequential rank  $Q_{10}^*$  among  $SD(RS, \mathbf{X}_1), \dots, SD(RS, \mathbf{X}_{10})$  is computed using equation (2.4). It is equal to 0.5. The observed value of the control statistic of the  $rMEWMA$  control chart,  $T_{10}$ , is computed using equation (2.5). It is equal to 0.100. Note that it is assumed that the starting value is equal to 0.  $T_{10}$  is larger than the lower control limit  $h$ , see Figure 2.3. It causes no concerns of a process change to the engineers and they assumed that the process is in-control. Thus, they wait until the next observation  $\mathbf{X}_{11} = (0.61, -0.37)'$  is obtained and compute the control statistic.

At time  $t = 11$ ,  $RS$  is equal to  $\{\mathbf{X}_2, \dots, \mathbf{X}_{11}\}$ .  $SD(RS, \mathbf{X}_{11})$  and  $Q_{11}^*$  are respectively 0.317 and 0.9. The control statistic  $T_{11}$  is equal to  $0.260 > h$  which causes no concerns of process change. The process engineers wait until another observation is obtained, and so on, until an out-of-control signal is generated.

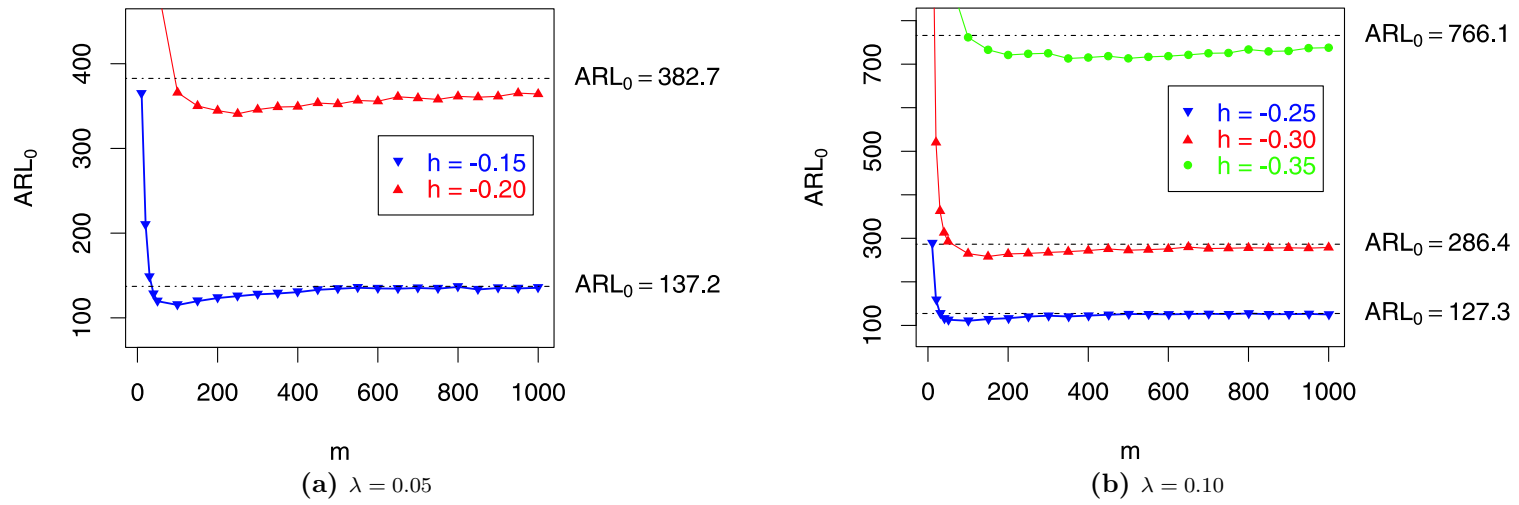
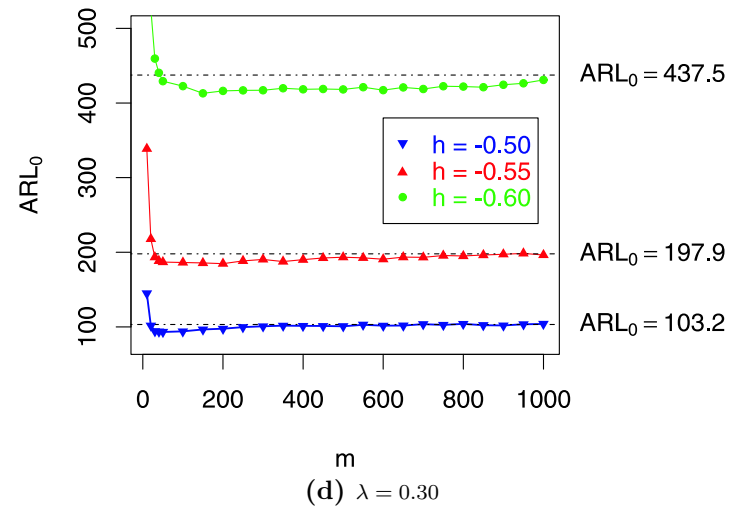
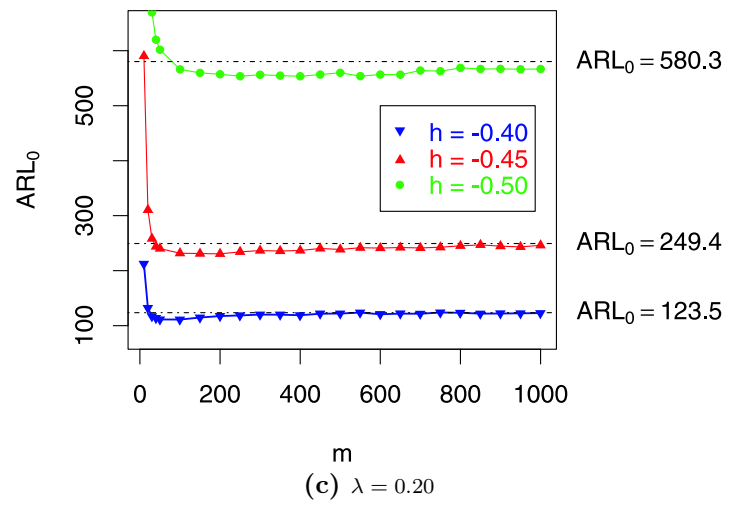


Figure 2.2: Simulated in-control ARL of  $r$ MEWMA control charts



**Figure 2.2:** Simulated in-control ARL of  $r$ MEWMA control charts (Continued)

**Table 2.2:** Illustrative example of the  $r$ MEWMA control chart

$t$	Observations $\mathbf{X}_t$		$SD(RS, \mathbf{X}_t)$	$Q_t^*$	$Q_t^m$	$T_t$
	$x_{t,1}$	$x_{t,2}$				
1	0.13	-0.09				
2	1.67	0.73				
3	1.00	-1.28				
4	-2.40	-0.68				
5	-0.04	0.89				
6	-0.02	-1.30				
7	-0.67	0.18				
8	0.83	-0.55				
9	-0.64	0.01				
10	-0.67	-0.83	0.250	8	0.5	0.100
11	0.61	-0.37	0.317	10	0.9	0.260
12	-0.29	-0.92	0.317	10	0.9	0.388
13	-0.58	0.06	0.342	10	0.9	0.435
14	0.05	-0.75	0.292	9	0.7	0.435
15	-0.14	1.48	0.150	3	-0.5	0.248
16	-0.21	-0.26	0.375	10	0.9	0.378
17	-0.14	-2.54	0.150	3	-0.5	0.203
18	0.58	-0.04	0.150	3.5	-0.4	0.082
19	-0.23	0.72	0.250	8	0.5	0.166
20	1.58	-0.39	0.150	2.5	-0.6	0.013

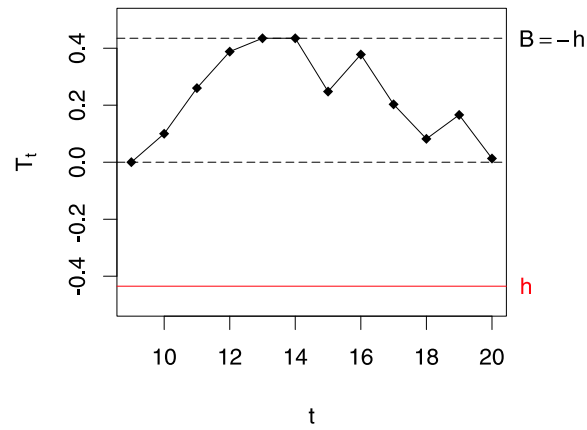


**Figure 2.3:** Plot of the  $r$ MEWMA Control Chart

## Simulation Results

In this chapter, simulations are conducted in order to assess the application of the proposed  $r$ MEWMA control charts. The effect of the use of reference samples of limited amount of observations on the performance of  $r$ MEWMA monitoring procedures is studied in section 3.1. In section 3.2, we examine the effect of the geometrical nature of simplicial depth on the performance of  $r$ MEWMA control charts.

In the following, Mahalanobis and simplicial  $r$ MEWMA control charts refer to the  $r$ MEWMA control charts based on Mahalanobis and simplicial depths, respectively. Note that in this chapter only the bivariate case is considered. This is explained by the computational difficulty of simplicial depth in  $\mathbb{R}^d$ ,  $d \geq 3$ , see section 2.1.

### 3.1 Effect of the Reference Sample Size on $r$ MEWMA Control Charts Performance

In section 2.3, the in-control ARL of  $r$ MEWMA control charts is approximated using the integral equation (2.6). It is assumed that a sufficiently large reference sample,  $m \rightarrow \infty$ , is available so that the in-control distribution can be estimated with negligible error. In practice, reference samples of limited amount of observations are used and the estimation effect may affect the performance of  $r$ MEWMA monitoring procedures.

In this section, a simulation study is conducted in order to examine the estimation effect on the desired in-control and out-of-control run length (RL) performances of  $r$ MEWMA control charts. A desired in-control and out-of-control RL performances mean that the empirical in-control and out-of-control RL distributions approach their asymptotic counterpart. Note that only the Mahalanobis  $r$ MEWMA control charts are considered. Indeed, the computation of simplicial depth is extremely time consuming for reference samples larger than 200 observations.

### 3.1.1 Simulation Study

The four Mahalanobis  $r$ MEWMA control charts with smoothing parameters  $\lambda = 0.05, 0.1, 0.2,$  and  $0.3$  are studied in detail. Their parameter combinations  $(\lambda, h$  and  $B)$  are chosen so that they have the same asymptotic in-control ARL equal to 200. Thus the respective values of  $h$  are  $-0.169, -0.279, -0.435,$  and  $-0.551$ . The different reflection boundaries  $B$  are chosen equal to  $-h$ . Different values are considered for the reference sample size  $m$ . Note that  $m = 10000$  is considered as  $m \approx \infty$ .

For the simulation, we generate random independent observations  $\{\mathbf{X}_t\}$  from a bivariate normal distribution with mean vector  $\boldsymbol{\mu}_0 = (0, 0)'$  and variance covariance matrix  $\Sigma_X$ . The shift scenario in the mean vector from  $\boldsymbol{\mu}_0$  to  $\boldsymbol{\mu}_1$  is considered to represent the out-of-control process. Its magnitude  $\delta$  is given by

$$\delta^2 = (\boldsymbol{\mu}_1 - \boldsymbol{\mu}_0)' \Sigma_X^{-1} (\boldsymbol{\mu}_1 - \boldsymbol{\mu}_0). \quad (3.1)$$

Other scenarios are not considered, for example a change in the in-control covariance matrix  $\Sigma_X$ . Note that in the context of multivariate normality,  $\delta$  is called the noncentrality parameter.

Since the multivariate normal distribution is elliptically symmetrical and the Mahalanobis depth is affine invariant, see Liu *et al.* (1999), the Mahalanobis  $r$ MEWMA control charts are directionally invariant. That is, their out-of-control ARL performance depends on a shift in the process mean vector  $\boldsymbol{\mu}$  only through the value of  $\delta$ . Thus, without any loss of generality, the shift is fixed in the direction of  $\mathbf{e}_1 = (1, 0)'$  and the variance covariance matrix  $\Sigma_X$  is taken to be the identity matrix  $\mathbf{I}$ . Note that due to the nonparametric nature of the  $r$ MEWMA control charts, the normality of the observations is not required and any other distribution could be used.

The simulation strategy proceeds as follows

1. Generate  $m - 1$  independent random vectors  $\mathbf{X}_1, \mathbf{X}_2, \dots, \mathbf{X}_{m-1}$ .
2. At time  $t \geq m$ , generate a random vector  $\mathbf{X}_t$  and add a shift of magnitude  $\delta$  given by equation (3.1). It is fixed in the direction  $\mathbf{e}_1 = (1, 0)'$ . Form the reference sample,  $RS = \{\mathbf{X}_{t-m+1}, \dots, \mathbf{X}_t\}$ , and compute data depths of all its observations, i.e.,  $D(\mathbf{X}_{t-m+1}), \dots, D(\mathbf{X}_t)$ .
3. Compute the control statistic  $T_t$  and check the in-control state. If the process is in-control, go to step 2. Otherwise the run-length is equal to  $t - m + 1$ .

The above steps are repeated a total of 100000 times.

### 3.1.2 Simulation Results

Tables A.1 to A.8 in Appendix A show summary statistics of the in-control ( $\delta = 0$ ) and out-of-control ( $\delta \neq 0$ ) run length (RL) distributions of the Mahalanobis  $r$ MEWMA

control charts. SDRL is the standard deviation of the run length.  $Q(.10)$ ,  $Q(.50)$ , and  $Q(.90)$  are respectively the 10th, 50th, and 90th percentiles of the in-control and out-of-control RL distributions. In the following,  $ARL_0$  and  $ARL_1$  are used to represent the in-control and out-of-control ARL, respectively. Similarly,  $Q_0(q)$  and  $Q_1(q)$  refer to the  $q$ th percentile of the in-control and out-of-control RL distributions, respectively. Note that  $Q_0(.50)$  and  $Q_1(.50)$  are respectively the in-control and out-of-control median RL.

### Performance of $r$ MEWMA Control Charts Based on Small Reference Samples

Tables A.1 to A.4 in Appendix A show that the four  $r$ MEWMA control charts with  $\lambda = 0.05, 0.1, 0.2,$  and  $0.3$  have an  $ARL_0$  performance approximately equal to the desired  $ARL_0$  of 200 when the respective reference samples of sizes  $m = 47, 41, 31,$  and  $28$  are used. Moreover,  $Q_0(.10)$ ,  $Q_0(.50)$  and  $Q_0(.90)$  are approximately equal to their asymptotic counterparts. However, Tables A.1 to A.4 in Appendix A and Figure 3.1 show that the  $ARL_1$ ,  $Q_1(.50)$ , and  $Q_1(.90)$  values of these control charts are much larger than the  $ARL_1$ ,  $Q_1(.50)$  and  $Q_1(.90)$  values of  $r$ MEWMA control charts with larger values of  $m$ . For example, consider the  $r$ MEWMA control chart with  $\lambda = 0.05$ . Table A.1 in Appendix A shows that the  $ARL_1$  and  $Q_1(.50)$  values for detecting a shift of magnitude  $\delta = 1.0$  are equal to 153.92 and 89, respectively, when  $m = 47$ . They are much larger than the  $ARL_1$  and  $Q_1(.50)$  values of 23.73 and 19, respectively, when  $m = 1000$ . That is, the control chart with  $m = 47$  detects the shift much slower than the one with  $m = 1000$ . Note that the  $Q_1(.50)$  values imply that there is a 50% of chance that the first out-of-control signal is given in less than 89 and 19 observations after the occurrence of the shift when  $m = 47$  and  $m = 1000$ , respectively.

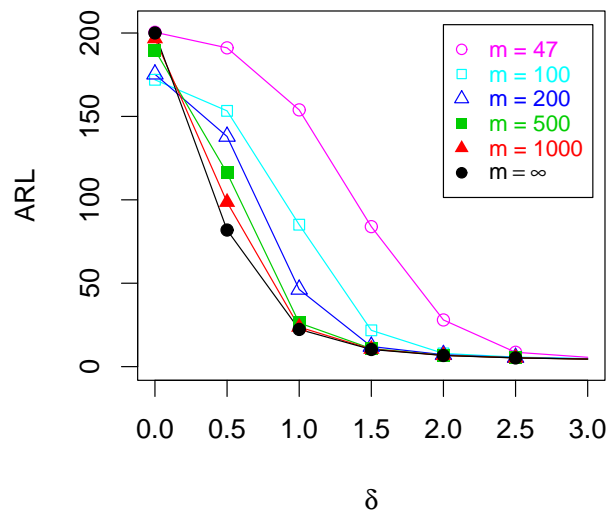
Therefore, even though that using *relatively* small reference samples achieves the desired in-control RL performance, this choice reduces considerably the  $r$ MEWMA control charts ability to quickly detect an out-of-control condition.

### Performance of $r$ MEWMA Control Charts Based on Moderate and Large Reference Samples

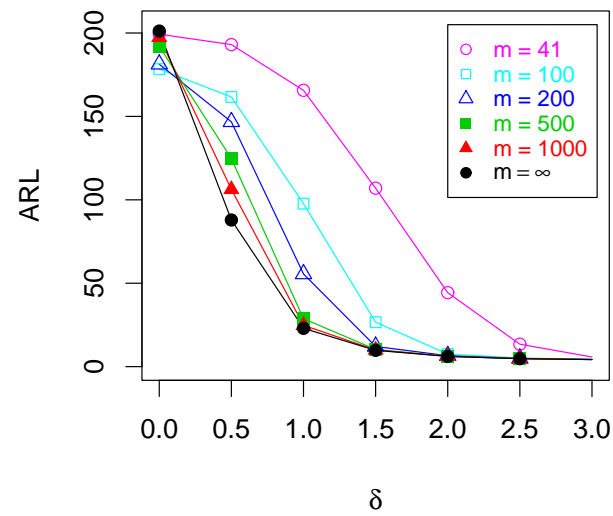
In the following, the three  $r$ MEWMA control charts with moderate and large reference samples are considered, i.e.,  $m = 100, 200, 500,$  and  $1000$ . Table 3.1 shows the percentage of decrement and increment in  $ARL_0$  and  $ARL_1$  values, respectively, with respect to the asymptotic  $ARL_0$  and  $ARL_1$  performances, i.e.,  $m = 10000$ .

#### In-Control Case ( $\delta = 0$ )

Table 3.1 and Figure 3.1 show that the  $ARL_0$  values of the  $r$ MEWMA control charts are shorter than the desired  $ARL_0$  of 200. That is, these control charts produce more false alarms than expected. However, interpretation based on the  $ARL_0$  values alone can be misleading. The  $Q_0(.90)$  values given in Tables A.1 to A.4 in Appendix A indicate that the larger percentiles of the in-control RL distributions affect the  $ARL_0$  values.



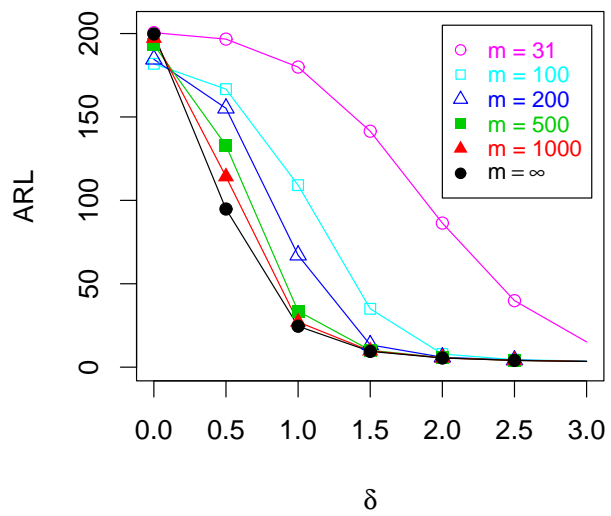
(a)  $\lambda = 0.05$



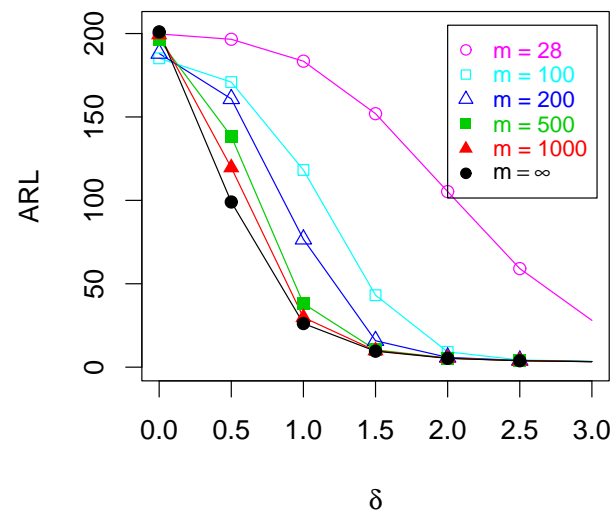
(b)  $\lambda = 0.10$

**Figure 3.1:** The ARL values of Mahalanobis  $r$ MEWMA control charts for mean shifts of size  $\delta$





(c)  $\lambda = 0.20$



(d)  $\lambda = 0.30$

**Figure 3.1:** The ARL values of Mahalanobis  $r$ MEWMA control charts for mean shifts of size  $\delta$  (Continued)

**Table 3.1:** Percentage of decrement and increment in the  $ARL_0$  and  $ARL_1$  values of Mahalanobis  $r$ MEWMA control charts with respect to the asymptotic  $ARL_0$  and  $ARL_1$  values, i.e.,  $m \approx \infty$

$m$	Shift magnitude						
	0.0	0.5	1.0	1.5	2.0	2.5	3.0
(a) $\lambda = 0.05$							
100	-14.03	+87.26	+281.27	+111.56	+18.71	+9.58	+7.10
200	-12.38	+68.49	+107.30	+17.30	+6.89	+4.02	+3.10
500	-5.13	+41.77	+17.34	+4.86	+2.54	+1.53	+1.11
1000	-1.68	+20.40	+6.32	+2.24	+1.20	+0.57	+0.44
(a) $\lambda = 0.10$							
100	-11.32	+83.91	+325.38	+172.67	+23.04	+8.19	+4.26
200	-9.89	+66.96	+141.84	+23.85	+6.86	+3.57	+1.65
500	-4.51	+41.92	+25.12	+5.53	+2.45	+1.26	+0.71
1000	-1.86	+20.91	+8.71	+2.66	+0.82	+0.42	+0.47
(a) $\lambda = 0.20$							
100	-8.95	+75.78	+344.44	+269.87	+43.90	+10.89	+5.85
200	-7.60	+63.70	+173.36	+41.44	+8.56	+4.46	+2.63
500	-3.24	+40.20	+36.70	+7.40	+2.91	+1.73	+0.88
1000	-1.26	+20.46	+10.35	+3.38	+1.28	+0.99	+0.29
(a) $\lambda = 0.30$							
100	-7.89	+72.59	+351.87	+350.42	+73.35	+12.21	+5.47
200	-6.44	+62.44	+193.12	+65.45	+11.15	+4.42	+2.13
500	-2.38	+39.73	+45.68	+8.56	+3.40	+1.82	+0.91
1000	-0.82	+20.81	+14.03	+3.44	+1.70	+0.78	+0.61

For example, consider the  $r$ MEWMA control chart with  $\lambda = 0.05$  and  $m = 200$ . Its  $ARL_0$  value is 12.38% shorter than its asymptotic value, see Table 3.1. Table A.1 in Appendix A shows that the  $Q_0(.10)$  value is equal to its asymptotic value of 26. The  $Q_0(.50)$  value is equal to 136. It is slightly shorter than its asymptotic value of 140. That is, the control chart produce in average a false alarm within 136 observations with a probability of 0.5 and within 140 observations with the same probability when  $m \approx \infty$ . Thus, the control chart does not suffer from the problem of early false alarms. However, the  $Q_0(.90)$  value is equal to 376. It is much shorter than its asymptotic value of 453. This implies that the larger percentiles affect the  $ARL_0$  value. In this case, practitioners may draw inaccurate conclusions about the in-control performance of the considered  $r$ MEWMA control chart based on the  $ARL_0$  value alone.

Now we will focus on the probabilities of the occurrence of early false alarms for the considered  $r$ MEWMA control charts. As mentioned in section 1.2, these probabilities are reflected in the lower percentiles of the in-control RL distributions. Table 3.2 gives the 5th, 10th, 20th, 30th, 40th and 50th percentiles of the in-control RL distributions of the four  $r$ MEWMA control charts. Table 3.2 shows that almost all lower percentiles are nearly the same as their asymptotic values. Only the  $Q_0(.40)$  and  $Q_0(.50)$  values of the  $r$ MEWMA control charts with  $100 \leq m \leq 200$  are slightly shorter than their asymptotic values.

Therefore, we can conclude that the observed decreases in the  $ARL_0$  values in Table 3.1 are caused by the shorter values of the larger percentiles. Practitioners should not fear for the problem of early false alarms when  $r$ MEWMA control charts are applied using reference samples of size  $m \geq 100$  observations.

### Out-of-Control Case ( $\delta \neq 0$ )

Table 3.1 and Figure 3.1 show that the  $ARL_1$  values of the  $r$ MEWMA control charts are larger than their asymptotic counterparts. As mentioned in section 1.2, interpretation based on the  $ARL_1$  values alone may lead to inaccurate conclusions. Thus, the lower percentiles and the median of the out-of-control RL distributions are investigated. They provide useful information about the ability of  $r$ MEWMA control charts to quickly detect an out-of-control condition.

First, we investigate the out-of-control performance of the four  $r$ MEWMA control charts for shifts of magnitude  $\delta \geq 1.5$ . Tables A.1 to A.4 in Appendix A show that the  $Q_1(.10)$  and  $Q_1(.50)$  values are nearly the same as their asymptotic values. However, the  $Q_1(.90)$  values are larger than their asymptotic values. That is, the  $ARL_1$  values are affected by some long runs. For example, consider the  $r$ MEWMA control chart with  $\lambda = 0.3$  and  $m = 100$ . Its  $ARL_1$  value for detecting a shift of magnitude  $\delta = 1.5$  is 350.42% larger than its asymptotic value, see Table 3.1. Table A.4 in Appendix A shows that the  $Q_1(.10)$  and  $Q_1(.50)$  values are nearly the same as their asymptotic counterparts.

**Table 3.2:** Lower percentiles of the in-control run length distributions of Mahalanobis  $r$ MEWMA control charts based on reference samples of size  $m$ 

$\lambda$	$m$	$Q_0(.05)$	$Q_0(.10)$	$Q_0(.20)$	$Q_0(.30)$	$Q_0(.40)$	$Q_0(.50)$
0.05	100	17	26	49	75	101	130
	200	17	26	48	74	103	136
	500	17	26	49	74	104	140
	1000	17	26	48	74	104	140
	$\infty$	17	26	49	75	105	140
0.10	100	15	26	49	74	101	132
	200	15	26	48	74	103	137
	500	15	26	48	74	105	140
	1000	15	25	48	75	105	141
	$\infty$	15	25	49	75	105	141
0.20	100	14	24	48	73	101	132
	200	14	24	47	72	102	136
	500	14	25	47	73	103	139
	1000	14	24	47	74	104	139
	$\infty$	14	24	48	74	104	139
0.30	100	13	24	47	73	101	133
	200	13	23	47	73	102	138
	500	13	24	47	74	105	141
	1000	13	24	47	74	105	141
	$\infty$	13	24	47	74	104	141

NOTE:  $Q_0(q) = q$ th percentile of the in-control run length distribution

**Table 3.3:** Lower percentiles of the out-of-control ( $\delta = 0.5$ ) run length distributions of the Mahalanobis  $r$ MEWMA control charts based on reference samples of size  $m$ 

$\lambda$	$m$	$Q_1(.05)$	$Q_1(.10)$	$Q_1(.20)$	$Q_1(.30)$	$Q_1(.40)$	$Q_1(.50)$
0.05	100	12	18	31	50	78	110
	200	12	16	27	40	57	82
	500	11	16	25	36	49	66
	1000	11	16	24	35	47	62
	$\infty$	11	16	24	34	45	59
0.10	100	11	16	31	52	82	114
	200	10	15	27	41	61	89
	500	10	15	25	37	52	71
	1000	10	15	25	36	49	66
	$\infty$	10	14	24	35	47	62
0.20	100	9	15	30	53	84	115
	200	9	14	27	43	64	95
	500	9	14	25	39	55	76
	1000	9	14	24	37	52	70
	$\infty$	9	13	24	36	49	65
0.30	100	9	15	31	55	86	118
	200	8	14	27	45	67	99
	500	8	14	26	40	57	79
	1000	8	13	25	38	54	73
	$\infty$	8	13	24	37	51	68

NOTE:  $Q_1(q) = q$ th percentile of the out-of-control run length distribution

The control chart detects the shift on average within 10 observations with a probability of 0.5 and within 8 observations with the same probability when  $m \approx \infty$ . However, the  $ARL_1$  value is affected by some long runs. The  $Q_1(.90)$  value is equal to 124. It is much larger than its asymptotic value of 18. Therefore, we can conclude that the ability of the four  $r$ MEWMA control charts to quickly detect shifts of magnitude  $\delta \geq 1.5$  is not affected when reference samples of size  $m \geq 100$  are used.

Now we investigate the out-of-control performance of the four  $r$ MEWMA control charts for shifts of magnitude  $\delta = 0.5$  and 1.0. Tables 3.3 and 3.4 show that the lower percentiles of the out-of-control RL distributions of  $r$ MEWMA control charts with  $100 \leq m \leq 200$  are larger than their asymptotic values. That is, the estimation effect affects the sensitivity of these control charts to react to shifts of magnitude  $\delta \leq 1.0$ . For  $r$ MEWMA control charts with  $500 \leq m \leq 1000$ , the lower percentiles of the out-of-control RL distribution are nearly the same or slightly larger than the asymptotic values. Therefore, we can conclude that using reference samples of size  $m \geq 500$  ensures that the  $r$ MEWMA control charts perform like ones with sufficiently large reference samples, i.e.,  $m \approx \infty$ . Their ability to quickly detect an out-of-control condition is not affected.

**Table 3.4:** Lower percentiles of the out-of-control ( $\delta = 1.0$ ) run length distributions of the Mahalanobis  $r$ MEWMA control charts based on reference samples of size  $m$ 

$\lambda$	$m$	$Q_1(.05)$	$Q_1(.10)$	$Q_1(.20)$	$Q_1(.30)$	$Q_1(.40)$	$Q_1(.50)$
0.05	100	7	9	12	16	21	28
	200	7	8	11	14	17	21
	500	7	8	11	13	16	19
	1000	7	8	11	13	16	19
	$\infty$	7	8	11	13	15	18
0.10	100	6	8	11	15	21	29
	200	6	7	10	13	17	22
	500	6	7	10	12	16	19
	1000	6	7	10	12	15	18
	$\infty$	6	7	10	12	15	18
0.20	100	5	7	10	15	22	34
	200	5	6	9	13	17	23
	500	5	6	9	12	16	20
	1000	5	6	9	12	15	19
	$\infty$	5	6	9	11	15	18
0.30	100	5	6	10	15	24	40
	200	4	6	9	13	18	25
	500	4	6	9	12	16	21
	1000	4	6	9	12	15	20
	$\infty$	4	6	8	11	15	19

NOTE:  $Q_1(q) = q$ th percentile of the out-of-control run length distribution

### Sample Size Requirements

In this section, it is shown that using large reference samples of size  $m \geq 500$  will reduce the estimation effect on the in-control and out-of-control performances of  $r$ MEWMA control charts. However, only the shift scenario in the mean vector is considered to represent the out-of-control process. The early false alarms produced by the  $r$ MEWMA control charts and the early detection of out-of-control conditions are mainly used to evaluate their in-control and out-of-control performances. The reader should be aware that the sample size recommendation may differ for other out-of-control scenarios. For example, a shift in the in-control covariance matrix.

The required large reference samples of size  $m \geq 500$  observations should not be a problem for the applications of  $r$ MEWMA monitoring procedures. Nowadays, advances in data collection activities as well as the computational power of digital computers have increased the available data sets in many industrial processes. However, practitioners should not neglect the estimation effect on the in-control and out-of-control performances of the  $r$ MEWMA control charts if for some industrial applications forming large reference samples might be problematic.

### Relation Between the Smoothing Parameter and the Reference Sample Size $m$

An important consideration is the relation between the smoothing parameter  $\lambda$  and the reference sample size  $m$ . Table 3.1 shows that the smaller the value of  $\lambda$ , the larger the reference sample size  $m$  is necessary for achieving desired  $ARL_0$  performance. This suggests that for a fixed reference sample size  $m$ ,  $r$ MEWMA control charts with smaller values of  $\lambda$  are more plagued by false alarms than charts with larger values of  $\lambda$ . Finally,  $r$ MEWMA control charts with smaller values of  $\lambda$  are more effective to detect small shifts and drifts in the process mean vector than charts with larger values of  $\lambda$ . This is a known property of the EWMA schemes.

## 3.2 Effect of the Geometrical Nature of Simplicial Depth on the Performance of $r$ MEWMA Control Charts

In this section, a simulation similar to that described in section 3.1.1 is conducted in order to study the in-control and out-of-control performances of the four simplicial  $r$ MEWMA control charts with  $\lambda = 0.05, 0.1, 0.2,$  and  $0.3$ . The simplicial depth is computed using the revised definition. Note that simplicial  $r$ MEWMA control charts are directionally invariant because the simplicial depth is affine invariant. For the simulation, 10000 replications are used and only reference samples of size  $m = 100$  and  $200$  observations are considered. This is due to the computational difficulty of the simplicial depth for large values of  $m$ , see section 2.1.

Tables A.5 to A.8 in Appendix A show summary statistics of the in-control ( $\delta = 0$ ) and out-of-control ( $\delta \neq 0$ ) run length distributions of the simplicial  $r$ MEWMA control charts. SDRL is the standard deviation of the run length.  $Q(.10)$ ,  $Q(.50)$ , and  $Q(.90)$  are respectively the 10th, 50th, and 90th percentiles of the in-control and out-of-control run length distributions.

In Figure 3.2, the  $ARL_0$  and  $ARL_1$  values of Mahalanobis and simplicial  $r$ MEWMA control charts are plotted for  $m = 100$  and  $200$ . To compare the control charts fairly, the  $ARL_0$  and  $ARL_1$  values of Mahalanobis  $r$ MEWMA control charts are calculated using the same number of replications of 10000. Figure 3.2 shows that the simplicial  $r$ MEWMA control charts have larger  $ARL_0$  and  $ARL_1$  values than charts based on Mahalanobis depth. Furthermore, the percentiles of their in-control and out-of-control RL distributions are slightly larger than the respective percentiles of Mahalanobis  $r$ MEWMA control charts. This suggests larger in-control and out-of-control run lengths. This is explained by the geometrical nature of simplicial depth. One drawback of its use in quality control is that it assigns the same depth to the extreme points of the reference sample. This reduces the ability of simplicial  $r$ MEWMA control charts to quickly react to process changes.

The extreme points of the reference sample play a central role in investigating the properties of simplicial  $r$ MEWMA control charts. Let  $RS$  denote a reference sample of size  $m > d$  observations from a  $d$ -variate continuous distribution. Let  $E^m$  denote the number of extreme points of  $RS$ . Stoumbos and Jones (2000) showed that the minimum simplicial depth that any point in  $RS$  can have is  $\frac{d+1}{2m}$  and that a point assumes this minimum depth only and only if it is an extreme point. They also showed that there always exist at least  $d + 1$  extreme points, i.e.,  $E^m \geq d + 1$ .

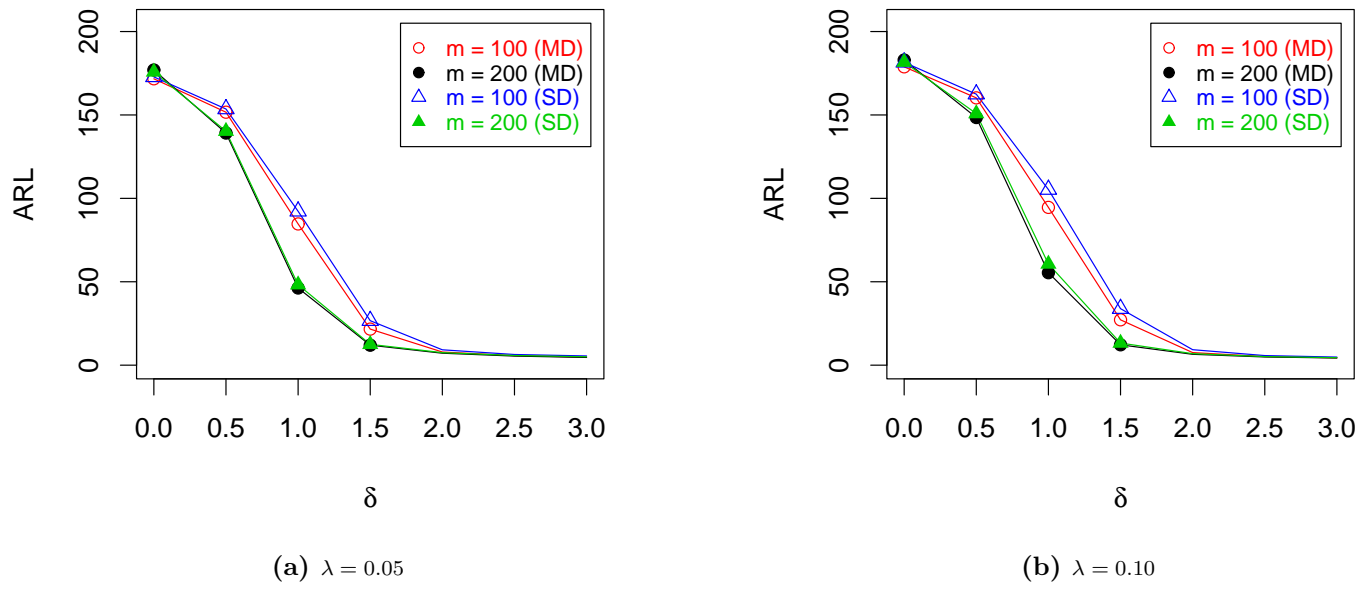
### 3.2.1 Lower Bounds to $Q_t^m$

In section 2.2, it is mentioned that the statistics  $Q_t^*$  and  $Q_t^m$  given by equations (2.3) and (2.4) are uniformly distributed on the  $m$  points  $\{1, 2, \dots, m\}$  and  $\{1/m - 1, 3/m - 1, \dots, 1 - 1/m\}$ , respectively. Indeed, it is assumed that the data depths of the observations of  $RS$  are continuous. This ensures that ties are not observed. Therefore the lower bounds to the statistics  $Q_t^*$  and  $Q_t^m$  ( $t \geq m$ ) given by equations (2.3) and (2.4) are

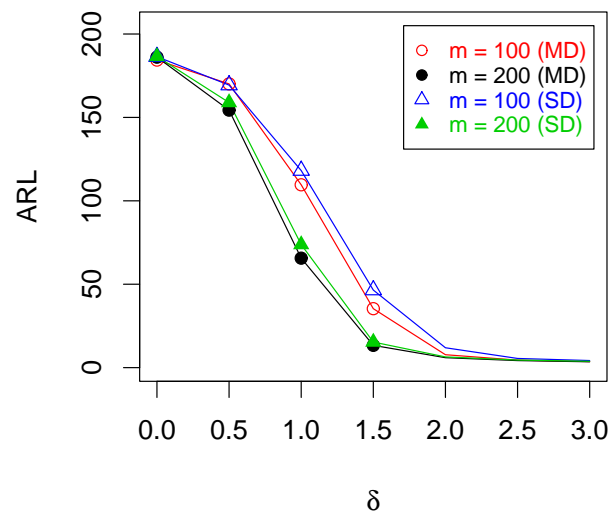
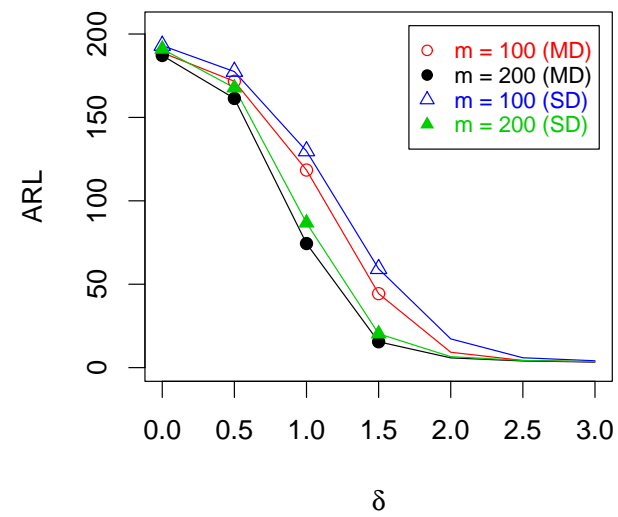
$$\begin{aligned} 1 &\leq Q_t^*, \\ \frac{1}{m} - 1 &\leq Q_t^m. \end{aligned} \tag{3.2}$$

However, for the simplicial  $r$ MEWMA monitoring procedure, the  $E^m \geq d + 1$  extreme points of  $RS$  are treated in an indistinguishable manner. They share the minimum simplicial depth of  $\frac{d+1}{2m}$ . The midrank of their simplicial depth is equal to  $(E^m + 1)/2$ .





**Figure 3.2:** The ARL of Mahalanobis (MD) and simplicial (SD)  $r$ MEWMA control charts for mean shifts of size  $\delta$

(c)  $\lambda = 0.20$ (d)  $\lambda = 0.30$ **Figure 3.2:** The ARL of Mahalanobis (MD) and simplicial (SD)  $r$ MEWMA control charts for mean shifts of size  $\delta$  (Continued)

**Table 3.5:** Lower bounds to  $Q_t^m$  when the Mahalanobis (MD) and simplicial (SD) depths are used ( $d = 2$ )

$m$	MD		SD
	$1/m - 1$	$(d + 1)/m - 1$	$E(E^m)/m - 1$
50	-0.980	-0.920	-0.834
100	-0.990	-0.960	-0.908
200	-0.995	-0.980	-0.950
500	-0.998	-0.992	-0.978
1000	-0.999	-0.996	-0.988
10000	-1.000	-1.000	-0.999

Therefore the lower bounds to the statistics  $Q_t^*$  and  $Q_t^m$  ( $t \geq m$ ) are now

$$\begin{aligned}
 1 &< \frac{d + 2}{2} \leq \frac{E^m + 1}{2} \leq Q_t^*, \\
 \frac{1}{m} - 1 &< \frac{d + 1}{m} - 1 \leq \frac{E^m}{m} - 1 \leq Q_t^m.
 \end{aligned}
 \tag{3.3}$$

More generally, Hueter (1994) derived an asymptotic expression for the expected number of vertices or extreme points on the convex hull of a bivariate normal sample of size  $m$ . It is given by

$$E(E^m) \approx 2\sqrt{2\pi\ln(m)},$$

where  $\pi = 3.142$  and  $\ln(\cdot)$  is the natural log function. Stoumbos and Jones (2000) found that, for a given finite value of  $m$ , this result overestimated the exact  $E(E^m)$  by a constant. They derived an accurate approximation for  $E(E^m)$  and  $Var(E^m)$ , where

$$E(E^m) \approx 2\sqrt{2\pi\ln(m)} - 1.6,$$

and

$$Var(E^m) \approx 1.291623\sqrt{\ln(m)}.$$

Therefore, the lower bounds to  $E(Q_t^*)$  and  $E(Q_t^m)$  can be approximated by

$$\begin{aligned}
 1 &< \frac{d + 2}{2} \leq \frac{E(E^m) + 1}{2} \leq E(Q_t^*), \\
 \frac{1}{m} - 1 &< \frac{d + 1}{m} - 1 \leq \frac{E(E^m)}{m} - 1 \leq E(Q_t^m).
 \end{aligned}
 \tag{3.4}$$

Now we assume that a change occurs in the process at time  $t \geq m$ . For example it can be represented by a shift in the in-control mean vector  $\mu_0$  or a change in the in-control covariance matrix  $\Sigma_X$ . At each sampling time  $t$ , the simplicial  $r$ MEWMA control statistic  $T_t$  wander in the direction of an out-of-control by  $\lambda Q_t^m$ , where

$$\lambda \left( \frac{1}{m} - 1 \right) < \lambda \left( \frac{d + 1}{m} - 1 \right) \leq \lambda \left( \frac{E(E^m)}{m} - 1 \right) \leq \lambda E(Q_t^m).$$

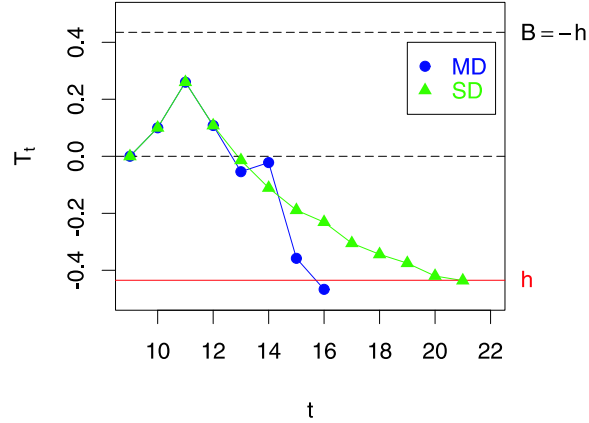


**Figure 3.3:** Plot of Mahalanobis (MD) and simplicial (SD)  $r$ MEWMA control charts

On the other hand, the Mahalanobis  $r$ MEWMA control statistic  $T_t$  wander fast in the direction of an out-of-control by  $\lambda Q_t^m$ , where

$$\lambda \left( \frac{1}{m} - 1 \right) \leq \lambda Q_t^m.$$

Table 3.5 shows the lower bounds to  $Q_t^m$  for different values of  $m$  when the Mahalanobis and simplicial depths are used. It shows that as  $m \rightarrow \infty$ , the lower bound of  $E(Q_t^m)$  approaches its limiting value of  $-1$ . This ensures that the simplicial  $r$ MEWMA control charts will behave similar to the Mahalanobis  $r$ MEWMA control charts.

### 3.2.2 Illustrative Example

To illustrate the effect of the geometrical nature of simplicial depth on the performance of  $r$ MEWMA control charts, we consider the example given in section 2.4. We assume that the process mean vector shifts from  $\boldsymbol{\mu}_0 = (0, 0)'$  to  $\boldsymbol{\mu}_1 = (2, 1)'$  at time  $t \geq 12$ .

At time  $t = 11$ , the two control statistics  $T_{11}$  of the Mahalanobis and simplicial  $r$ MEWMA control charts are equal to 0.26. Figure 3.3 shows that the Mahalanobis  $r$ MEWMA control chart is more sensitive to the shift and detect it after 5 observations. However, using the simplicial depth, the shift is detected after 11 observations.

After the occurrence of the shift, observations  $\mathbf{X}_t$ ,  $t = 12, \dots, 16$ , are extreme points to  $RS = \{\mathbf{X}_{t-9}, \dots, \mathbf{X}_t\}$ . Table 3.6 shows that the Mahalanobis  $r$ MEWMA control statistic  $T_t$  wander fast in the direction of an out-of-control. For example, at  $t = 16$ , using the Mahalanobis depth, the sequential rank of  $MD(RS, \mathbf{X}_{16})$  among  $MD(RS, \mathbf{X}_7), \dots, MD(RS, \mathbf{X}_{16})$  is equal to 1. The Mahalanobis  $r$ MEWMA control statistic  $T_{16}$  wander in the direction of an out-of-control by  $-0.18$  and an out-of-control signal is given. However, observation  $\mathbf{X}_{16}$  share the minimum simplicial depth of 0.15 with 5 other

extreme points. Therefore, the sequential midrank of  $SD(RS, \mathbf{X}_{16})$  among  $SD(RS, \mathbf{X}_7), \dots, SD(RS, \mathbf{X}_{16})$  is equal to 3.5 and the simplicial  $r$ MEWMA control statistic  $T_{16}$  wander in the direction of an out-of-control only by  $-0.08$ .

In conclusion, simplicial  $r$ MEWMA control charts are less powerful than Mahalanobis  $r$ MEWMA control charts when reference samples of limited amount of observations are used. This is due to the geometrical nature of simplicial depth.

**Table 3.6:** Illustrative example of the effect of the lower boundary to  $Q_t^m$  on the out-of-control performance of the  $r$ MEWMA control charts

$t$	Observations $\mathbf{X}_t$		Mahalanobis depth				Simplicial depth				
	$x_{t,1}$	$x_{t,2}$	$MD$	$Q_t^*$	$Q_t^{10}$	$T_t$	$SD$	$E^m$	$Q_t^*$	$Q_t^m$	$T_t$
11	0.61	-0.37	0.749	10	0.9	0.260	0.317	6	10	0.9	0.260
12	1.71	0.08	0.271	3	-0.5	0.108	0.150	5	3	-0.5	0.108
13	1.42	1.06	0.208	2	-0.7	-0.054	0.150	5	3	-0.5	-0.014
14	2.05	0.25	0.157	1	-0.9	-0.022	0.150	5	3	-0.5	-0.111
15	1.86	2.48	0.123	1	-0.9	-0.358	0.150	5	3	-0.5	-0.189
16	1.79	0.74	0.163	1	-0.9	-0.467	0.150	6	3.5	-0.4	-0.231
17	1.86	-1.54					0.150	4	2.5	-0.6	-0.305
18	2.58	0.96					0.150	5	3	-0.5	-0.344
19	1.77	1.72					0.150	5	3	-0.5	-0.375
20	3.58	0.61					0.150	5	2.5	-0.6	-0.420
21	3.18	2.79					0.150	5	3	-0.5	-0.436

## Performance Comparisons

In this chapter, the performances of the proposed  $r$ MEWMA control charts and the parametric alternative procedure are compared using simulations. In section 4.1, the parametric multivariate EWMA control chart is introduced. In section 4.2, the simulation study is described. The results are given in section 4.3.

### 4.1 The Parametric Multivariate EWMA Control Chart

The parametric multivariate EWMA ( $p$ MEWMA) control chart is introduced by Lowry *et al.* (1992). This chart is used to monitor the mean vector  $\boldsymbol{\mu}$  of a  $d$ -variate process observations,  $\mathbf{X} = (x_1, \dots, x_d)'$ . The authors assumed that the in-control mean vector  $\boldsymbol{\mu}_0$  and covariance matrix  $\Sigma_X$  of the observations  $\{\mathbf{X}_t\}$  are known. For this control chart, the vectors of EWMA's are defined as

$$\mathbf{z}_t = \mathbf{r}(\mathbf{X}_t - \boldsymbol{\mu}_0) + (\mathbf{I} - \mathbf{r})\mathbf{z}_{t-1}, \quad (4.1)$$

$t = 1, 2, \dots$ , where the smoothing matrix  $\mathbf{r}$  is a  $d \times d$  diagonal matrix whose diagonal elements are  $0 < r_i \leq 1$ ,  $i = 1, 2, \dots, d$ , and the starting value  $\mathbf{z}_0$  is usually chosen to be equal to 0. Lowry *et al.* (1992) suggests using  $r_i = r$ ,  $i = 1, 2, \dots, d$ , if there is no practical reason to weight past observations differently. The control statistic of the  $p$ MEWMA control chart is

$$T_t^2 = \mathbf{z}_t' \Sigma_{z_t}^{-1} \mathbf{z}_t,$$

$t = 1, 2, \dots$ , where  $\Sigma_{z_t}$  is the covariance matrix of  $\mathbf{z}_t$  given by

$$\Sigma_{z_t} = \frac{r[1 - (1 - r)^{2t}]}{2 - r} \Sigma_X.$$

Lowry *et al.* (1992) mentioned that it may be more likely that the process will stay in control for a while and then shift to an out-of-control state. Therefore, they suggest the

use of asymptotic covariance matrix,  $i \rightarrow \infty$ . That is,

$$\Sigma_{z_t} \approx \frac{r}{2-r} \Sigma_X. \quad (4.2)$$

Note that the use of the exact covariance matrix or the asymptotic covariance matrix leads to two different monitoring procedures. The exact covariance matrix can be used in equation (4.1) if it is believed that there may be some initial process disturbances. In this case, the  $p$ MEWMA control chart has the fast initial response (FIR) and then detects more quickly initial process disturbances.

The  $p$ MEWMA control chart produces an out-of-control signal as soon as  $T_t^2 > L$ , where  $L > 0$  represents the chart's upper control limit. It is usually determined so that the  $p$ MEWMA control chart achieves a desired in-control ARL.

In practice, the in-control mean vector  $\boldsymbol{\mu}_0$  and covariance matrix  $\Sigma_X$  of the monitored observations  $\{\mathbf{X}_t\}$  are rarely known. A common practice is to collect data over a substantial amount of time when the process is in-control to estimate them. Moreover, this data could be used to check the assumptions of independence and multivariate normality.

For the estimated version of the  $p$ MEWMA control chart,  $\boldsymbol{\mu}_0$  and  $\Sigma_X$  are replaced by their respective estimators  $\hat{\boldsymbol{\mu}}_0$  and  $\hat{\Sigma}_X$ . Thus, the vectors of EWMA's are given by

$$\mathbf{z}_t = \mathbf{r}(\mathbf{X}_t - \hat{\boldsymbol{\mu}}_0) + (\mathbf{I} - \mathbf{r})\mathbf{z}_{t-1},$$

$t = 1, 2, \dots$ , where  $\mathbf{z}_0 = \mathbf{0}$ . The control statistic is defined as

$$T_t^2 = \mathbf{z}_t' \hat{\Sigma}_{z_t}^{-1} \mathbf{z}_t,$$

$t = 1, 2, \dots$ , where  $\hat{\Sigma}_{z_t}$  is given by

$$\hat{\Sigma}_{z_t} = \frac{r[1 - (1-r)^{2t}]}{2-r} \hat{\Sigma}_X.$$

The asymptotic form of  $\hat{\Sigma}_{z_t}$  is

$$\hat{\Sigma}_{z_t} \approx \frac{r}{2-r} \hat{\Sigma}_X.$$

Note that the  $p$ MEWMA control chart with  $r_i = 1$ ,  $i = 1, 2, \dots, d$ , is the Hotelling's  $T^2$  control chart.

For a  $p$ MEWMA control chart, it is assumed that the underlying distribution of the  $d \times 1$  quality vector is multivariate normal. Stoumbos and Sullivan (2002) and Testik *et al.* (2003) investigated the effect of non-normality on its statistical performance. They considered the multivariate  $t$ -distribution to represent a large-tailed distribution and the multivariate gamma to represent a skewed distribution. Stoumbos and Sullivan (2002) noted that a control chart for the mean vector would be distribution free in the sense that its performance would be sensitive to changes in the mean vector, but independent of all other aspects of the control statistic's distribution, as determined by the higher moments.



They concluded that using  $r \in [0.02, 0.05]$ , the  $p$ MEWMA control charts are insensitive to departures from multivariate normality. That is, this choice ensures in-control performance comparable to that with multivariate normal observations. Furthermore, they are very effective at detecting process shifts of any size or direction even for highly skewed and extremely heavy-tailed multivariate distributions.

## 4.2 Simulation Study

In this section, the in-control and out-of-control performances of the  $r$ MEWMA and  $p$ MEWMA control charts are compared using simulations. The shift scenario in the process mean vector from  $\boldsymbol{\mu}_0$  to  $\boldsymbol{\mu}_1$  when the higher moments of the distribution are fixed is considered to represent the out-of-control process. Its magnitude is given by equation (3.1). The four  $r$ MEWMA control charts with  $\lambda = 0.05, 0.1, 0.2$  and  $0.3$  and the  $p$ MEWMA control charts with  $r = 0.05$  are considered. As mentioned, using  $r = 0.05$ , the  $p$ MEWMA control chart is insensitive to departure from multivariate normality.

The  $p$ MEWMA control charts with estimated parameters are designed similar to the  $r$ MEWMA control charts in order to compare their in-control and out-of-control RL performances fairly. That is, at time  $t \geq m$ , the reference sample comprised of the  $m > 1$  most recent observations taken from the process is used to estimate  $\boldsymbol{\mu}_0$  and  $\Sigma_X$ .

Reference samples of sizes  $m = 200$  and  $m \approx \infty$  (i.e.,  $m = 10000$ ) are considered. In fact, reference samples of size  $m = 200$  may be practical in many industrial applications. In this case, the parameters are unknown and the estimation effect should not be neglected, see section 3.1. The case  $m \approx \infty$  is similar to the parameter known case. In fact, a sufficiently large reference sample is available so that the in-control parameters  $\boldsymbol{\mu}_0$  and  $\Sigma_X$  of the  $p$ MEWMA control charts and the in-control distributions of the  $r$ MEWMA control charts can be estimated with negligible error.

To compare all control charts fairly when  $m = 200$ , we need to adjust their control limits so that their in-control ARL is approximately the same. Table 4.1 shows the adjusted ( $m = 200$ ) and asymptotic control limits ( $m \approx \infty$ ) of all control charts. The adjusted control limits are obtained using simulation, where we generate independent random vectors  $\{\mathbf{X}_t\}$  from the bivariate normal distribution with mean vector  $\boldsymbol{\mu}_0 = (0, 0)'$  and variance covariance matrix equal to the identity matrix.

Table 4.1 shows that the control limit of the  $p$ MEWMA control chart is shrunk. The effect of the use of adaptive estimates  $\hat{\boldsymbol{\mu}}_0$  and  $\hat{\Sigma}_X$  in place of known parameters  $\boldsymbol{\mu}_0$  and  $\Sigma_X$  increases the  $ARL_0$  values. This result is different of the traditional  $p$ MEWMA control charts where estimates of  $\boldsymbol{\mu}_0$  and  $\Sigma_X$  from an in-control Phase I reference sample are used in the monitoring phase (Phase II). In this case, Champ and Jones-Farmer (2005) showed that a dramatic increase in the number of false alarms is observed because of the reduced  $ARL_0$  values and percentiles of the in-control RL distribution.

**Table 4.1:** Adjusted and asymptotic control limits of the  $r$ MEWMA and  $p$ MEWMA control charts

$m$	$p$ MEWMA		$r$ MEWMA		
	$r$	0.05	$\lambda$		
	0.05		0.10	0.20	0.30
200	7.200	-0.176	-0.284	-0.440	-0.555
$\infty$	7.346	-0.159	-0.279	-0.435	-0.551

For the  $p$ MEWMA control charts, the asymptotic covariance matrix given by equation (4.2) is used. In fact, the use of a fast initial response (FIR) feature increases the probability of early false alarms. Stoumbos and Sullivan (2002) noted that in the presence of non-multinormal observations this would impair the ability to achieve robust performance.

Similar to Stoumbos and Sullivan (2002), we consider the multivariate  $t$ -distribution to represent a large-tailed distribution and the multivariate gamma distribution to represent a skewed distribution. For a complete discussion about the motivation of this choice see Stoumbos and Sullivan (2002). We consider  $t(v)$  observations with degrees of freedom values of  $v = 3, 6, 20$  and  $100$ . Stoumbos and Sullivan (2002) noted that with degrees of freedom below 3, the second moment is undefined so the  $p$ MEWMA control chart statistic is also undefined. For the  $G(\alpha, 1)$ , we consider observations having shape parameter values of  $\alpha = 1, 4, 16$  and  $64$ . Note that  $t(3)$  and  $G(1, 1)$  depart from multinormality greatly with respect to the third/or fourth moments. As  $v$  and  $\alpha$  increase, the  $t$  and gamma distributions, respectively, approach multivariate normality. Note that only results with  $t(3)$  and  $G(1, 1)$  distributions are reported in this work.

For the multivariate normal and  $t$ -distributions, the  $p$ MEWMA and  $r$ MEWMA control charts are directionally invariant. That is, their ARL performance depends on a shift in the process mean vector  $\boldsymbol{\mu}$  only through the value of  $\delta$  given by equation (3.1). Note that for the  $p$ MEWMA control charts, this property holds only when a diagonal smoothing matrix  $\mathbf{r}$  is used, see Lowry *et al.* (1992). Thus, without any loss of generality, the shift is fixed in the direction of  $\mathbf{e}_1 = (1, 0)'$  and  $\Sigma_X$  is taken to be equal to  $\mathbf{I}$  and  $v/(v-2)\mathbf{I}$  for the multivariate normal and  $t$ -distributions, respectively.

For the multivariate gamma distribution, the  $p$ MEWMA and  $r$ MEWMA control charts are directionally not invariant. Stoumbos and Sullivan (2002) showed that the shift direction affects the detection power of the  $p$ MEWMA control charts. Similar to Stoumbos and Sullivan (2002) we report the ARL averaged over a uniform distribution (all directions being equally likely) for the shift directions. The shift directions were generated using the algorithm suggested by Johnson (1987) (p. 127). A new shift direction is generated for each simulation run.  $\Sigma_X$  equal to  $\mathbf{I}$  is used for the simulations. Note that

the details but not the general conclusions depend on this choice of parameter settings.

The simulation strategy is similar to that described in section 3.1.1. The results are based on 10000 replications. The simplicial depth is computed using the revised definition. The random  $t$  and gamma observations are generated similar to Stoumbos and Sullivan (2002).

### 4.3 Simulation Results

Tables A.9 through A.17 in Appendix A presents the in-control ( $\delta = 0$ ) and out-of-control ( $\delta \neq 0$ ) performances of the  $r$ MEWMA and  $p$ MEWMA control charts for multivariate normal,  $t(3)$  and  $G(1, 1)$  distributions with various parameters. The Mahalanobis and simplicial depths are used for the  $r$ MEWMA control charts. Similar as in Chapter 3,  $ARL_0$  and  $ARL_1$  represent the in-control and out-of-control average run lengths, respectively.  $Q_0(q)$  and  $Q_1(q)$  refer to the  $q$ th percentile of the in-control and out-of-control run length distributions, respectively.

#### 4.3.1 Comparison of Performances of Mahalanobis $r$ MEWMA and $p$ MEWMA Control Charts

In this section, the in-control ( $\delta = 0$ ) and out-of-control ( $\delta \neq 0$ ) RL performances of  $r$ MEWMA and  $p$ MEWMA control charts are compared. Note that only Mahalanobis  $r$ MEWMA control charts with  $\lambda = 0.05$  are considered.

##### In-Control Case ( $\delta = 0$ )

Table 4.2 gives the  $ARL_0$ ,  $Q_0(.10)$ ,  $Q_0(.50)$  and  $Q_0(.90)$  values of the  $p$ MEWMA and Mahalanobis  $r$ MEWMA control charts for  $m = 200$  and  $m \approx \infty$ . It shows that using reference samples of size  $m = 200$  observations, the  $ARL_0$ ,  $Q_0(.10)$ ,  $Q_0(.50)$  and  $Q_0(.90)$  values of the  $p$ MEWMA control charts with bivariate  $t(3)$  and  $G(1, 1)$  observations are shorter than the respective values with bivariate normal observations. That is,  $p$ MEWMA control charts with bivariate  $t(3)$  and  $G(1, 1)$  observations are more plagued by false alarms than with bivariate normal observations. This might be explained by the fact that  $p$ MEWMA control charts are designed assuming the multivariate normality of the observations. In the other hand, the Mahalanobis  $r$ MEWMA control charts have approximately equal  $Q_0(.10)$ ,  $Q_0(.50)$  and  $Q_0(.90)$  values with bivariate normal,  $t(3)$  and  $G(1, 1)$  observations. This is explained by their distribution-free design.

Table 4.2 shows that the  $ARL_0$ ,  $Q_0(.10)$ ,  $Q_0(.50)$  and  $Q_0(.90)$  values of the  $p$ MEWMA control charts are approximately equal or shorter than the respective values of the Mahalanobis  $r$ MEWMA control charts. Note that only the  $Q_0(.50)$  value of the  $p$ MEWMA control chart with bivariate normal observations is slightly larger than the respective value of the Mahalanobis  $r$ MEWMA control chart. Thus, we can conclude that  $p$ MEWMA

**Table 4.2:** In-control ( $\delta = 0$ ) run length properties of Mahalanobis  $r$ MEWMA and  $p$ MEWMA control charts with bivariate normal,  $t(3)$  and  $G(1,1)$  distributions. Reference samples of size  $m = 200$  and  $m \approx \infty$  are used.

$\delta$		$p$ MEWMA			$r$ MEWMA		
		N	$t(3)$	$G(1,1)$	N	$t(3)$	$G(1,1)$
$m = 200$							
0.0	ARL	201.56	153.67	192.90	202.94	200.14	203.20
	$Q_1(.10)$	32	24	30	30	30	30
	$Q_1(.50)$	143	114	140	158	156	157
	$Q_1(.90)$	451	337	429	438	429	439
$m \approx \infty$							
0.0	ARL	199.10	194.95	196.60	201.93	199.17	200.54
	$Q_1(.10)$	34	28	30	27	27	25
	$Q_1(.50)$	145	137	136	140	140	140
	$Q_1(.90)$	445	440	441	467	452	465

control charts are more plagued by false alarms than Mahalanobis  $r$ MEWMA control charts for extremely heavy-tailed and highly skewed distributions when reference samples of size  $m = 200$  observations are used. For the asymptotic in-control performance, Table 4.2 shows that the two control charts have approximately the same performances.

#### Out-of-Control Case ( $\delta \neq 0$ )

Tables A.9 through A.17 in Appendix A show that the  $ARL_1$  values of  $p$ MEWMA control charts are shorter than the respective values of Mahalanobis  $r$ MEWMA control charts. The difference is large for small shifts in the mean vector of magnitude  $\delta \leq 1.0$ . However, interpretation based on the  $ARL_1$  values alone can be misleading. An investigation of the percentiles of the out-of-control run length distributions is needed.

First, we investigate the performance of the two control charts to detect shifts in the mean vector of magnitude  $\delta \geq 1.5$ . Table 4.3 shows that the  $Q_1(.10)$  and  $Q_1(.50)$  values of the  $r$ MEWMA and  $p$ MEWMA control charts are nearly equal. That is, the two control charts have nearly the same performance when  $m = 200$  and  $m \approx \infty$ .

Now, we compare the performances of Mahalanobis  $r$ MEWMA and  $p$ MEWMA control charts for detecting shifts in the mean vector of magnitude  $\delta \leq 1.0$ . The  $Q_1(.90)$  values in Table 4.4 show that the  $ARL_1$  values of Mahalanobis  $r$ MEWMA control charts are more affected by some long runs more than the  $ARL_1$  values of  $p$ MEWMA control charts. For example, using reference samples of size  $m = 200$  observations, the  $ARL_1$  value of the Mahalanobis  $r$ MEWMA control chart with  $G(1, 1)$  observations is equal to 93.73. It is larger than the  $ARL_1$  value of 11.89 of the  $p$ MEWMA control chart. The  $Q_1(.90)$  value of Mahalanobis  $r$ MEWMA control chart is equal to 346. It is much larger than the respective value of 18 of the  $p$ MEWMA control chart. That is, the  $ARL_1$  value of the Mahalanobis  $r$ MEWMA control chart is affected by some extremely long runs.

Table 4.4 shows that the  $Q_1(.10)$  and  $Q_1(.50)$  values of  $p$ MEWMA control charts are much shorter than the respective values of Mahalanobis  $r$ MEWMA control charts when bivariate normal observations are monitored than when bivariate  $t(3)$  and  $G(1, 1)$  observations are monitored. Indeed, it is expected that  $p$ MEWMA control charts perform much better than Mahalanobis  $r$ MEWMA control charts when the normality assumption is met. As mentioned, they are designed assuming the multivariate normality of the observations.

When  $\delta = 0.5$ , the  $Q_1(.50)$  values of Mahalanobis  $r$ MEWMA control charts with  $t(3)$  and  $G(1, 1)$  observations are nearly equal to the double of the respective values of  $p$ MEWMA control charts when  $m = 200$ . The difference decreases when  $m \approx \infty$ . When  $\delta = 1.0$ , the  $Q_1(.10)$  and  $Q_1(.50)$  values of Mahalanobis  $r$ MEWMA control charts with bivariate  $t(3)$  and  $G(1, 1)$  observations approach the respective values of  $p$ MEWMA control charts when  $m = 200$ . They are nearly the same when  $m \approx \infty$ .

**Table 4.3:** Out-of-control ( $\delta > 1.0$ ) run length properties of Mahalanobis  $r$ MEWMA and  $p$ MEWMA control charts with bivariate normal,  $t(3)$  and  $G(1,1)$  distributions. Reference samples of size  $m = 200$  and  $m \approx \infty$  are used.

$\delta$		$p$ MEWMA			$r$ MEWMA		
		N	$t(3)$	$G(1,1)$	N	$t(3)$	$G(1,1)$
$m = 200$							
1.5	ARL	7.51	7.16	7.42	12.55	7.62	21.59
	$Q_1(.10)$	5	5	5	6	5	5
	$Q_1(.50)$	7	7	7	10	7	8
	$Q_1(.90)$	10	10	10	21	10	19
2.0	ARL	5.57	5.29	5.48	7.51	5.81	6.54
	$Q_1(.10)$	4	4	4	5	5	5
	$Q_1(.50)$	5	5	5	7	6	6
	$Q_1(.90)$	7	7	7	11	7	8
2.5	ARL	4.44	4.26	4.42	5.73	5.17	5.33
	$Q_1(.10)$	3	3	3	4	5	5
	$Q_1(.50)$	4	4	4	5	5	5
	$Q_1(.90)$	6	5	6	8	6	6
3.0	ARL	3.78	3.61	3.74	4.90	4.93	5.03
	$Q_1(.10)$	3	3	3	4	4	5
	$Q_1(.50)$	4	3	4	5	5	5
	$Q_1(.90)$	5	5	5	6	5	5
$m \approx \infty$							
1.5	ARL	7.17	7.06	7.16	10.31	6.76	8.74
	$Q_1(.10)$	5	5	5	6	5	5
	$Q_1(.50)$	7	7	7	9	6	7
	$Q_1(.90)$	10	9	10	17	9	14
2.0	ARL	5.28	5.23	5.26	6.64	5.36	5.82
	$Q_1(.10)$	4	4	4	5	5	5
	$Q_1(.50)$	5	5	5	6	5	5
	$Q_1(.90)$	7	7	7	9	6	7
2.5	ARL	4.24	4.19	4.21	5.23	4.79	5.01
	$Q_1(.10)$	3	3	3	4	4	4
	$Q_1(.50)$	4	4	4	5	5	5
	$Q_1(.90)$	5	5	5	7	5	6
3.0	ARL	3.55	3.51	3.53	4.51	4.29	4.56
	$Q_1(.10)$	3	3	3	4	4	4
	$Q_1(.50)$	3	3	3	4	4	5
	$Q_1(.90)$	4	4	4	5	5	5

**Table 4.4:** Out-of-control ( $\delta \leq 1.0$ ) run length properties of Mahalanobis  $r$ MEWMA and  $p$ MEWMA control charts with bivariate normal,  $t(3)$  and  $G(1,1)$  distributions. Reference samples of size  $m = 200$  and  $m \approx \infty$  are used.

$\delta$		$p$ MEWMA			$r$ MEWMA		
		N	$t(3)$	$G(1,1)$	N	$t(3)$	$G(1,1)$
$m = 200$							
0.5	ARL	33.31	33.00	33.39	163.26	119.62	163.88
	$Q_1(.10)$	12	11	12	18	14	12
	$Q_1(.50)$	25	24	25	98	52	55
	$Q_1(.90)$	59	58	58	390	325	440
1.0	ARL	11.86	11.42	11.89	54.23	18.07	93.73
	$Q_1(.10)$	7	6	7	9	7	7
	$Q_1(.50)$	11	10	11	23	12	15
	$Q_1(.90)$	18	17	18	115	26	346
$m \approx \infty$							
0.5	ARL	26.78	28.25	26.87	82.82	44.98	280.41
	$Q_1(.10)$	12	12	12	16	13	10
	$Q_1(.50)$	23	25	23	58	34	36
	$Q_1(.90)$	47	48	47	182	91	782
1.0	ARL	11.19	11.31	11.28	22.41	11.69	30.14
	$Q_1(.10)$	7	7	7	8	7	6
	$Q_1(.50)$	11	11	11	18	11	12
	$Q_1(.90)$	17	16	17	42	18	69

### Results Summary

The results show that Mahalanobis  $r$ MEWMA control charts are less powerful than  $p$ MEWMA control charts to react to shifts in the mean vector of magnitude  $\delta \leq 1.0$ . This is no surprise because Mahalanobis  $r$ MEWMA control charts only use the rank information of the data depth measures of the observations. Thus, it can wander to the direction of an out-of-control of no more than  $1/m - 1$  per sample. On the other hand, the parametric design of  $p$ MEWMA control charts imply that they use the information of the observations. They can wander to the direction of an out-of-control by any value per sample.

### 4.3.2 Performance of Mahalanobis and Simplicial $r$ MEWMA Control Charts

First, the effect of widening the control limits on the  $ARL_1$  performance of  $r$ MEWMA control charts is discussed. Tables A.9 through A.17 in Appendix A show that the different  $r$ MEWMA control charts achieve desired  $ARL_0$  performance for all considered distributions. However, their sensitivity to react to process changes is reduced compared to charts with asymptotic control limits. The  $ARL_1$  values and percentiles of the out-of-control run length distributions are inflated when control limits are widened. Note that this is inevitable. The probability of crossing the control limit  $h$  becomes larger when  $h$  is widened.

The  $Q_1(.90)$  values in Tables A.9 through A.17 in Appendix A show that the  $ARL_1$  values of simplicial  $r$ MEWMA control charts are more affected by long runs than the  $ARL_1$  values of Mahalanobis  $r$ MEWMA control charts. Furthermore, the  $Q_1(.10)$  and  $Q_1(.50)$  values show that simplicial  $r$ MEWMA control charts are more powerful to quickly detect shifts in the mean vector when bivariate  $G(1, 1)$  observations are monitored.

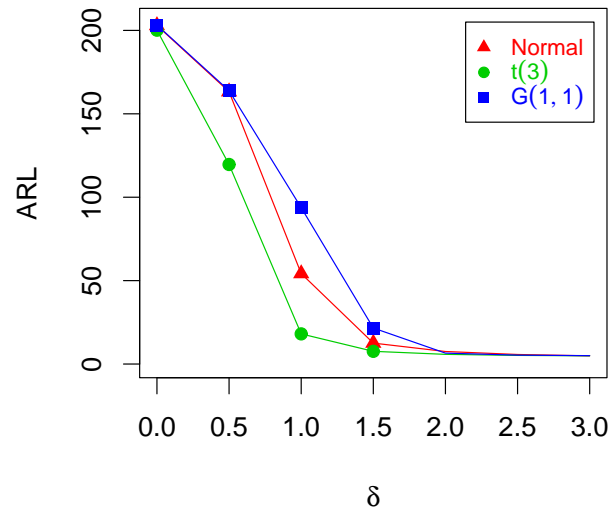
Finally, Mahalanobis and simplicial  $r$ MEWMA control charts are more sensitive to react to shifts in the mean vector when the distribution is heavy-tailed,  $t(3)$ , than normal. However, they are less powerful to highly skewed,  $G(1, 1)$ , distribution. For example, Figure 4.1 shows the  $ARL$  values of Mahalanobis and simplicial  $r$ MEWMA control charts with bivariate normal,  $t(3)$  and  $G(1, 1)$  observations. The smoothing parameter  $\lambda$  and the reference sample size  $m$  are equal to 0.05 and 200, respectively.

## 4.4 Discussion and Conclusion

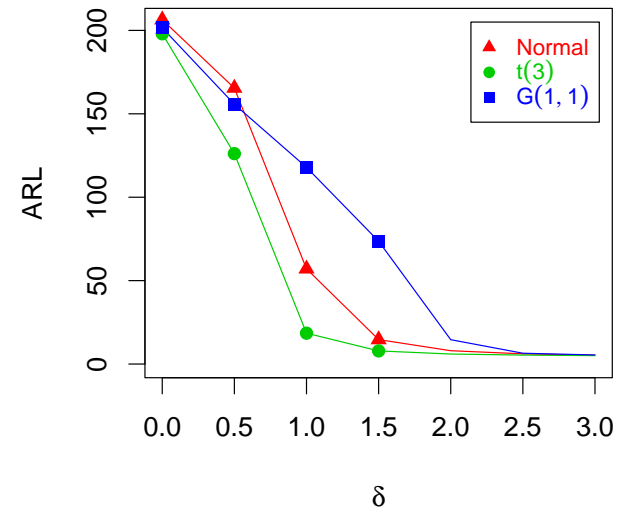
In this chapter, we compared the in-control and out-of-control performances of  $r$ MEWMA and  $p$ MEWMA control charts. The results show that  $p$ MEWMA control charts are more effective to detect sustained shifts of small magnitude in the mean vector. However, only the sustained shift scenario in the mean vector is considered to represent the out-of-control process. It is known that  $p$ MEWMA control charts are designed to have excellent



performance in detecting sustained shifts in the mean vector. Furthermore, Stoumbos and Sullivan (2002) mentioned that designing  $p$ MEWMA control charts to be insensitive to deviations from normality in the higher moments, including kurtosis, has the side effect of decreased sensitivity to isolated outlying process observations. In this case,  $r$ MEWMA control charts might be used. We are currently investigating this issue. Moreover, we are investigating the performance of  $r$ MEWMA control charts to monitor process variability.



(a) Mahalanobis  $r$ MEWMA Control Charts



(b) simplicial  $r$ MEWMA Control Charts

**Figure 4.1:** The ARL of (a) Mahalanobis and (b) simplicial  $r$ MEWMA control charts with adjusted control limits for mean shifts of size  $\delta$

## **Part II**

# **Monitoring the BTA Deep-Hole Drilling Process**

This page intentionally left blank

## The BTA Deep-Hole Drilling Process

In this chapter, the BTA deep-hole drilling process is introduced. In section 5.1, the drilling machine, drilling tool and principles of the process are reviewed. Then, the dynamic process disturbances are described in section 5.2. Finally, a previous experimental investigation conducted in order to study the dynamics of the process and its main results are reviewed in section 5.3.

### 5.1 The Drilling Process

Deep hole drilling methods are used for producing holes with a high length-to-diameter ratio, good surface finish and straightness. For drilling holes with a diameter of 20 mm and above, the BTA deep-hole machining principle is usually employed. Deep-hole drilling means that  $l/D \geq 3$ , where  $l$  and  $D$  are the length and the diameter of the hole to be machined, respectively. The special construction of this tool leads to long holes with very smooth walls and a high degree of straightness. As mentioned, the BTA deep-hole drilling process is usually the final step in the production of expensive workpieces.

#### 5.1.1 The Drilling Machine

In this section, we briefly review the BTA deep-hole drilling machine. For more details, see Weinert *et al.* (2002). The machine tool has six main components: two drive units for the rotary motion of the workpiece and the rotary and translation motion of the tool, the machine bed, the oil supply device containing the starting bush, the damper, and the tool-boring bar assembly. Figure 5.1 shows the BTA deep-hole drilling machine. Drilling can be performed in three different ways:

1. Turning tool and standing workpiece

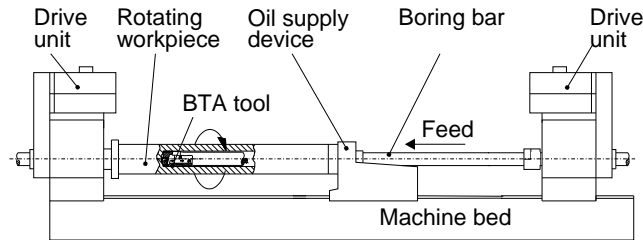


**Figure 5.1:** BTA deep-hole drilling machine

2. Standing tool and turning workpiece
3. Turning tool and workpiece in opposite directions

The following parameters can be influenced on the machine:

- The axial feed ( $f$ ) in mm/rev
- The cutting velocity or cutting speed ( $v_c$ ) in m/min
- The flow rate of the oil ( $\dot{V}$ ) in l/min
- The position of the damper
- The operating-pressure of the damper

The *cutting velocity* is automatically controlled and therefore not exactly on target in the process. This is taken into account by measuring the true number of revolutions per second which then allows the effect of the variation in this parameter to be inferred. The *axial feed* influences the speed of the boring substantially, since it determines the thickness of the chips which are removed by the cutting edge. The *flow rate of the oil* determines the speed of transportation of the chips from the cutting edge and the cooling and lubrication of the process. It also influences the damping properties of the whole assembly. The *damper* serves to prevent dynamic disturbances, see section 5.2. It can be positioned along the boring bar. Its position can be fixed on the machine bed or relative to the drive unit of the tool. The pressure with which the damper is clamped to the boring bar, is determined by the machine operator. If a disturbance is detected, the operator can vary the position and the pressure until it disappears.

### 5.1.2 The Drilling Tool and Principle of the Process

In this section, the BTA tool and principle of the drilling process are discussed. The BTA tool has only one cutting edge and two or three guiding pads, see Figures 5.2 and 5.3.

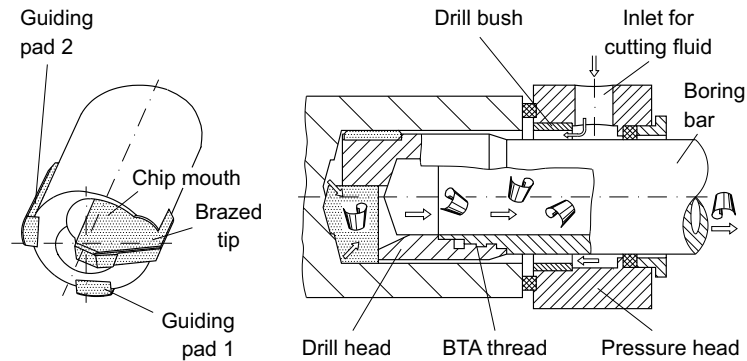


**Figure 5.2:** Working principle of the BTA deep-hole drilling

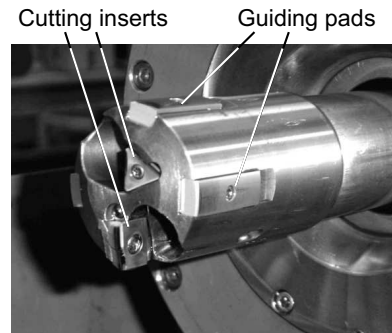


**Figure 5.3:** Boring tool as used in the experiments

In contrast to conventional twist drills, the tool has an asymmetric cutting edge. This induces a nonzero radial component of the cutting force, which leads to forces pushing outwards against the walls of the hole. Therefore the tool has to be guided at the start of the process until its self guiding action becomes effective. For this purpose, the BTA deep-hole drilling machine is equipped with a stationary starting bush integrated in the oil supply device, see Figure 5.2. The necessary guiding action during the starting phase of the process is achieved through the radial forces pushing the guide pads of the boring head onto the internal cylindrical surface of the starting bush. With increasing drilling depth, the boring head together with its guide pads enters the bore hole and the function of the starting bush is taken over by the bore hole wall.

The lubrication oil or cutting fluid flows through the outside of the tool to the cutting edge. Therefore, the chips are pushed out of the workpiece via the chip mouth and through the boring bar, see Figure 5.2. Thus, the chips cannot contact and damage the bore hole wall surface. Hence, a high quality of the holes can be achieved.

## 5.2 Process Disturbances

The machining of bore holes with high length-to-diameter ratio implies the use of slender tool-boring assemblies featuring low static and dynamic stiffness properties. This in turn leads to the process being susceptible to dynamic disturbances usually classified as either chatter vibration or spiralling. This limits the productivity and accuracy of the drilling process and therefore the good surface roughness and roundness of the produced holes. In mechanical engineering, the quality of a hole might be measured by roughness and roundness. The roughness measurements describe the deviation of the surface from the ideal totally smooth surface. Note that the surface roughness produced by a turning operation depends on the cutting tool geometry and tool path traversed throughout the workpiece. Roundness measures the deviation of the machined hole from an optimal circle. For more details, see Theis (2004).

For the drilling process, chatter is a form of unwanted and excessive self excited vibration between the tool and the workpiece. It leads to a poor surface finish of the workpiece. Usually, its effect is restricted to radial chatter marks at the bottom of the bore hole. In extreme cases it damages the boring wall by causing marks, called chatter marks, on the cylindrical surface of the bore hole, see Figure 5.4. The effect of chatter on

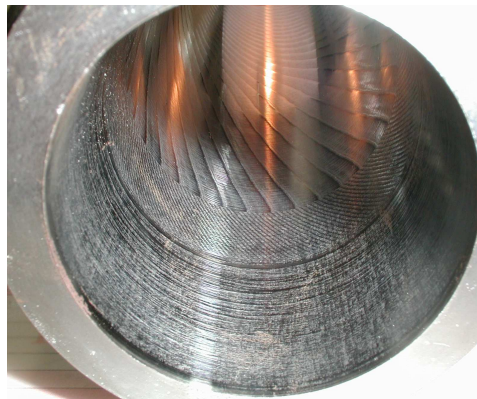


**Figure 5.4:** Radial chatter marks

the BTA tool are more severe. It leads to excessive wear of the cutting edges and guiding pads of the tool. This has a deteriorating effect on the machine tool life and therefore the reliability and safety of the machining operation.

Spiralling is a periodic movement of the tool around the center of the boring bar. It damages the workpiece severely. It leads to a multi lobe-shaped deviation of the cross section of the hole from absolute roundness which constitutes a significant impairment of the workpiece. Figure 5.5 shows the effect of spiralling on the workpiece.



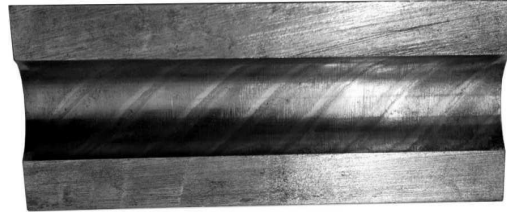


**Figure 5.5:** Effect of spiralling on the bore hole wall

### 5.3 Experimental Investigation

In order to study the dynamics of the process, several drilling experiments are conducted according to a given experimental design. The experiments were carried out on a CNC BTA deep hole drilling machine type Giana GGB 560, see Figure 5.6, with a bed length of 10.4 m, a maximum spindle speed of  $1600 \text{ min}^{-1}$ , a maximum feed rate of  $5700 \text{ mm/min}$  and a maximum spindle power of 125 kW. A commercially available multi-edge BTA solid boring tool has been employed. It is equipped with three guiding pads and two cutting inserts and has a nominal external diameter of 60 mm, see Figure 5.7. The workpiece material was C60 with an external diameter of 83 mm and a length of 500 mm. The experiments were carried out with a stationary tool and rotating workpiece. This was chosen because an appropriate measuring device to transmit the signals of drilling torque and feed force from the rotating boring bar was not available. The experimental setup is illustrated in Figure 5.8. The process parameters were varied within the following ranges according to a central composite experimental design comprising of 21 experiments, see Theis (2004):

- Cutting speed  $v_c$ : 60 - 120 m/min,
- Feed  $f$ : 0.12 - 0.25 mm,
- Oil flow rate  $\dot{V}$ : 200 -400 L/min.

The damper was not considered in order to allow the system to evolve to chatter and spiralling. Note that there are some uncontrollable influences such as the temperature of the boring bar oil and more importantly the wear of the cutting edges and the guiding pads. During these experiments several on-line measurements were sampled. Chatter is easily recognized in the on-line measurements by a fast increase of the dynamic part of the torque, force and acceleration signals. However, the drilling torque measurements yield the earliest and most reliable information about the transition from stable operation to chatter. They are recorded using strain gauges applied to the boring bar close to its clamped end. For a complete discussion about the experimental setup, see Weinert *et al.* (2002).



**Figure 5.6:** Deep-hole drilling machine Giana GGB 560



**Figure 5.7:** BTA deep-hole drilling tool as used for the experimental investigation

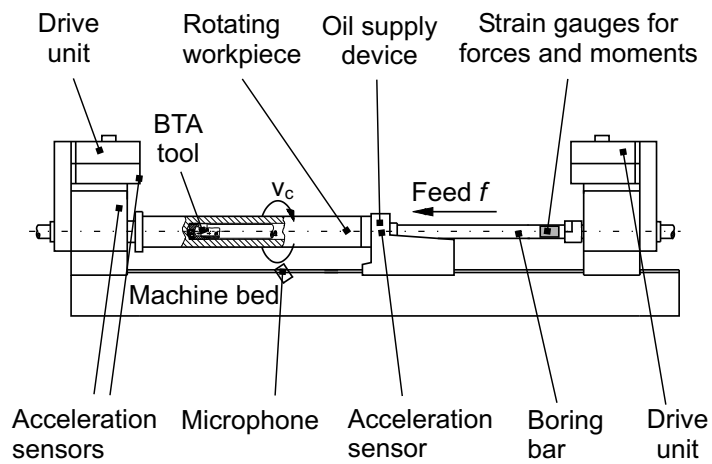


**Figure 5.8:** Experimental setup

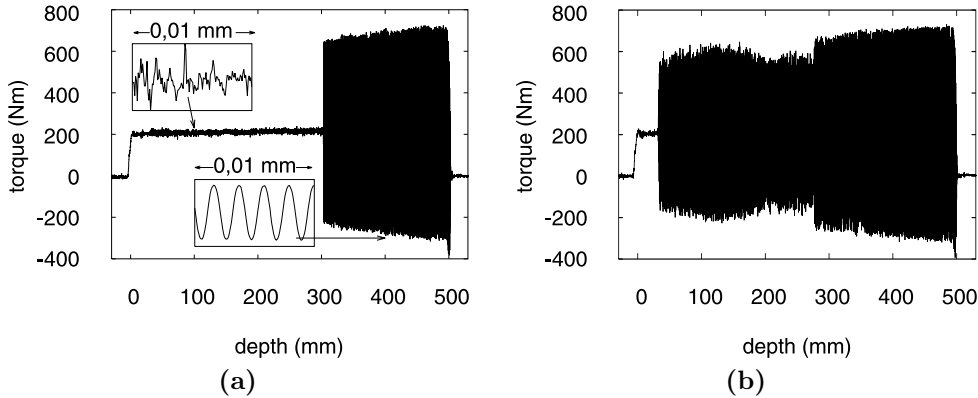


**Figure 5.9:** Two time series of the drilling torque from experiments with the same parameters

In these experiments, it was observed that experiments with identical machine parameters can exhibit qualitatively different behavior. For example, Figure 5.9 shows the evolution of the torque in two experiments with the same machine parameters, feed  $f = 0.185$  mm/rev, cutting speed  $v_c = 90$  m/min and oil flow rate  $\dot{V} = 300$  l/min. The two time series are recorded with a sampling rate of  $S = 20000$  Hz. The whole drilling process takes almost six minutes. In the first experiment, only one kind of chatter vibration is observed, see Figure 5.9a. First, the drilling process is stable and the distribution of the measured data is almost Gaussian with a very low amount of additional structure. Approximately after depth 300 mm, a rapid but smooth increase of the torque is observed. The observed time series is very smooth and periodic. This means that chatter vibration is present. In the second experiment, chatter starts right after leaving the bushing, approximately depth 32 mm, see Figure 5.9b. The amplitude of the torque rapidly increased approximately after depth 280 mm, which means that a change of the structure of chatter vibration have occurred. In both experiments, the BTA tool leaves the workpiece and the torque decreases to the starting value of 0 Nm after depth 500 mm.

The spectrograms of the drilling torque showed clearly that single frequencies dominate the process when chatter vibration is observed. These frequencies are mostly related to the eigenfrequencies of the boring bar. Figure 5.10 shows the spectrogram of an exemplary process showing varying dynamic states. The cutting parameters are feed  $f = 0.185$  mm/rev, cutting speed  $v_c = 90$  m/min and oil flow rate  $\dot{V} = 300$  l/min. In this case, the spectrogram is a pictorial representation of the frequency content of the drilling torque over depth (mm). Usually, this representation is useful for signals whose frequency characteristics change over time (non-stationary). In Figure 5.10, frequencies are plotted on the vertical axis. The intensity of each frequency is represented with a scale of colors.

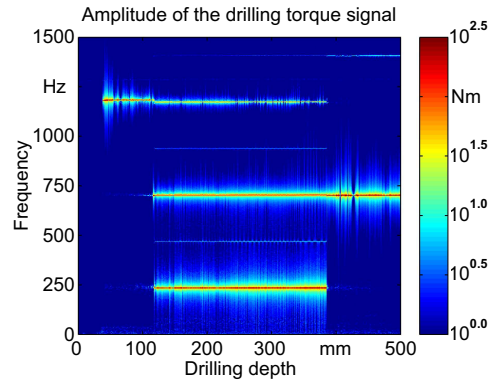


**Figure 5.10:** Spectrogram calculated from drilling torque data

Note that this spectrogram is constructed by breaking the drilling torque into small segments in time, then finding the fast fourier transform (FFT) of each segment. This yields the frequency content. Figure 5.10 shows that the process exhibits an initial non-chatter phase followed by three phases during which the process is in different states of chatter. These states can be distinguished by the different dominating frequencies of approximately 234 Hz, 703 Hz, and 1183 Hz, respectively. Theis (2004) studied the features of the development of amplitudes of the drilling torque over time. He determined all the relevant frequencies of the process and showed that the most prominent frequency bands are near 234 Hz, 703 Hz, and 1183 Hz. In fact, the chatter states can be distinguished by these different dominating frequencies in all experiments.

### 5.3.1 A Drilling Depth Dependency of Chatter Frequency

Figure 5.11 shows a plot of the different process phases over the drilling depth for the 21 experiments. A horizontal line in the graph represents one drilling experiment. For each experiment, the corresponding process parameters and the experiment number in the experimental design are given. Colored line segments indicate chatter vibration with a dominating frequency according to the graph legend. Chatter vibration is observed in all experiments. Figure 5.11 shows that chatter vibration is observed at later stages of the process only in 6 experiments. In the others, chatter is observed straight after the guiding pads left the starting bush. The observed dynamic states always occurred in the following sequence: drilling without chatter vibration followed by chatter vibration at approximately 1183 Hz, 234 Hz, and 703 Hz, respectively. In the majority of the experiments only a subset of the overall observed states occurred. Weinert *et al.* (2002) noted that the transitions from stable drilling to chatter as well as from one chatter state to another one are not sudden but are result of a long-term process over minutes.

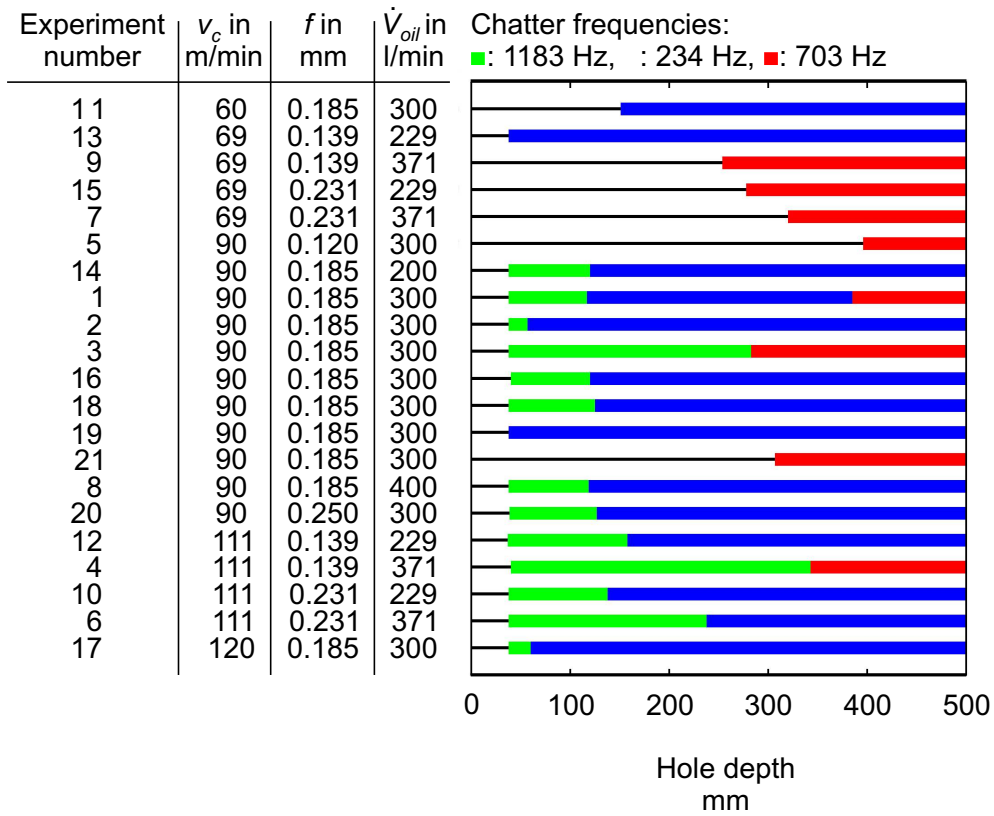


**Figure 5.11:** Occurrence of the non-chatter state and the three observed states of chatter as a function of the drilling depth and the process parameters  $v_c$ ,  $f$  and  $\dot{V}_{oil}$

However, chatter observed directly after the guiding pads left the starting bush occurs spontaneous. Figure 5.11 shows a drilling depth dependency of the chatter frequency. In fact,

- Chatter around 234 Hz is observed at different stages of the process. In 11 experiments, it is observed after the high-frequency (1183 Hz) chatter. In experiments #13 and #19, it is developed straight after the guiding pads left the starting bush. In experiment #11, it is observed at later stage of the process, namely after depth 150 mm.
- Chatter around frequency 703 Hz is developed only at later stages of the process. In all the 21 experiments, there is no transition from 703 Hz chatter to any other chatter state. In this sense, 703 Hz chatter seems to be the most stable.
- Chatter around 1183 Hz is only observed as initial process chatter vibration. In fact, right after leaving the starting bush the process is more likely to enter the 1183 Hz chatter state. Note that this kind of chatter is the less stable. Always, a transition to 234 Hz or 703 Hz chatter occurs.

### 5.3.2 Mechanical Interpretation

Weinert *et al.* (2002) proposed a mechanical interpretation that explains the temporal development of the process dynamics. The authors showed that the drilling depth dependency of chatter is caused by slowly varying boundary conditions. In fact, they identified the stiffness and damping effects through the contact between the stuffing box within the oil supply device and the boring bar as the main influencing factors, see Figure 5.12.

For the drilling process, the stuffing box is used to prevent the lubrication oil to go outside. A relative translatory motion between the boring bar and the stuffing box during the drilling process is necessary. Therefore, the point of contact between the stuffing box and boring bar changes during drilling. Moreover, the stuffing box exerts a constant friction on the boring bar and therefore a drilling depth damping effect on the torsional modes, 234 Hz, 703 Hz, and 1183 Hz. Note that in engineering applications a “distributed parameter system”, such as the boring bar, is modelled as a collection of distinct harmonic oscillators, each representing a vibrational mode of the entire apparatus. The frequency and effective damping ratio of each mode are computed in laboratory tests. Generally, only the lowest frequency modes are considered if the peaks in the power spectrum of the vibratory response are sufficiently separated.

Weinert *et al.* (2005) showed that in the beginning of the drilling process the damping of the third mode 1183 Hz due to the stuffing box is close to its minimum. Therefore, the amplitudes of frequency 1183 Hz increases. This explains that chatter vibration with 1183 Hz occurs as initial phase chatter. In accordance with the increased damping of the

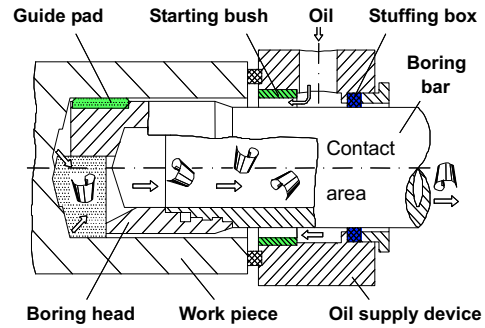


**Figure 5.12:** Cross sectional illustration of the BTA deep-hole drilling principle showing the location of the contact between stuffing box and boring bar

third mode transitions to the first mode 234 Hz occur further along the process. Towards the end of the drilling process, the damping effect of the stuffing box on the second 703 Hz reaches a minimum. This explains that chatter vibration associated with frequency 703 Hz was only observed towards the end of the process.



## Time Varying Process Dynamics

As mentioned in section 5.3, the experimental investigation shows that during the drilling process time varying dynamics can be observed while drilling with identical machine parameters. It consists of alternating chatter and non-chatter phases as well as sudden changes of frequency during chatter phases.

In this chapter, previous work to understand and to predict the temporal development of the process is reviewed. Based on it, we propose a modelling approach in order to setup the proposed *r*MEWMA monitoring procedure in Chapter 8. First, the van der Pol equation is introduced in section 6.1. Then, a purely phenomenological model based on the van der Pol equation that describes the transition from stable drilling to chatter vibration in one frequency is reviewed in section 6.2. Finally, time series analysis and modelling of the amplitude of the relevant frequencies of the process are proposed in section 6.3.

### 6.1 Introduction to Dynamical Systems Theory: The van der Pol Equation

The theory of dynamical systems is an area of mathematics used to describe the behavior of complex systems by employing differential and difference equations. Ozaki (1980) mentioned that nonlinear random vibrations are typically described by second-order differential equations of the form

$$\ddot{x}(t) + f(\dot{x}(t)) + g(x(t)) = \eta(t),$$

where  $f(\dot{x}(t))$  is called the damping force,  $g(x(t))$  is called the restoring force of the oscillation and  $\eta(t)$  is a random disturbance.

In this work, we will focus on the limit cycle behavior which is typical for processes of van der Pol equation type,

$$\ddot{x}(t) + \epsilon(a^2 - x(t)^2)\dot{x}(t) + \omega^2bx(t) = 0, \quad (6.1)$$

where  $\epsilon$  is a parameter that determines the degree of nonlinearity,  $a$  characterizes the degree of nonlinear saturation, and  $f_0 = \omega/2\pi$  is the frequency of the free running oscillator. This equation was described in connection with electrical circuit. It describes oscillations generated by a triode valve under excitation. In this equation, the restoring force is linear. However, the damping force is nonlinear and could vary between positive and negative values. The solution of this equation becomes periodic as  $t \rightarrow \infty$ . It is not constrained to be sinusoidal in character. The parameter  $\epsilon$  determines the properties of the periodic solution. When  $\epsilon > 0$ , the fixed point  $x = 0$  is an attractor of equation (6.1), i.e. the dynamic systems tends to approach this value with increasing time. When  $\epsilon < 0$ , the oscillations of the system are very stable for large  $\epsilon$ . As  $\epsilon$  decreases the stability of the system decreases as well. In this case, the van der Pol oscillator represents a physical system. For small oscillations, energy is fed into the system. Whereas for large oscillations, energy is taken from the system. For such systems, large oscillations are damped, due to the positive damping. While small oscillations are magnified due to the negative damping. This is known as limit cycle behavior and implies that the system has a “self-exciting” mechanism. That is, the process shows a stochastic behavior whose oscillations are sustained not by external disturbances but by their own nonlinear structure. In fact, assuming  $\epsilon > 0$

1. for  $x^2 < a^2$ , the system has negative damping force and it starts to oscillate and diverge
2. for  $x^2 > a^2$ , the system has positive damping force and it starts to damp out.

The interplay of these two opposite effects, negative damping for small  $x$  and positive damping for large  $x$  produces the steady oscillation of a certain amplitude, which is called a limit cycle. Tong (1990), page 27, stated

*“...Physically, limit cycles represent the (now dynamic) stationary state of sustained oscillations which does not depend on initial conditions but depends exclusively on the parameters of the system, that is they are intrinsic properties ...”*

The van der Pol equation may also be extended to the stochastic van der Pol equation given by

$$\ddot{x}(t) + \epsilon(a^2 - x(t)^2)\dot{x}(t) + \omega^2bx(t) = \eta(t),$$

where  $\eta(t)$  is an external random disturbance. That is, the system is perturbed by  $\eta(t)$  which produces a perturbed limit cycle process.

## 6.2 Modelling the Drilling Torque by a Stochastic Differential Equation

Weinert *et al.* (2002) used dynamical systems to model the process. At a first stage, they are not interested in an exact and global modelling of all microscopic details of the drilling process, but only in a local description of adequate accuracy to predict disturbances sufficiently early and to provide insights into how to react in order to prevent them. Therefore, they proposed a phenomenological approach with a special emphasis on the temporal neighborhoods of instabilities or state transitions from stable drilling to chatter vibration and back.

The authors proposed a phenomenological model based on the van der Pol equation (6.1) to describe the transition from stable drilling to chatter vibration in one frequency. In fact they noted that the different kinds of solutions of (6.1) qualitatively coincide with the experimentally observed states in the drilling process. They proposed to model the transition by Hopf bifurcation in the van der Pol equation. Therefore, the drilling torque is described by

$$\ddot{x}(t) + \epsilon(t)\left(b^2 - x(t)^2\right)\dot{x}(t) + w^2x(t) = W(t), \quad (6.2)$$

where  $x(t)$  is the drilling torque,  $b$  and  $w$  are constants,  $\epsilon(t)$  is a bifurcation parameter and  $W(t)$  is a white noise process. Here  $w$  describes the behavior of a prominent frequency component at 703 Hz, see section 5.3. Note that the authors included  $W(t)$  in order to model all the uncontrollable parameters of a drilling experiment, as well as the microscopic details of the drilling process. In this case, Hopf bifurcation occurs in the system when a stable fixed point becomes unstable to form a limit cycle, as  $\epsilon(t)$  varies from positive to negative values. That is, the periodic solution of equation (6.2) changes from a stable fixed point to limit cycles as the process changes from stable drilling to chatter. For further details and motivation of the choice of this phenomenological model, see Weinert *et al.* (2002).

Weinert *et al.* (2004) noted that the proposed model correctly accounts for a subset of experimental results, especially when chatter occurs later during the process. This is because in most of these experiments only the single frequency 703 Hz is dominant in producing chatter. Naturally, the model fails to capture all aspects of the process when this assumption becomes invalid, which is always the case for experiments which start to chatter during the initial phase. These show a more varied and complex behavior since there are always at least two, but in most cases three dominant frequencies that are involved in chatter. Phenomenologically, one observes alternations between distinct chatter states where different frequencies dominate singly or in combination with their harmonics. Furthermore, the frequencies affect each other either by excitatory or inhibitory interaction.

### 6.3 Modelling the Amplitudes of Relevant Frequencies

In section 5.3, it is noted that the single frequencies of approximately 234, 703, and 1183 Hz dominate the process when chatter vibration is observed. Furthermore, it is known that their amplitudes are not normally distributed, see Theis (2004). A natural idea is to monitor the amplitudes of these frequencies using the proposed nonparametric  $r$ MEWMA control charts, see Chapter 2, in order to detect the start of the transition from stable drilling to chatter vibration. However, it is necessary to check if the amplitudes of these frequencies are independent because  $r$ MEWMA control charts are developed to monitor independent observations.

#### 6.3.1 Time Series Analysis

In this section, time series analysis is used to check the independence assumption of the amplitudes of the relevant frequencies. Data sets from experiments where chatter vibration is observed at later stages in the process are used. These experiments are run numbers #5, #7, #9, #11, #15, and #21 of the experimental design, see Figure 5.11. For each data set, data collected before the occurrence of chatter vibration can be used to check the presence of autocorrelation in the amplitude of the relevant frequencies during stable drilling. Chatter vibration is developed and its effect is apparent on the bore hole wall after depths 340 mm, 250 mm, 150 mm, 270 mm, and 300 mm in experiments #7, #9, #11, #15, and #21 of the experimental design, respectively. Experiment #5 is the most stable experiment of the experimental design. In fact, chatter vibration is developed after depth 400 mm and slight chatter marks are observed on the bore hole wall at the end of the process.

The transition from stable drilling to chatter vibration is not sudden but a result of long term process over minutes. In each experiment, it is expected to start before the mentioned depths and during it the process may not be stable. Furthermore, the process is not stable when the guiding pads of the BTA tool leave the starting bush, see section 5.1.2, and the BTA tool enters the bore hole completely. These two physical changes occur approximately at depths 32 mm and 110 mm, respectively.

The independence assumption is checked using the Ljung-Box test in different time windows of length 200 observations. Note that in the following analysis, the amplitude of frequencies 234, 703, and 1183 Hz are considered in all experiments. The test statistics and p-values are reported in Tables C.1 to C.6 in Appendix C.

Table C.1 in Appendix C shows that the amplitudes of the three frequencies in experiment #5 are almost independent before the occurrence of chatter vibration i.e., depth  $\leq 400$  mm. This can be explained by the fact that experiment 5 is the most stable experiment in the experimental design. For the experiments #7, #9, #11, #15, and #21, the total number of time windows before the occurrence of chatter vibration is equal to

81. The null hypothesis of independence of the amplitudes of the three frequencies is rejected 47 times, see Tables C.2 to C.6 in Appendix C. In some time windows, the autocorrelation can be explained by the instabilities of the process caused by the mentioned physical changes (i.e., guiding pads of the BTA tool leave the starting bush, the BTA tool enters the bore hole completely and the start of the transition from stable drilling to chatter vibration). However, the autocorrelation seems to be an inherent part of the process in the others time windows. In this case, it cannot be ignored and need to be modelled.

The observations are moderately positively autocorrelated. This kind of autocorrelation should be distinguished from the autocorrelation in the amplitudes of the three frequencies during chatter vibration. After the occurrence of chatter vibration, the total number of time windows for the three frequencies is 75. The null hypothesis of independence of the amplitudes of the three frequencies is rejected 58 times. In this case, the amplitudes are highly positively autocorrelated. The presence of this high autocorrelation indicates the presence of some variability which should be removed rather than modelled. Furthermore, it can provide the basis for active process control as a tool for minimizing short term variability.

In conclusion, we assume that the amplitudes of the relevant frequencies might be autocorrelated during stable drilling. This autocorrelation is not explained by the mentioned physical changes of the process and seems to be an inherent part of the process. Therefore, it cannot be ignored and need to be modelled.

### 6.3.2 Autoregressive Approximation

In section 1.2, it is mentioned that residual control charts are adequate SPC procedures when the data are autocorrelated. In this case, a model of the autocorrelative structure of the data is needed. This can be achieved by fitting an appropriate time series model to the observations.

In this section, a time series modelling approach of the amplitudes of the relevant frequencies of the process is proposed in order to setup the monitoring procedure in Chapter 8. Theis (2004) described the development of the amplitudes of these frequencies using a logistic function. He showed that his approximation is directly connected to the phenomenological model given by equation (6.2). In fact, he considered  $x(t)$  as a harmonic process

$$x(t) = R(t)\cos(2\pi f + \phi),$$

where  $f \in [0, \pi/2]$  and  $\phi$  is the corresponding phase. He showed that

$$2\frac{dR(t)}{dt} + \epsilon(t)R(t) \left( b^2 - \frac{R(t)^2}{2} \right) = \frac{W(t)}{w}, \quad (6.3)$$

is the amplitude-equation for the differential equation in (6.2) if there is only one frequency present in the process. Assuming  $\Delta t$  is sufficiently small and by discretization of equation (6.3), the amplitudes of the relevant frequencies may be described by

$$R_t = \phi_{1,t}R_{t-1} + \phi_{2,t}R_{t-1}^3 + \varepsilon_t, \quad (6.4)$$

where  $\phi_{1,t} = (1 - b^2\epsilon(t)/2)$  and  $\phi_{2,t} = \epsilon(t)/4$  are time varying parameters and  $\varepsilon_t$  is normally distributed with mean 0 and variance  $\sigma_\varepsilon^2$ . As discussed in sections 6.1 and 6.2, the bifurcation parameter  $\epsilon(t)$  should be small when the process is stable and large when there is chatter. That is, the nonlinear term  $\phi_{2,t}R_{t-1}^3$  in equation (6.4) only becomes important when there is chatter. Therefore, we propose to approximate the amplitudes of the relevant frequencies by the linear autoregressive part AR(1) of equation (6.4)

$$R_t \approx \phi_{1,t}R_{t-1} + \varepsilon_t.$$

The empirical evidence of this approximation is studied in section 6.3.3 using real data.

To estimate the AR(1) model parameters, a moving window of length  $m$  is used. Moving window techniques are useful to estimate model parameters which are time varying assuming stationarity only locally. The window moves in each period covering  $m$  observations  $R_{t-m+1}, R_{t-m+2}, \dots, R_t$ . In each window, parameters  $\phi_1, \beta$  and  $\sigma_\varepsilon$  of the linear regression model

$$R_t = \beta_t + \phi_{1,t}R_{t-1} + \varepsilon_t. \quad (6.5)$$

are estimated and used to calculate the residuals, given by

$$e_t = R_t - \hat{\phi}_{1,t-k}R_{t-1} - \hat{\beta}_{t-k}, \quad (6.6)$$

where  $\hat{\phi}_{1,t-k}$  and  $\hat{\beta}_{t-k}$  are estimates of the regression parameters  $\phi_1$  and  $\beta$  at time  $t - k$ ,  $k \geq 1$ . Note that  $\beta$  is included because there is a general shift in the amplitudes after depth 32 mm due to a change in the physical conditions of the process, see section 5.1.2. The use of  $\hat{\phi}_{1,t-k}$  and  $\hat{\beta}_{t-k}$  in equation (6.6) is motivated by the fact that using the estimated parameters at time  $t$  to calculate the residuals may rather serve to mask changes than to detect them, see section 8.4. Note that in the following work, the residuals are calculated using  $k = 1$ . However, as  $k$  increases, the residuals will unavoidably be larger.

### 6.3.3 Empirical Results: Diagnostic Checks of the Residuals

In this section, the empirical evidence of time series modelling of the amplitudes of the relevant frequencies during stable drilling is studied using the amplitudes of the dominating frequencies obtained from experiments #5, #7, #9, #11, #15, and #21 of the experimental design. That is frequency 703 Hz in experiments #5, #7, #9, #15, and #21 and frequency 234 Hz in experiment #11, see Figure B.1 in Appendix B. At time  $t \geq 100$ , the 100 most recent amplitudes of each frequency are used to estimate

the parameters of the AR(1) model given by equation (6.5). The choice of  $m = 100$  is motivated in section 8.3.3. The first 100 residuals are calculated using equation

$$e_t = R_t - \hat{\phi}_{1,100}R_{t-1} - \hat{\beta}_{100},$$

where  $\hat{\phi}_{1,100}$  and  $\hat{\beta}_{100}$  are estimates of the regression parameters  $\phi_1$  and  $\beta$  at time 100.

In the previous section it is indicated that the amplitudes of the relevant frequencies given by equation (6.4) are approximated by an AR(1) model within each time window. That is, the nonlinear term  $\phi_{2,t}R_{t-1}^3$  in equation (6.4) is not important before chatter. This assumption is checked using the Teräsvirta *et al.* (1993) statistical test for nonlinear dependence. This test is used for nonlinear residual structure, after linear structure has been removed by fitting the AR(1) model. The idea behind this test is by fitting the linear AR(1) model to the data, the inherent nonlinear structure has been swept into the residuals. The same time windows of length 200 observations as in section 6.3.1 are used to test for neglected nonlinearity for the regression (6.5).

Tables C.7 to C.12 in Appendix C show the calculated test statistics and p-values for the residuals of the dominating frequency in each experiment.

Before the occurrence of chatter vibration, the total number of time windows of the residuals of the considered frequencies is equal to 37. Tables C.7 to C.12 in Appendix C show that the null hypothesis of linearity is rejected 11 times. 4 rejections can be explained by the change in the dynamics of the process when the guiding pads of the BTA tool leave the starting bush, see Tables C.9, C.10, C.11, and C.12. 5 rejections occur before the occurrence of chatter vibration, see Tables C.7, C.9, C.10, C.11, and C.12. They are explained by the start of the transition from stable drilling to chatter vibration.

Moreover, the independence and normality assumptions are checked. In fact, if the AR(1) model fits the data well, the residuals will be “approximately” independent. As mentioned, this is a basic assumption for the application of the proposed  $r$ MEWMA control charts. The normality assumption is important only for control charts that are designed based on the normal distribution. Indeed, the statistical properties of these charts are exact only if this assumption is satisfied, see section 1.2.

The Ljung-Box and Shapiro-Wilks tests are used to test the independence and normality assumptions of the residuals, respectively. The same time windows of length 200 observations used for the Teräsvirta-Lin-Granger nonlinearity test are considered. The results are reported in tables C.7 to C.12 in Appendix C for the residuals of the dominating frequencies in each experiment. The results show that the null hypothesis of independence of the residuals is rejected only 6 times before the occurrence of chatter vibration. As mentioned, the total number of time windows is 36. 5 rejections can be explained by the change in the dynamics of the process when the guiding pads leave the starting bush, see Tables C.8, C.9, C.11, and C.12 in Appendix C. The hypothesis of normality is rejected in all time windows.

In conclusion, during stable drilling the amplitudes of the relevant frequencies of the process can be approximated by the AR(1) model given by equation (6.5). The residuals are independent. However, they are not normally distributed.

## 6.4 Conclusion

In this chapter, previous work and results of the project are reviewed. The phenomenological model used to describe the transition from stable drilling to chatter vibration is reviewed. Time series analysis of the amplitudes of the relevant frequencies showed that they might be autocorrelated during stable drilling. Therefore, we proposed a time series model in order to remove this autocorrelation. Its empirical evidence is studied. This model is used in chapter 8 in order to setup the monitoring strategy.



# Nonlinear Time Series Modelling of the the Drilling Process

**A**mplitude-dependent exponential autoregressive time series models are introduced by Ozaki and Oda (1978) and Ozaki (1980) in an attempt to reproduce certain features of nonlinear random vibration theory. They are able to reveal certain types of nonlinear dynamics such as fixed points and limit cycles.

In this chapter, these models are used to model the drilling process in order to characterize its time varying dynamics. Furthermore, this modelling approach provides an on-line monitoring strategy using control charts. In section 7.2, the properties of the nonlinear exponential autoregressive time series models are reviewed. The estimation of their parameters is discussed in section 7.3. These models are used to model the drilling torque in section 7.4. Finally, exponential autoregressive time series models based control charts are proposed in section 7.5.

## 7.1 Basic Definitions

In this section, we give an explicit definition of fixed or singular points and limit cycles of a general discrete time difference equation,

$$x_t = f(x_{t-1}, \dots, x_{t-p}). \quad (7.1)$$

These definitions are given by Ozaki (1985).

### Definition 7.1.1 Fixed or singular point

*A fixed point of equation (7.1) is a point  $\xi$ , for which every trajectory of equation (7.1) beginning sufficiently near  $\xi$  approaches it either for  $t \rightarrow \infty$  or  $t \rightarrow -\infty$ . If it approaches*

$\xi$  for  $t \rightarrow \infty$  we call  $\xi$  a stable fixed point, and if it approaches  $\xi$  for  $t \rightarrow -\infty$  we call  $\xi$  an unstable fixed point.

### Definition 7.1.2 Limit cycle

A limit cycle of equation (7.1) is an “isolated” and “closed” trajectory  $x_{t+1}, x_{t+2}, \dots, x_{t+q}$ , where  $q$  is a positive integer.

“Closed” means that if the initial values  $(x_1, \dots, x_p)$  belong to the limit cycle, then  $(x_{1+kq}, \dots, x_{p+kq}) = (x_1, \dots, x_p)$  for any integer  $k$ . “Isolated” means that every trajectory beginning sufficiently near the limit cycle approaches it either for  $t \rightarrow \infty$  or  $t \rightarrow -\infty$ . If it approaches the limit cycle for  $t \rightarrow \infty$  we call it a *stable limit cycle*, and if it approaches the limit cycle for  $t \rightarrow -\infty$  we call  $\xi$  an *unstable limit cycle*. The smallest integer  $q$  which satisfies definition 7.1.2 is called the period of the limit cycle of equation (7.1). Ozaki (1985) noted that the fixed point can be considered to be a limit cycle of period 1 but he distinguishes it because it has a significantly different physical meaning.

## 7.2 Amplitude-dependent Exponential Autoregressive Time Series Models

Amplitude-dependent exponential autoregressive (ExpAr) time series models have simple structure similar to the autoregressive (AR) time series models except for the state-dependent coefficients. An ExpAr time series model is given by

$$x_t = \left( \phi_1 + \pi_1 e^{-\gamma x_{t-1}^2} \right) x_{t-1} + \dots + \left( \phi_p + \pi_p e^{-\gamma x_{t-1}^2} \right) x_{t-p} + e_t, \quad (7.2)$$

where  $\{e_t\}$  is a sequence of i.i.d. random variables, usually with zero mean and finite variance.  $\gamma, \phi_i, \pi_i, i = 1, \dots, p$ , are constants,  $p$  is the model order. The nonlinearity of the process comes from the exponential form. This function renders the dynamics of the series locally linear but globally nonlinear. The autoregressive coefficients of the model are amplitude dependent. They depend on  $x_{t-1}$ . They change from  $\phi_i + \pi_i$  to  $\phi_i$  as  $|x_{t-1}|$  changes from zero to  $+\infty$ . That is, whenever  $|x_{t-1}|$  becomes large, the coefficients  $(\phi_i + \pi_i e^{-\gamma x_{t-1}^2}) \rightarrow \phi_i$  for  $i = 1, 2, \dots, p$ . Whenever  $|x_{t-1}|$  becomes small, the coefficients  $(\phi_i + \pi_i e^{-\gamma x_{t-1}^2}) \rightarrow \phi_i + \pi_i$  for  $i = 1, 2, \dots, p$ . The nonlinear coefficient  $\gamma$  acts as a scaling factor. It modifies the effect of  $x_{t-1}$  in the term  $e^{-\gamma x_{t-1}^2}$ .

Haggan and Ozaki (1981) showed that the ExpAr time series model exhibits a limit cycle behavior under the following conditions

- i) All the roots of the characteristic equation

$$\lambda^p - \phi_1 \lambda^{p-1} - \phi_2 \lambda^{p-2} - \dots - \phi_p = 0.$$

lie inside the unit circle. Therefore  $x_t$  starts to damp out when  $|x_{t-1}|$  becomes too large.

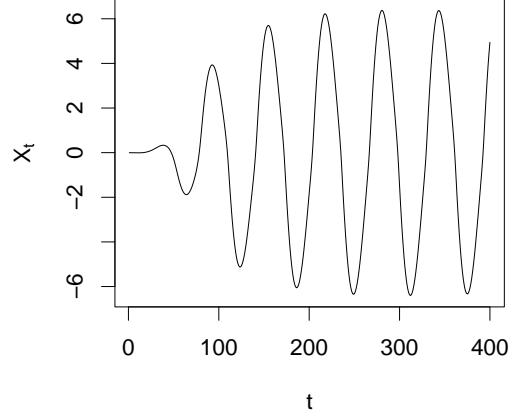


**Figure 7.1:** Limit cycle obtained for the model  $x_t = (1.95 + 0.23e^{-x_{t-1}^2})x_{t-1} - (0.96 + 0.24e^{-x_{t-1}^2})x_{t-2} + e_t$

ii) Some roots of the characteristic equation

$$\lambda^p - (\phi_1 + \pi_1)\lambda^{p-1} - (\phi_2 + \pi_2)\lambda^{p-2} - \dots - (\phi_p + \pi_p) = 0.$$

lie outside the unit circle. Therefore  $x_t$  starts to oscillate and diverge for small  $|x_{t-1}|$ .

The results of these two effects are expected to produce a similar sort of self excited oscillation as the van der Pol equation, see section 6.1. Figure 7.1 shows the limit cycles obtained for the model

$$x_t = (1.95 + 0.23e^{-x_{t-1}^2})x_{t-1} - (0.96 + 0.24e^{-x_{t-1}^2})x_{t-2} + e_t.$$

where the coefficients satisfy the above conditions (i) and (ii).

The above two conditions are necessary for the existence of a limit cycle but not sufficient. A sufficient condition is

iii)

$$\left(1 - \sum_{i=1}^p \phi_i\right) / \sum_{i=1}^p \pi_i > 1 \text{ or } \left(1 - \sum_{i=1}^p \phi_i\right) / \sum_{i=1}^p \pi_i < 0.$$

The condition (iii) guarantees that a fixed point does not exist for the ExpAr time series model. For example, the model

$$x_t = (1.80 + 4.00e^{-x_{t-1}^2})x_{t-1} - (0.97 + 0.10e^{-x_{t-1}^2})x_{t-2}.$$

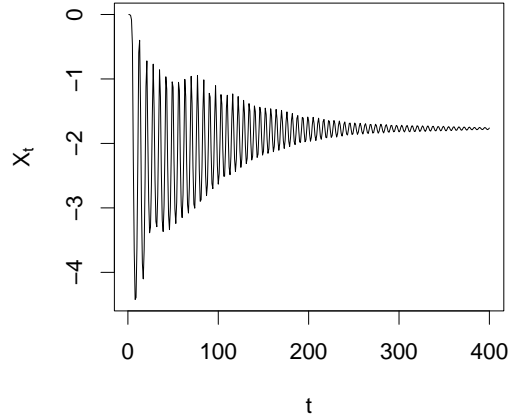


**Figure 7.2:** Singular point obtained for the model  $x_t = (1.80 + 4.00e^{-x_{t-1}^2})x_{t-1} - (0.97 + 0.10e^{-x_{t-1}^2})x_{t-2}$

satisfies conditions (i) and (ii) but the trajectory of  $x_t$  converges to a singular or fixed point  $\xi$ , see Figure 7.2. It holds that

$$\xi = \left(1.8 + 4e^{-\xi^2}\right) \xi - \left(0.97 + 0.1e^{-\xi^2}\right) \xi.$$

In this case, the singular point exists because the coefficients does not satisfy condition (iii). That is

$$0 < \left(1 - \sum_{i=1}^2 \phi_i\right) / \sum_{i=1}^2 \pi_i < 1.$$

Some ExpAr time series models without satisfying condition (iii) still have a limit cycle. Ozaki (1982) noted that this is because the fixed points themselves of the model are unstable. The following condition is used to check whether the fixed points are stable or not whenever the condition (iii) is unsatisfied.

- iv) The fixed point of an ExpAr time series model, if it exists, is stable if and only if the roots of the equation

$$\lambda^p - \beta_1 \lambda^{p-1} - \beta_2 \lambda^{p-2} - \dots - \beta_p = 0,$$

lie inside the unit circle, where the  $\beta_i$ 's are given by

$$\beta_1 = \frac{\pi_1 + \phi_1 \sum_{j=1}^p \pi_j - \pi_1 \sum_{j=1}^p \phi_j}{\sum_{j=1}^p \pi_j} + 2 \left( 1 - \sum_{j=1}^p \phi_j \right) \log \left( \frac{1 - \sum_{j=1}^p \phi_j}{\sum_{j=1}^p \pi_j} \right),$$

$$\beta_i = \frac{\pi_i + \phi_i \sum_{j=1}^p \pi_j - \pi_i \sum_{j=1}^p \phi_j}{\sum_{j=1}^p \pi_j}, (i = 2, 3, \dots, p).$$

## 7.3 Estimation of the ExpAr Models

### 7.3.1 Maximum Likelihood Estimate

The maximum likelihood estimate  $\hat{\gamma}$  is obtained by minimizing the variance of the prediction errors

$$J(\theta) = \sigma_e^2 = \frac{1}{N-p} \sum_{j=p+1}^N \left( x_t - \sum_{i=1}^p (\phi_j + \pi_j e^{-\gamma x_{t-i}^2}) x_{t-i} \right)^2,$$

where  $\theta = (\phi_1, \dots, \phi_p, \pi_1, \dots, \pi_p, \gamma)$ , see Shi *et al.* (2001), and  $N$  is the total number of observations. Such estimation is a commonly time consuming nonlinear optimization procedure. Moreover, it can be proved that  $J(\theta)$  for the nonlinear coefficient  $\gamma$  is not convex and multiple local optima may exist. Therefore, there is no guarantee that a derivative-based method will converge to the global optimum.

To overcome this problem, Haggan and Ozaki (1981), Shi and Aoyama (1997) and Baragona *et al.* (2002) proposed alternative estimation procedures. Haggan and Ozaki (1981) proposed an approximate straightforward estimation method. First, a pre-specified interval for the  $\gamma$  value is fixed. This interval is divided in sub-intervals, so that a grid of candidate  $\gamma$  values is built. Then, the parameters  $\{\phi_i, \pi_i\}$ ,  $i = 1, 2, \dots, p$ , are estimated by linear least squares problem on centered series. The order  $p$  of the fitted model is selected by use of the Akaike information criterion (AIC), given by

$$AIC(p) = (N-p) \log \hat{\sigma}_e^2 + 2(2p+1),$$

where  $p$  is the order of the model to be considered and  $\hat{\sigma}_e^2$  is the least squares estimate of the residual variance of the model.

Shi and Aoyama (1997) and Baragona *et al.* (2002) used a genetic algorithm to estimate the parameters of the model. The genetic algorithm is a class of global optimization procedures distinguished from other optimization techniques by using concepts from population genetics to guide the search. Its basic principles are crossover, mutation

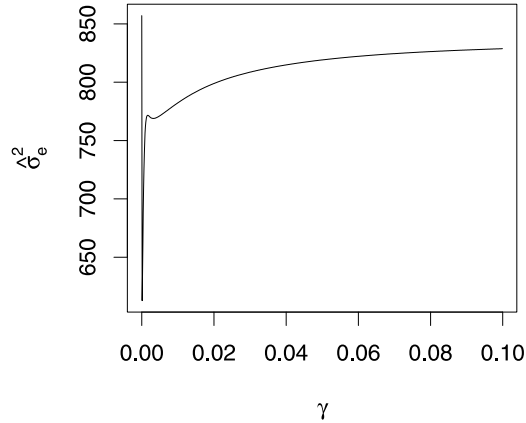


**Figure 7.3:** Illustration of the “golf-hole-like” problem

and selection. However, for large values of  $\{x_t\}$ , the objective function  $J(\theta)$  may have a “golf-hole-like” problem. Genetic algorithms are not applicable to this kind of hard problems. For example, the fluctuations in a far-infrared laser data, see example 4 of Shi and Aoyama (1997), are considered with a time lag  $p = 3$ . Figure 7.3 shows that the deep minimum of  $J(\theta)$  being of “golf-hole-like” character. The genetic algorithm used by the authors failed to find this global optima.

### 7.3.2 Real-time Estimate

The estimation procedures proposed by Haggan and Ozaki (1981), Shi and Aoyama (1997) and Baragona *et al.* (2002) involve computation difficulties and are not suitable for use in manufacturing systems (real-time), where CPU-time and memory are important. The important task of a real-time estimation procedure is the fast determination of the nonlinear coefficient  $\gamma$ . The estimation of the other coefficients  $\{\phi_i, \pi_i\}$ ,  $i = 1, 2, \dots, p$ , in the model is only a linear least squares problem whenever  $\gamma$  is determined. Shi *et al.* (1998) noted that in terms of the mechanism of the ExpAr time series model to reveal the limit cycle or cyclical behavior, the scaling parameter  $\gamma$  takes the role of adjusting the instantaneous roots of the model. Whenever the state  $x_{t-1}$  becomes far away from the equilibrium point,  $\{\phi_i + \pi_i e^{-\gamma x_{t-1}^2}\}$  terms in the ExpAr time series model should approach  $\phi_i$ . That is, the nonlinear term  $e^{-\gamma x_{t-1}^2}$  should approach zero, so that the resulting model has all roots less than unit to force the next state  $x_t$  not to diverge further. From this viewpoint, Shi *et al.* (2001) proposed a heuristic determination of the nonlinear coefficient  $\gamma$  from the original data set, and defined

$$\gamma_0 = -\frac{\log \delta}{\max x_i^2}, \quad (7.3)$$

where  $\delta$  is a small number (i.e.,  $\delta = 0.0001$ ),  $1 \leq i < N$  and  $N$  is the length of the data series. Fixing  $\gamma = \gamma_0$ , the model coefficients can insist on changing toward constants  $\phi_i$  even if the observation moves far away from the equilibrium, since  $\exp\{\max x_i^2\} = \delta$ , i.e., approximately zero. Moreover, fixing  $\gamma = \gamma_0$ , the model coefficients  $\{\phi_t + \pi_t e^{-\gamma x_{t-1}^2}\}$  can always approach  $\phi_i + \pi_i$  when the state  $x_{t-1}$  moves to zero. So the instantaneous model may have some roots outside the unit circle to force the next state to increase. Thus, based on fixing  $\gamma_0 = \gamma$ , though it is not optimal, the ExpAr time series model is still assured to reveal the limit cycle behavior of the underlying time series.

## 7.4 Modelling the Drilling Torque Using ExpAr Time Series Models: Experimental Results

In Chapter 6, it is mentioned that a model based on the van der Pol equation is used to describe the transition from stable drilling to chatter vibration. It is used due to the nonlinear time varying dynamics of the process, see section 6.2. In the previous section, it is shown that the ExpAr time series models are able to reveal complex nonlinear dynamics such as singular point and limit cycle. Therefore, we propose to use the ExpAr time series models to describe the drilling torque and to characterize this time varying dynamics.

The ExpAr time series model is used to fit the drilling torque moments in experiment #21 of the experimental design. The data are recorded with a sampling rate of  $S = 20000$  Hz and consist of 6807552 observations, see Figure 5.9a. For the problem of on-line monitoring of the drilling process, a common way is to segment on-line measurements of the drilling torque. Then, it becomes very important to achieve fast decision-making about the dynamics through inference and analysis of the estimated time ExpAr time series model in each segment. Therefore, the data are divided into segments of length 4096, which is used by Theis (2004) to calculate the periodograms. In each segment, the ExpAr( $p$ ) time series model is fitted to centered data. The parameters are estimated using the real-time estimation procedure with  $\delta = 0.0001$  in equation (7.3).

The choice of a proper model order  $p$  is not an easy task. Figure 7.4 shows the AIC criterion for two time series segments before and after chatter. It is clear that the AIC criterion is decreasing as  $p$  increases. This may be explained by the autocorrelation function. Figure 7.5 shows the autocorrelation function for the two time series segments. It shows that for the first segment the autocorrelation decreases as  $p$  increases. For the second segment, the autocorrelation shows the existence of a periodic behavior. The selection of a model without a big enough lag will unavoidably result in larger residuals. We think that the selection of  $p = 40$  is a reasonable choice. For statistical interpretation, a model with lag 40 (i.e., 81 parameters) is often out of the imagination of an analyst. In practice, it is easy to justify the use of a model with 81 parameters for 4096 observations.

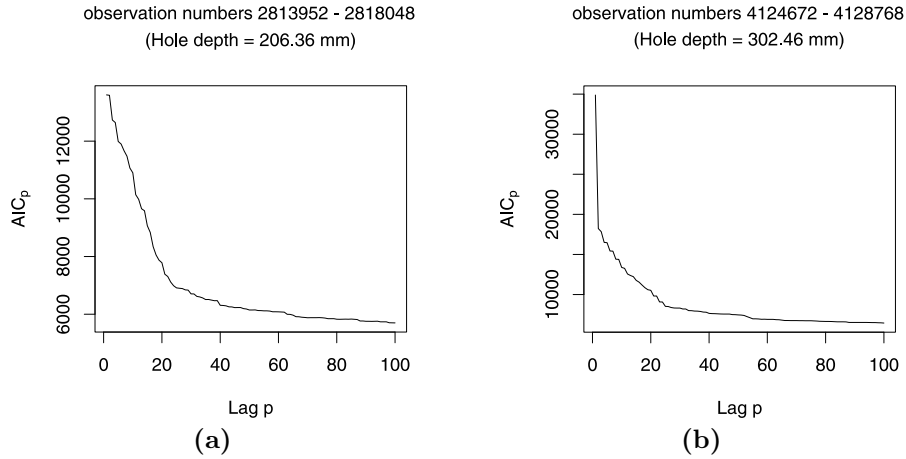


**Figure 7.4:** AIC criterion of two time series segments (a) before chatter (b) after chatter

Moreover, the nature of collected data in this process, “data-rich” environment, justifies the use of such models.

### 7.4.1 Diagnostic Checks

For model diagnostic, the residuals are plotted against hole depth in (mm) in Figure 7.6. Note that there is a slight increase in the variance of the residuals after depth 300 mm. That is during chatter vibration. This increase is clear in Figure 7.7. This figure shows the least squares estimate of the residual variance,  $\hat{\sigma}_e^2$ , of the model against hole depth in mm. We also check whether the errors are probably centered, symmetric and Gaussian. Figure 7.8 shows the histograms of the errors over two segments during stable drilling and chatter. They have a symmetric shape around zero and Gaussian appearance. However, the null hypothesis of normality of the residuals is rejected in all time segments using the Kolmogorov Smirnov test. This is explained by the presence of outliers. As a final check, the fitted model is simulated using the estimated coefficients and residual variance. The first  $p = 40$  values of the drilling torque in each segment are used as initial values. In fact, a model which cannot reproduce a similar series by simulation is certainly not interesting to statisticians and engineers. The result shows that the simulated values behave similar to the observed data. In conclusion, the estimated ExpAr(40) model provide a good fit to the drilling torque measurements.

### 7.4.2 Description of the Time Varying Dynamics

An important question is whether the ExpAr(40) time series model describes the nonlinear time varying dynamics of the process, see section 6.2. In section 7.2, we mentioned



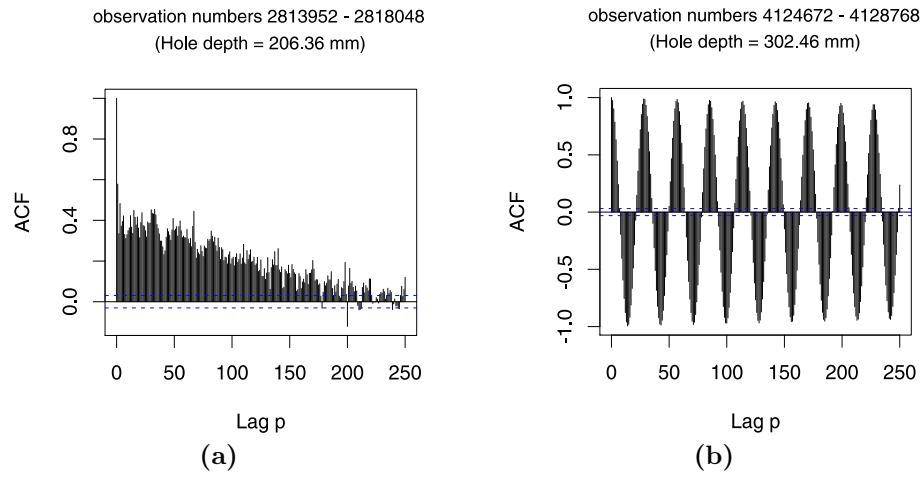


**Figure 7.5:** Autocorrelation function of two time series segments (a) before chatter (b) after chatter

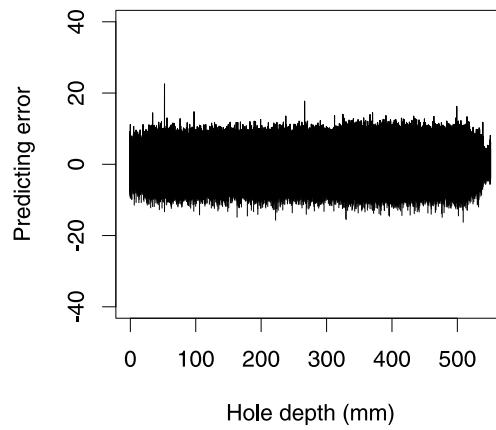


**Figure 7.6:** Plot of the residuals

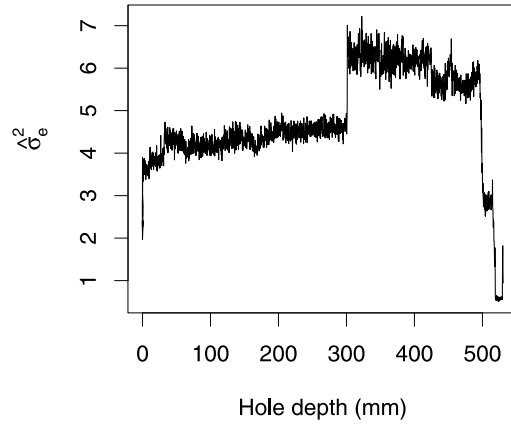


**Figure 7.7:** The least squares estimate of the residual variance,  $\hat{\sigma}_e^2$

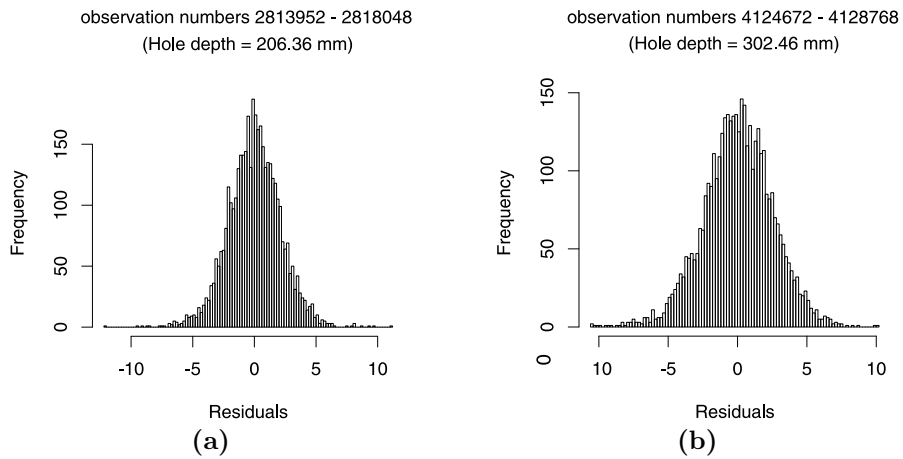


**Figure 7.8:** Histograms of the predicted errors (a) before chatter (b) after chatter

that the ExpAr time series model exhibit the limit cycle behavior under some conditions. These conditions are checked in each data segment. Figure 7.9 shows the results. It is clear that these conditions are satisfied during chatter vibration (depth  $\geq 300$  mm). This result is obvious for engineers. It is used by Weinert *et al.* (2002) in order to propose the phenomenological model that describes the transition from stable drilling to chatter, see section 6.2. In fact, it is known that machine tool chatter is a nonlinear oscillation of the limit cycle type, which can be regarded as an intrinsic property independent of process working conditions and measuring noise, see Tobias (1965).

In conclusion, it is shown that using the ExpAr(40) time series model, an on-line procedure can be used to answer questions about the nonlinear time varying dynamics of the process. Its real-time implementation can be guaranteed. Furthermore, it can be used to decide whether the process is stable or not. Shi *et al.* (1998) proposed the limit cycle behavior as criterion of chatter occurrence. Shi *et al.* (2001) used the limit cycle behavior for monitoring the dynamics evolution of boiling water reactor (BWR) oscillation.

## 7.5 ExpAr( $p$ ) Time Series Models Based Control Charts

In this section, we propose ExpAr times series models based control charts. Usually, time series based control charts are used to monitor the residuals. That is, a time series model is used to fit the data and to calculate the residuals. However, the drilling process is characterized by the large amount of data and therefore residuals. For example, more than 4000000 residuals are available in experiment #21 before the occurrence of chatter vibration. This causes the inapplicability of monitoring the residuals. Therefore, we propose to monitor the parameters of the ExpAr( $p$ ) time series model. The two parameters  $\hat{\gamma}$  and  $\hat{\sigma}_e^2$  might be monitored. For the monitoring procedure, the drilling torque moments are divided into segments with a given length  $N_0$ . In each segment, the ExpAr( $p$ ) time series model is fitted to the centered data and parameters  $\gamma$  and  $\sigma_e^2$  are estimated. Note that in the following, the index  $t$  refers to the segment number  $t$  of length  $N_0$ . For the monitoring procedure, we propose the rank based univariate EWMA ( $r$ UEWMA) control chart proposed by Hackl and Ledolter (1992).

### Monitoring $\{\hat{\gamma}\}$

At time  $t \geq m$ , the sequential rank of  $\hat{\gamma}_t$  among  $RS = \{\hat{\gamma}_{t-m+1}, \dots, \hat{\gamma}_t\}$  is given by

$$Q_t^* = 1 + \sum_{i=t-m+1}^t I(\hat{\gamma}_t > \hat{\gamma}_i).$$

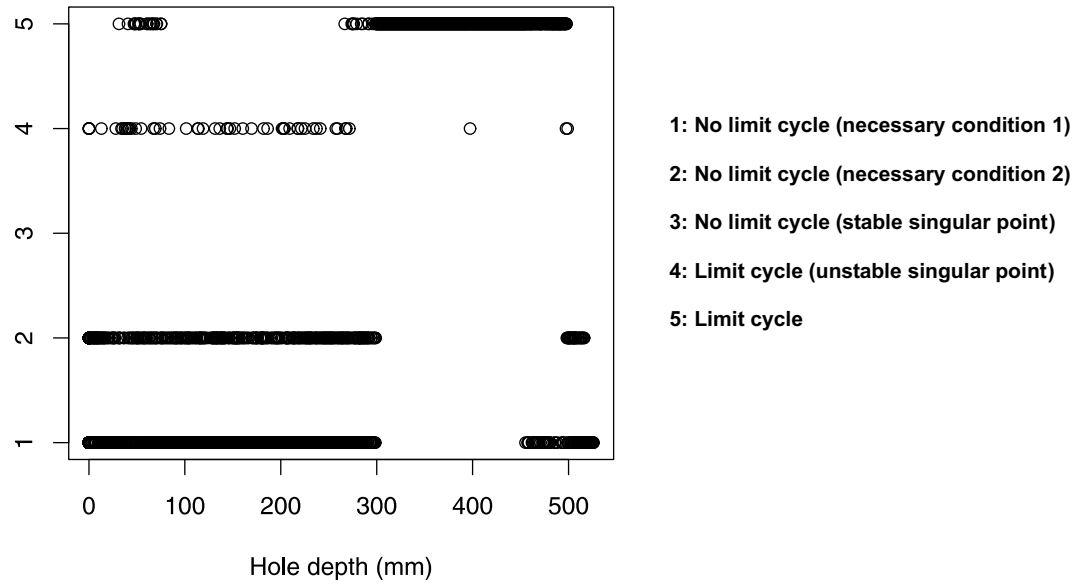


**Figure 7.9:** Description of the time varying dynamics of the drilling process (experiment #21)

The standardized sequential rank  $Q_t^m$  is computed using equation (2.4). The control statistic  $T_t$  is computed as follows

$$T_t = \min\{B_1, (1 - \lambda_1)T_{t-1} + \lambda_1 Q_t^m\},$$

$t = 1, 2, \dots$ , where  $B_1$  is an upper reflection boundary,  $T_0$  is a starting value, usually set equal to zero, and  $0 < \lambda_1 \leq 1$ . The process is considered in-control as long as  $T_t \geq h_1$ , where  $h_1 < 0$  is a lower control limit. Note that, the lower-sided EWMA is considered because the statistic  $Q_t^m$  is “higher the better”. Indeed, an increase in  $\hat{\gamma}_t$  means a process improvement.

### Monitoring $\{\hat{\sigma}_e^2\}$

Similarly, the sequential rank of  $\hat{\sigma}_{e,t}^2$  among  $RS = \{\hat{\sigma}_{e,t-m+1}^2, \dots, \hat{\sigma}_{e,t}^2\}$  is given by

$$Q_t^* = 1 + \sum_{i=t-m+1}^t I(\hat{\sigma}_{e,t}^2 > \hat{\sigma}_{e,i}^2).$$

The standardized sequential rank  $Q_t^m$  is computed using equation (2.4). In this case, the EWMA recursion is given by

$$T_t = \max\{B_2, (1 - \lambda_2)T_{t-1} + \lambda_2 Q_t^m\},$$

$t = 1, 2, \dots$ , where  $B_2$  is a lower reflection boundary,  $T_0$  is a starting value and  $0 < \lambda_2 \leq 1$ . The process is considered in-control as long as  $T_t \leq h_2$ , where  $h_2 > 0$  is an upper control limit. In this case, the upper-sided EWMA is considered because the statistic  $S_t^m$  is “lower the better”. Indeed, a decrease in  $\hat{\sigma}_e^2$  means a process improvement.

## 7.6 Conclusion

The main objective of this chapter is to investigate whether ExpAr time series models can be used to model the drilling process and to setup an on-line monitoring strategy. The results show that they provide an explanation of the nonlinear time varying dynamics of the process namely fixed points and limit cycles. Finally, ExpAr time series based control charts are proposed. They are used to monitor the drilling process using several data sets in Chapter 8.

This page intentionally left blank

## Experimental Results

In this chapter, the proposed  $r$ MEWMA and ExpAr( $p$ ) time series based control charts are used to monitor the drilling process using several data sets of run numbers #5, #7, #9, #11, #15, and #21 of the experimental design. In these experiments chatter vibration is observed at later stages in the process. Thus, data collected before its occurrence can be used to evaluate the performance of the control charts during stable drilling.

For the drilling process, a successful monitoring procedure would detect all changes in the physical conditions of the process and especially the start of the transition from stable drilling to chatter. It should produce few false alarms during stable drilling in order to avoid unnecessary process adjustments. Moreover, it should be easy to visualize and interpret for the process operator.

### 8.1 Experimental Settings

Table 8.1 gives the cutting parameters, sampling rates and series lengths of the drilling torque and the amplitudes of the relevant frequencies in each experiment. The drilling torque is recorded with a sampling rate  $S = 20000$  Hz. They are divided into segments of length  $N = 4096$  observations to calculate the periodograms. The use of different cutting speeds  $v_c$  and feeds  $f$  leads to different sampling rates of the amplitudes of the relevant frequencies and therefore series lengths. The boring tool moves with a velocity  $v = v_c f / (2\pi r)$ , where  $r$  is the radius of the workpiece. An amplitude  $R_t$  of each frequency is obtained at  $vN/S$  mm of drilling.

Figure 5.11 shows the occurrence of chatter vibration in each experiment. It is determined by the inspection of chatter marks on the bore hole wall of the workpiece. It is observed after hole depths 400, 340, 250, 150, 270, and 300 mm in experiments #5,

**Table 8.1:** Experimental settings

Experiment Number	Cutting Parameters			Sampling Rate		Series Length	
	$f$ (mm)	$v_c$ (m/min)	$\dot{V}_{oil}$ (L/min)	Drilling Torque (Hz)	$R$ (mm)	Drilling Torque	$R$
#5	0.120	90	300	20000	$19.456 \cdot 10^{-2}$	10506240	2565
#7	0.231	69	371	20000	$28.672 \cdot 10^{-2}$	7131136	1741
#9	0.139	69	371	20000	$17.408 \cdot 10^{-2}$	11747328	2868
#11	0.185	60	300	20000	$20.139 \cdot 10^{-2}$	10178560	2485
#15	0.231	69	229	20000	$28.672 \cdot 10^{-2}$	7266304	1774
#21	0.185	90	300	20000	$30.037 \cdot 10^{-2}$	6807552	1662



#7, #9, #11, #15, and #21, respectively. Chatter is dominated by frequency 703 Hz in experiments #5, #7, #9, #15, and #21 and frequency 234 Hz in experiment #11, see Figure B.1 in Appendix B. Data obtained after the occurrence of chatter are not used. Indeed, the objective of the use of control charts is to detect the start of the transition from stable drilling to chatter vibration in order to quickly adjust the process and not to signals when chatter is observed.

## 8.2 Transition from Stable Drilling to Chatter Vibration

The start of the transition from stable drilling to chatter vibration is not sudden as it may be expected from Figure B.1 in Appendix B. It is increasing with time, see Weinert *et al.* (2002). Its identification is very important for the investigation of the empirical performance of the different control charts. A successful monitoring procedure would quickly detect this change in the dynamics of the process and not only signals when chatter is observed. This allows the process engineers to quickly adjust the process and avoid the occurrence of chatter vibration.

The mechanical interpretation proposed by Weinert *et al.* (2002), see section 5.3.2, is used to identify the start of the transition from stable drilling to chatter vibration. First, experiments #5, #7, #9, #15, and #21 are investigated. As mentioned, chatter vibration is dominated by frequency 703 Hz in these frequencies. Figures 8.1 to 8.6 show the means of the amplitudes of frequencies 234, 703, and 1183 Hz within segments of length 5 mm. They show that in all experiments frequency 1183 Hz dominate the process in the beginning of drilling. As noted in section 5.3.2, the damping effect due to the stuffing box of torsional mode 1183 Hz is close to its minimum. After that, the amplitudes of frequency 703 Hz increase and dominate the process. This is explained by a change in the boundary conditions of the process. The damping effect changes from torsional mode 1183 Hz to 703 Hz. The transition from stable drilling to chatter vibration starts when a fast increase in the amplitudes of frequencies 703 Hz is observed. Finally, the process is subject to chatter vibration when the damping effect of torsional mode 703 Hz reaches a critical value. Therefore, the amplitudes of frequency 703 Hz explode and chatter is observed, see Figure B.1 in Appendix B.

Moreover, there are two known physical changes in the process that should be considered. First, it is known that the guiding pads of the BTA tool leave the starting bush approximately at depth 32 mm, see section 5.1.2. From previous experiments, the process has been observed to either stay stable or start with chatter vibration, see Weinert *et al.* (2002). This change in the physical condition of the process induces a sudden increase in the amplitudes of the relevant frequencies. In fact, before that depth, the vibrations of the tool are strongly damped by the starting bush supporting the guiding pads and the amplitudes are low. The fact that the guiding pads leave the starting bush induces

a sudden change in the dynamics of the process, caused by the tool being freed. This explains that there is always an increase in all amplitudes of the relevant frequencies, see Figure B.1 in Appendix B. Secondly, it is known that depth 110 mm is approximately the position where the tool enters the bore hole completely. Theis (2004) noted that this might lead to changes in the dynamics of the process because the boring bar is slightly thinner than the tool and therefore the pressures in the hole may change.

## 8.3 Monitoring Strategies

### 8.3.1 Residual $r$ MEWMA Control Charts

In chapter 6, it is shown that the amplitudes  $R_t$  of frequencies 234, 703 and 1183 Hz might be autocorrelated during stable drilling. This autocorrelation is a normal and unremovable part of the process. Then, monitoring  $\mathbf{R}_t = (R_{t,234}, R_{t,703}, R_{t,1183})'$  will lead to an ineffective strategy that produces out-of-control signals because of the presence of autocorrelation. In this case, residual control charts are adequate SPC procedures suggested by several authors, see section 1.2. As mentioned, this procedure requires a model of the autocorrelative structure of the data which can be achieved by fitting an appropriate time series model to the observations. For this reason, the autoregressive approximation of the amplitudes of the relevant frequencies proposed in section 6.3.2 is used. The  $m > 1$  most recent observations  $R_{t-m+1}, \dots, R_t$  of each frequency are used to estimate the parameters of the AR(1) model given by equation (6.5). The residuals are calculated using equation (6.6). Note that  $k = 5$  is used in equation (6.6) in order to avoid the masking problem, see section 8.4. The  $r$ MEWMA control charts are used to monitor the residual vectors  $\mathbf{e}_t = (e_{t,234}, e_{t,703}, e_{t,1183})'$ ,  $t \geq m$ . In the following, we will omit the word residual from residual  $r$ MEWMA control charts.

In this chapter, only Mahalanobis  $r$ MEWMA control charts are considered because the calculation of simplicial depth in  $\mathbb{R}^3$  is extremely time consuming, see section 2.1.

### 8.3.2 ExpAr(40) Time Series Based $r$ UEWMA Control Charts

The drilling torque observations are divided into segments of length 4096. In each segment, the ExpAr(40) time series model is fitted to the centered data. The nonlinear coefficient  $\gamma$  of the model is estimated using the heuristic approach described in section 7.3.2 with  $\delta = 0.0001$  in equation (7.3). The other parameters  $\{\phi_i, \pi_i\}$ ,  $i = 1, 2, \dots, 40$ , of the model are estimated using the least squares method. The resulting estimated parameters  $\hat{\gamma}$  and  $\hat{\sigma}_e^2$  of all segments are monitored using the  $r$ UEWMA control charts, see section 7.5. Note that in the following  $r$ UEWMA $^{\hat{\gamma}}$  and  $r$ UEWMA $^{\hat{\sigma}}$  refer to the ExpAr(40) time series based  $r$ UEWMA control charts used to monitor  $\{\hat{\gamma}_t\}$  and  $\{\hat{\sigma}_{e,t}^2\}$ ,  $t = 1, 2, \dots$ , respectively.

**Table 8.2:** Adjusted control limits of the  $r$ MEWMA and UMEWMA control charts

$m$	$r$ MEWMA $\lambda$			$r$ UEWMA $\hat{\tau}$ $\lambda_1$			$r$ UEWMA $\hat{\sigma}$ $\lambda_2$		
	0.10	0.30	0.50	0.10	0.30	0.50	0.10	0.30	0.50
Control limit	-0.318	-0.593	-0.756	-0.318	-0.593	-0.756	0.318	0.593	0.756
Reflection boundary	0.318	0.593	0.756	0.318	0.593	0.756	-0.318	-0.593	-0.756

### 8.3.3 Choice of the Control Charts Parameters

For the different control charts, reference samples of size  $m = 100$  observations are used because the monitoring procedures should start before depth 32 mm. As noted chatter vibration may be observed after that depth. Furthermore, large reference samples can not be used due to the time varying dynamics of the process. In all experiments, 100 amplitudes are obtained at 19.456 - 30.037 mm of drilling. Note that the statistical performance of  $r$ MEWMA and  $r$ UEWMA control charts may be poor when reference samples of size 100 observations are used. That is, the control charts may signal frequently with no assignable causes presents and do not quickly detect changes in the process, see section 3.1.

The  $r$ MEWMA and  $r$ UEWMA control charts with smoothing parameters equal to 0.1, 0.3 and 0.5 are considered. Their control limits and reflection boundaries are chosen so that they all have an in-control ARL equal to 370. This choice should avoid excessive false alarm signals. The control limits are adjusted using simulation. As noted in section 3.1, the estimation effect should not be neglected when reference samples of size  $m = 100$  observations are used. Table 8.2 gives the adjusted control limits and reflection boundaries of the different control charts.

### 8.3.4 Experimental Results

Tables 8.3 to 8.7 show the out-of-control signals produced by the different control charts in all experiments. All control charts produced out-of-control signals at  $32 \leq \text{depth} \leq 50$  mm. That is, they detect the change in the dynamics of the process when the guiding pads leave the starting bush. Most control charts did not signal at  $100 \leq \text{depth} \leq 125$  mm. That is, when the BTA tool enters the bore hole completely. Figures 8.1 to 8.6. show that there is a decrease in the amplitudes of frequency 1183 Hz after depth 110 mm in all experiments. This explains that most control charts fail to detect the change in the dynamics of the process when the BTA tool enters the bore hole completely.

**Table 8.3:** Out-of-control signals of the different control charts (experiment #5)

Hole Depth (mm)	Residual $r$ MEWMA			$r$ UEWMA $\hat{\gamma}$			$r$ UEWMA $\hat{\sigma}_e^2$		
	$\lambda$			$\lambda_1$			$\lambda_2$		
	0.1	0.3	0.5	0.1	0.3	0.5	0.1	0.3	0.5
$\leq 32$	0	0	1	0	0	0	0	0	0
32-50	43	15	10	21	4	2	0	7	39
50-75	0	0	0	0	0	0	0	0	0
75-100	0	0	0	0	0	0	0	0	0
100-125	0	0	0	6	1	0	0	0	1
125-150	0	0	1	2	2	1	0	0	0
150-175	0	0	0	4	1	0	0	0	0
175-200	0	1	0	0	0	0	0	0	0
200-225	0	0	0	0	0	0	0	0	0
225-250	0	0	0	0	0	0	0	0	0
250-275	1	0	1	0	0	0	3	8	12
275-300	7	3	0	13	4	3	13	37	72
300-325	0	2	2	12	4	2	8	21	53
325-350	5	5	4	0	0	0	0	0	1
350-375	14	8	5	25	11	9	1	1	0
375-400	43	29	25	91	50	30	30	38	38

In the following we will focus on the capability of the different control charts to detect the start of the transition from stable drilling to chatter vibration in each experiment.

### Experiment #5

As mentioned, experiment #5 is the most stable experiment of the experimental design and only slight chatter marks are observed on the bore hole wall at the end of the process, after depth 400 mm. This may be explained by the low cutting speed used, see Table 8.1. Chatter vibration is dominated by frequency 703 Hz.

Figure 8.1 shows that a change in the damping effect of the stuffing box from torsional mode 1183 Hz to 703 Hz occurs after depth 250 mm. The  $r$ MEWMA control charts with  $\lambda = 0.1$  and 0.5 produce two out-of-control signals at depths 258 and 251 mm, respectively, see Table 8.3. The three  $r$ UEWMA $^{\hat{\sigma}}$  control charts produce many out-of-control signals. Then, a first increase in the amplitudes of frequency 703 Hz is observed at  $275 \leq \text{depth} \leq 350$  mm. All control charts detect this change in the dynamics of the process and produce out-of-control signals. The transition from stable drilling to chatter vibration starts after depth 350 mm. Indeed, a fast increase in the amplitudes of frequency 703 Hz is observed. All control charts detect it and many out-of-control signals are produced until depth 400 mm.

Note that few out-of-control signals are not related to known changes in the dynamics of the process. They are produced by the two  $r$ MEWMA control charts with  $\lambda = 0.3$

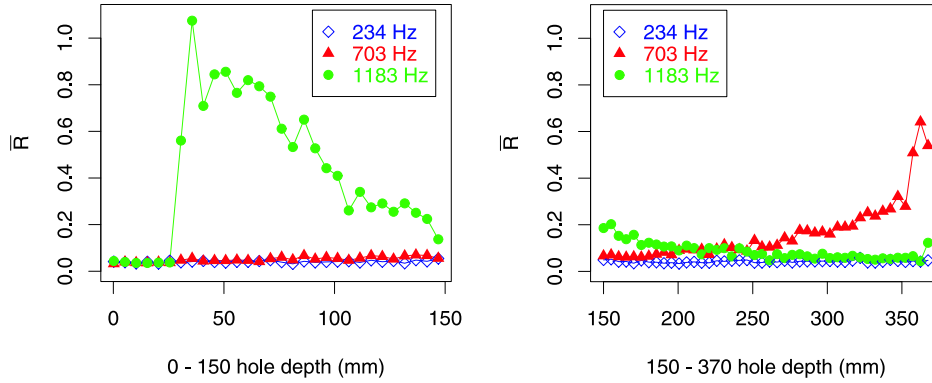


**Figure 8.1:** Means of the amplitudes of frequencies 234, 703 and 1183 Hz within segments of length 5 mm in experiment #5

and 0.5 at depths 178 and 141 mm, respectively, and  $r\text{UEWMA}^{\hat{\sigma}}$  control charts at  $125 \leq \text{depth} \leq 175$  mm.

#### Experiment #7

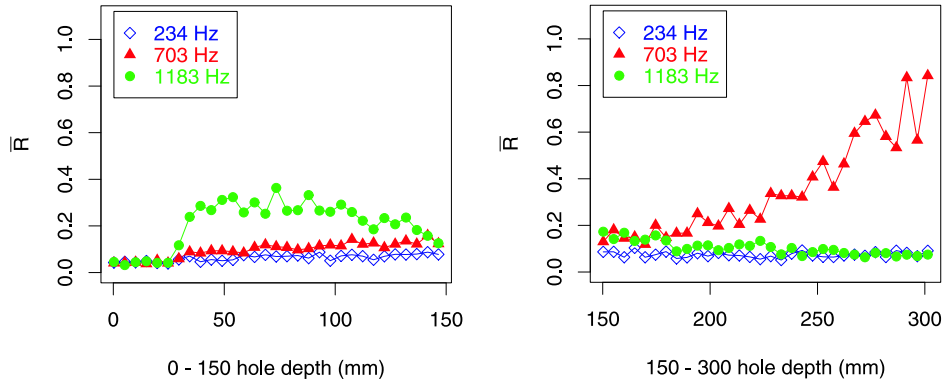
In this experiment, chatter vibration is dominated by frequency 703 Hz. Its effect is apparent on the bore hole wall after depth 340 mm.

Figure 8.2 shows that a change in the damping effect of the stuffing box from torsional mode 1183 Hz to 703 Hz occurs after depth 175 mm. Frequency 703 Hz dominates the process and a first increase in its amplitudes is observed at  $225 \leq \text{depth} \leq 275$  mm. Only the  $r\text{MEWMA}$  control charts with  $\lambda = 0.1$  and  $r\text{UEWMA}^{\hat{\sigma}}$  control charts with  $\lambda_2 = 0.1$  and 0.3 produce out-of-control signals, see Table 8.4. A second increase is observed at  $275 \leq \text{depth} \leq 300$  mm. It is detected by the three  $r\text{MEWMA}$  control charts. However the different  $r\text{UEWMA}$  control charts did not signal. The transition to chatter vibration starts after depth 300 mm. All control charts detect it. Similar as for experiment #5, few out-of-control signals are not related to known changes in the dynamics of the process.

#### Experiment #9

In this experiment, chatter vibration is dominated by frequency 703 Hz. Its effect is observed on the bore hole wall after depth 250 mm.

Figure 8.3 shows that the transition from stable drilling to chatter occurs approximately after depth 200 mm. All control charts detect this transition and many out-of-control signals are produced after that depth, see Table 8.5. Note that the three  $r\text{UEWMA}^{\hat{\sigma}}$  control charts produce many out-of-control signals at all depth segments, except at  $175 \leq \text{depth} \leq 200$  mm.



**Figure 8.2:** Means of the amplitudes of frequencies 234, 703 and 1183 Hz within segments of length 5 mm in experiment #7

**Table 8.4:** Out-of-control signals of the different control charts (experiment #7)

Hole Depth (mm)	Residual $r$ MEWMA			$r$ UEWMA $\hat{\gamma}$			$r$ UEWMA $\hat{\sigma}_e^2$		
	$\lambda$			$\lambda_1$			$\lambda_2$		
	0.1	0.3	0.5	0.1	0.3	0.5	0.1	0.3	0.5
$\leq 32$	0	0	0	0	0	0	0	0	0
32-50	59	28	17	8	2	2	62	33	19
50-75	13	1	1	0	0	0	20	1	1
75-100	0	0	0	0	0	0	0	0	0
100-125	2	0	0	5	5	2	0	0	0
125-150	0	1	1	0	0	0	4	2	0
150-175	0	0	0	0	0	0	0	0	0
175-200	0	0	0	0	0	0	0	0	0
200-225	0	0	0	0	0	0	0	0	0
225-250	4	0	0	0	0	0	17	2	0
250-275	0	0	0	0	0	0	0	0	0
275-300	3	2	1	0	0	0	0	0	0
300-325	52	42	33	51	44	43	38	36	25
325-350	50	11	2	31	18	15	56	10	2

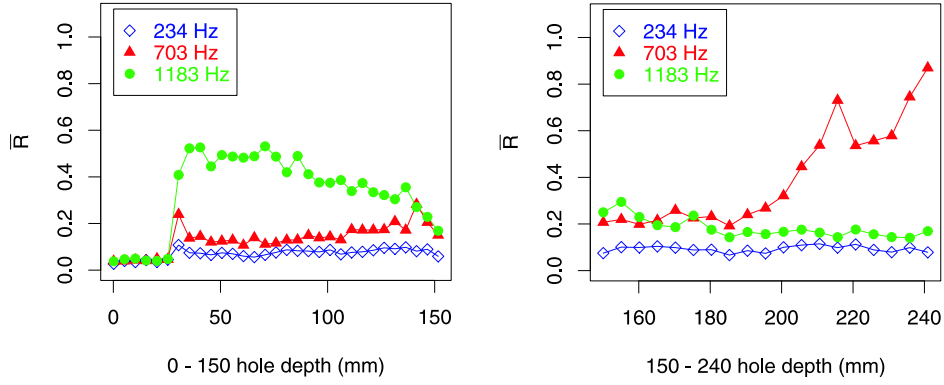


**Figure 8.3:** Means of the amplitudes of frequencies 234, 703 and 1183 Hz within segments of length 5 mm in experiment #9

**Table 8.5:** Out-of-control signals of the different control charts (experiment #9)

Hole Depth (mm)	Residual $r$ MEWMA			$r$ UEWMA $\hat{\gamma}$			$r$ UEWMA $\hat{\sigma}_e^2$		
	$\lambda$			$\lambda_1$			$\lambda_2$		
	0.1	0.3	0.5	0.1	0.3	0.5	0.1	0.3	0.5
$\leq 32$	0	0	0	4	2	2	39	19	13
32-50	75	29	16	10	3	4	62	25	13
50-75	0	0	0	7	5	2	31	18	14
75-100	0	1	1	0	0	0	47	10	3
100-125	2	1	1	1	0	0	80	32	18
125-150	1	1	1	0	0	0	15	2	0
150-175	7	1	1	0	0	0	10	10	8
175-200	0	1	1	0	0	0	0	0	0
200-225	18	4	2	1	0	0	60	24	6
225-250	14	14	15	11	12	12	20	11	9

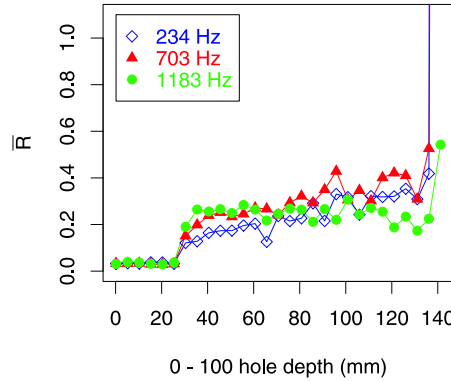


**Figure 8.4:** Means of the amplitudes of frequencies 234, 703 and 1183 Hz within segments of length 5 mm in experiment #11

**Table 8.6:** Out-of-control signals of the different control charts (experiment #11)

Hole Depth (mm)	Residual $r$ MEWMA			$r$ UEWMA $\hat{\gamma}$			$r$ UEWMA $\hat{\sigma}_e^2$		
	$\lambda$			$\lambda_1$			$\lambda_2$		
	0.1	0.3	0.5	0.1	0.3	0.5	0.1	0.3	0.5
$\leq 32$	0	0	0	16	4	3	12	0	0
32-50	73	38	25	38	4	1	65	52	39
50-75	0	0	0	3	0	0	31	27	10
75-100	3	1	0	0	0	0	35	9	1
100-125	4	3	2	0	0	0	22	0	0
125-150	26	14	10	34	29	28	78	52	32
150-175	36	14	9	51	21	11	25	2	0

**Experiment #11**

In this experiment, chatter vibration is dominated by frequency 234 Hz. Its effect is observed on the bore hole wall after depth 140 mm.

Figure 8.4 shows that the amplitudes of frequencies 234 Hz, 703 Hz and 1183 Hz increased after approximately depth 30 mm. In contrast to the other experiments, none of the three frequencies dominates the process at the beginning of drilling. Chatter vibration is developed suddenly before 140 mm. Figure 8.4 shows that there is not a distinguishable start of transition from stable drilling to chatter vibration. Indeed, a sudden large increase is observed in the amplitudes of frequencies 234 Hz and 703 Hz. The respective thresholds are 200 and 70, see Figure B.1 in Appendix B. Table 8.6 shows that all control charts detect the sudden development of chatter vibration. Similar as in experiment #9, the three  $r$ UEWMA $\hat{\sigma}$  control charts produce many out-of-control signals in most of the depth segments.



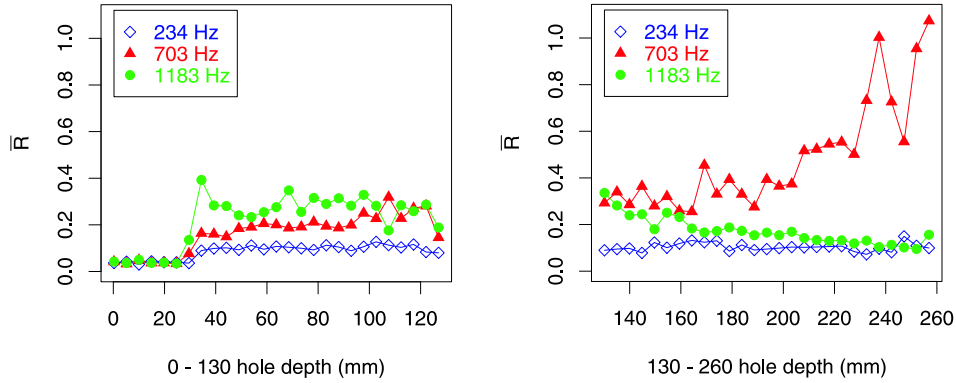


**Figure 8.5:** Means of the amplitudes of frequencies 234, 703 and 1183 Hz within segments of length 5 mm in experiment #15

#### Experiment #15

In this experiment, chatter vibration is dominated by frequency 703 Hz. Its effect is observed on the bore hole wall after depth 270 mm.

Figure 8.5 shows that frequency 1183 Hz dominates the process at the beginning of drilling. The change in the damping effect of the stuffing box from torsional mode 1183 Hz to 703 Hz occurs approximately after 160 mm. Frequency 703 Hz dominates the process. A fast increase in their amplitudes is observed after depth 225 mm. This means that the transition from stable drilling to chatter vibration occurs approximately at that depth. The three  $r$ MEWMA control charts detect the start of this transition and produce many out-of-control signals until depth 275 mm, see Table 8.7. Most of the  $r$ UEWMA control charts did not detect the start of this transition. Indeed, only  $r$ UEWMA $^{\hat{\sigma}}$  control charts with  $\lambda_2 = 0.3$  and  $0.5$  signals at  $225 \leq \text{depth} \leq 250$  mm.

#### Experiment #21

In this experiment, chatter vibration is dominated by frequency 703 Hz. Its effect is apparent on the bore hole wall after depth 300 mm. Figure 8.6 shows that a change in the boundary conditions occurs approximately after depth 210 mm. Frequency 703 Hz dominates the process and a first increase in its amplitudes is observed at  $210 \leq \text{depth} \leq 250$  mm, see Table 8.8. The three  $r$ MEWMA control charts detect this change in the dynamics of the process. They signal at  $200 \leq \text{depth} \leq 250$  mm. The different  $r$ UEWMA control charts signal only at  $200 \leq \text{depth} \leq 225$  mm. The transition from stable drilling to chatter vibration starts after depth 250 mm. A fast increase in the amplitudes of frequency 703 Hz is observed. The different control  $r$ MEWMA and  $r$ UEWMA $^{\hat{\gamma}}$  control charts detect the start of this transition and produce many out-of-control signals at  $250 \leq \text{depth} \leq 300$  mm. However,  $r$ UEWMA $^{\hat{\sigma}}$  produced out-of-control signals only at

**Table 8.7:** Out-of-control signals of the different control charts (experiment #15)

Hole Depth (mm)	Residual $r$ MEWMA			$r$ UEWMA $\hat{\gamma}$			$r$ UEWMA $\hat{\sigma}_e^2$		
	$\lambda$			$\lambda_1$			$\lambda_2$		
	0.1	0.3	0.5	0.1	0.3	0.5	0.1	0.3	0.5
$\leq 32$	0	0	0	1	1	1	1	0	0
32-50	58	39	28	57	20	9	63	50	37
50-75	6	0	0	2	0	0	9	0	0
75-100	0	1	0	0	0	0	0	0	0
100-125	0	1	0	1	1	1	0	0	0
125-150	0	0	0	0	0	0	13	1	0
150-175	1	1	0	0	0	0	0	0	0
175-200	0	0	0	1	0	0	31	17	13
200-225	2	1	0	0	0	0	0	0	0
225-250	5	2	3	0	0	0	0	1	1
250-275	22	19	18	35	31	30	16	16	16

$250 \leq \text{depth} \leq 275$  mm. Similar as experiments #9 and #11,  $r$ UEWMA $\hat{\sigma}$  produced many out-of-control signals in many depth segments.

### Results Summary

The results show that the three  $r$ MEWMA control charts quickly detect the start of the transition from stable drilling to chatter vibration in the considered experiments. That is, chatter may be avoided if corrective actions are taken after these signals. Furthermore, most of the out-of-control signals produced by the three  $r$ MEWMA control charts are related to changes in the dynamics of the process. Indeed, few out-of-control signals are not explained. For example, only 2 out-of-control signals are not related to any known change in the dynamics of the process in experiment #5. Therefore, we can conclude that  $r$ MEWMA control charts do not produce many false alarms during stable drilling, which avoid unnecessary process adjustments. However,  $r$ UEWMA control charts are less powerful than  $r$ MEWMA control charts. This is explained by the “non-optimal” estimation procedure of the ExpAr(40) time series model parameters and the choice of the time lag  $p$ .

## 8.4 The Masking Problem

In section 8.3.1, it is mentioned that the residuals of the amplitudes of frequencies 234, 703 and 1183 Hz are computed using  $k = 5$  in equation (6.6) in order to avoid the masking problem. In fact, one limitation of the use of adaptive estimates to calculate the residuals is the “masking” or parameter adaptation problem. If an early process

**Table 8.8:** Out-of-control signals of the different control charts (experiment #21)

Hole Depth (mm)	Residual $r$ MEWMA			$r$ UEWMA $\hat{\gamma}$			$r$ UEWMA $\hat{\sigma}_e^2$		
	$\lambda$			$\lambda_1$			$\lambda_2$		
	0.1	0.3	0.5	0.1	0.3	0.5	0.1	0.3	0.5
$\leq 32$	0	0	0	1	3	2	0	0	0
32-50	53	24	15	60	18	10	59	37	21
50-75	0	0	0	19	4	1	12	0	0
75-100	2	1	0	0	0	0	0	0	0
100-125	0	0	0	0	0	0	16	6	2
125-150	0	0	0	0	0	0	32	2	0
150-175	0	1	1	3	1	1	0	1	2
175-200	0	0	0	0	0	0	57	10	3
200-225	0	1	1	4	2	1	32	8	3
225-250	15	3	2	0	0	0	0	0	0
250-275	21	1	1	5	1	0	1	1	1
275-300	6	1	1	5	1	2	0	0	0
300-325	66	27	21	0	0	0	0	0	0

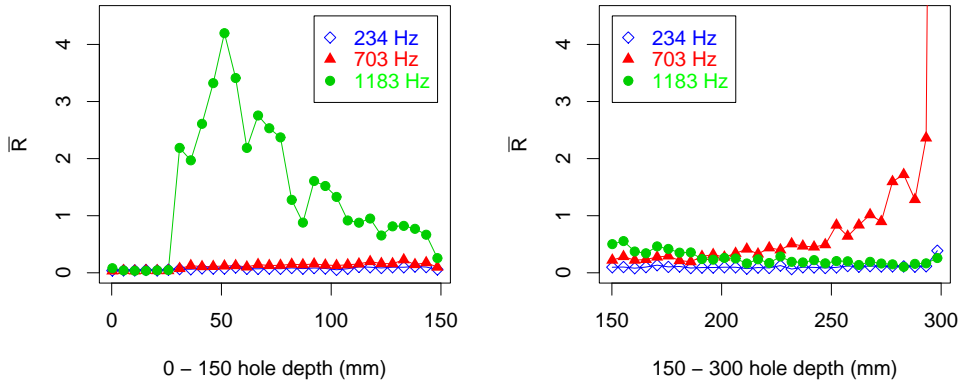


**Figure 8.6:** Means of the amplitudes of frequencies 234, 703 and 1183 Hz within segments of length 5 mm in experiment #21

**Table 8.9:** Out-of-control signals of the two  $r$ MEWMA control charts using  $k = 1$  and  $k = 5$  in equation (6.6) ( $252.91 \leq \text{depth} \leq 258.32$  mm)

Observation number	Hole depth	$r$ MEWMA $k = 1$	$r$ MEWMA $k = 5$
842	252.91		
843	253.21		
⋮			
847	254.42		×
848	254.72		
⋮			
860	258.32	×	

change is not quickly detected, then the parameter estimates may be adversely affected by the change, thus masking the shift from future detection. To illustrate this problem we consider the Mahalanobis  $r$ MEWMA control chart with  $\lambda = 0.3$ ,  $h = -0.593$  and  $B = -h$  used to jointly monitor the residuals of the amplitudes of frequencies 234, 703 and 1183 Hz in experiment #21. The residuals are calculated using  $k = 1$  and  $k = 5$  in equation (6.6).

Messaoud *et al.* (2004) showed that the transition from stable drilling to chatter vibration starts at depth 252.91 mm ( $t = 842$ ). Table 8.9 shows that using  $k = 5$  in equation (6.6), the  $r$ MEWMA control chart quickly detect the change in the dynamics of the process after 5 observations, see Figure 8.7. However, using  $k = 1$  in equation (6.6), the  $r$ MEWMA control chart is less powerful. The first out-of-control signal is observed after 18 observations (depth = 258.32 mm). The reason is that the change is quickly transferred to the adaptive estimated parameters. Figure 8.8 shows that using  $k = 1$ , observation  $\mathbf{e}_{842}$  is outside the data cloud. This is due to the fact that the residuals of the amplitudes of the three frequencies are computed using  $\hat{\beta}_{841}$  and  $\hat{\phi}_{1,841}$  in equation (6.6). They are estimated before the start of the transition from stable drilling to chatter vibration. The Mahalanobis depth of  $\mathbf{e}_{842}$  and its rank are equal to 0.030 and 1, respectively, see Table 8.10. This causes the  $r$ MEWMA control statistic  $T_{842}$  to wander to the direction of an out-of-control, see Figure 8.7. At  $t = 843$ , the residuals of the amplitudes of the three frequencies are computed using  $\hat{\beta}_{842}$  and  $\hat{\phi}_{1,842}$  in equation (6.6). Table 8.10 shows that the change is quickly transferred to  $\hat{\phi}_{1,842}$  (frequency 703 Hz). Therefore, observation  $\mathbf{e}_{843}$  is deep in the data cloud or reference sample, see Figure 8.8. The Mahalanobis depth of  $\mathbf{e}_{843}$  and its rank are equal to 0.446 and 77, respectively. This causes the  $r$ MEWMA control statistic  $T_{843}$  to wander in a direction opposite of an out-of-control, see Figure 8.7.

**Table 8.10:** Illustration of the masking problem

Observation number $t$	Hole depth (mm)	234 Hz		703 Hz		1183 Hz		$MD$	$Q_t^*$	$Q_t^m$	$T_t$
		$\hat{\beta}_{t-1}$	$\hat{\phi}_{1,t-1}$	$\hat{\beta}_{t-1}$	$\hat{\phi}_{1,t-1}$	$\hat{\beta}_{t-1}$	$\hat{\phi}_{1,t-1}$				
836	251.11	0.090	0.022	0.448	0.020	0.183	0.107	0.463	84	0.67	0.303
837	251.41	0.090	0.023	0.447	0.026	0.179	0.119	0.430	80	0.59	0.389
838	251.71	0.091	0.021	0.448	0.025	0.181	0.105	0.261	45	-0.11	0.239
839	252.01	0.089	0.030	0.449	0.023	0.183	0.096	0.700	95	0.89	0.434
840	252.31	0.090	0.027	0.452	0.021	0.182	0.106	0.120	4	-0.93	0.025
841	252.61	0.089	0.031	0.451	0.037	0.180	0.114	0.223	33	-0.35	-0.087
842	252.91	0.090	0.033	0.434	0.088	0.181	0.113	0.030	1	-0.99	-0.358
843	253.21	0.089	0.042	0.399	0.203	0.181	0.106	0.446	77	0.53	-0.092
844	253.51	0.090	0.045	0.383	0.239	0.181	0.116	0.120	4	-0.93	-0.343

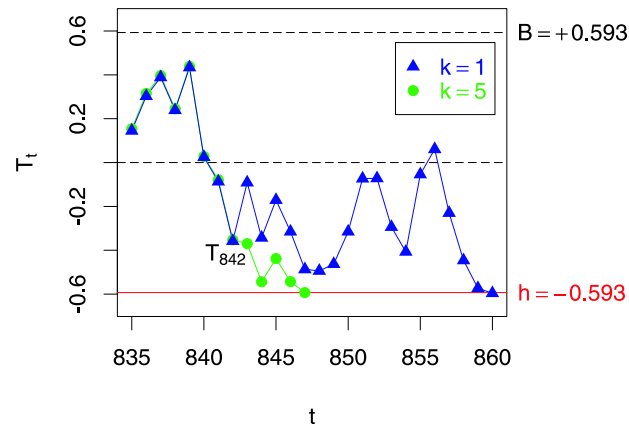


**Figure 8.7:** Plot of the the two  $r$ MEWMA control charts with  $\lambda = 0.3$  and using  $k = 1$  and  $k = 5$  in equation (6.6) ( $835 \leq t \leq 860$ )

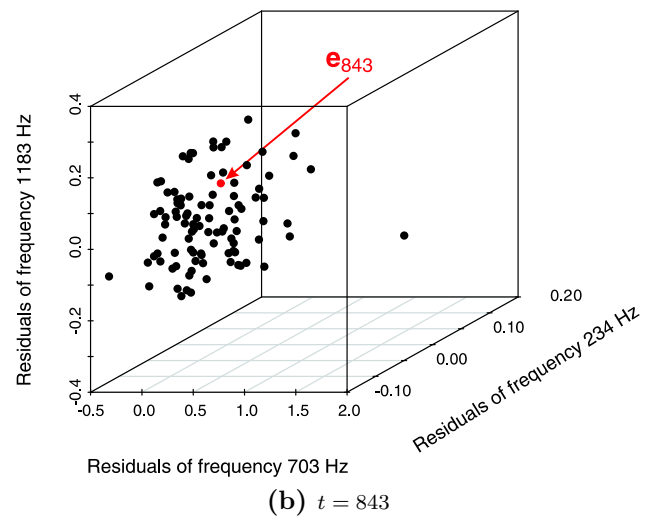
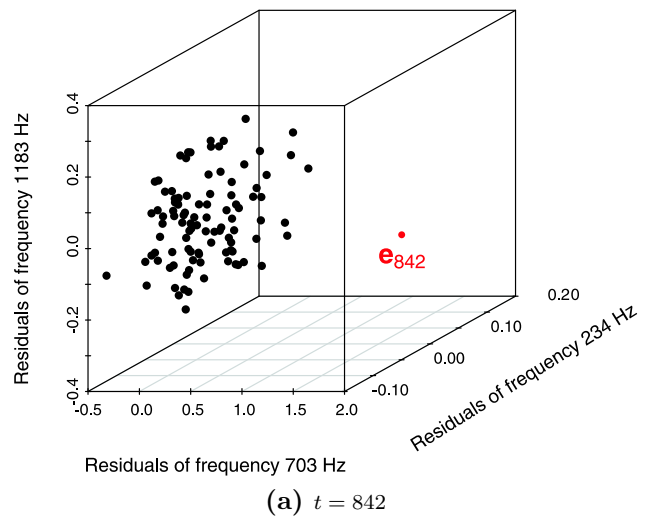


**Figure 8.8:** Plot of  $E_t = \{\mathbf{e}_{t-100+1}, \dots, \mathbf{e}_t\}$  (a)  $t = 842$  and (b)  $t = 843$

This page intentionally left blank



## Summary and Future Work

The main objective of this thesis is to develop on-line monitoring procedures for the early and reliable detection of chatter vibration in the BTA deep-hole drilling process. This chapter summarizes the content of thesis and identifies some important directions for future research.

### 9.1 Summary

In the first part of the thesis, a new distribution-free control chart for monitoring processes with multivariate quality measurements is developed. As it is shown in this thesis, the normality assumption of the collected data from the process is not valid. The main idea of the proposed  $r$ MEWMA control chart is to represent each multivariate observation by its corresponding data depth. In Chapter 2, data depths and the principles used to construct the new  $r$ MEWMA control chart are introduced. Its statistical design with respect to the asymptotic in-control ARL performance is proposed.

In Chapter 3, two important issues for the application of  $r$ MEWMA control charts are discussed. First, the effect of the use of reference samples of limited amount of observations on the in-control and out-of-control performances of  $r$ MEWMA monitoring procedures is studied using simulations. General recommendations for the required reference sample sizes so that the in-control and out-of-control performances of  $r$ MEWMA control charts approach their asymptotic counterparts are given. Second, it is shown that the geometrical nature of simplicial depth imply that simplicial  $r$ MEWMA control charts are less powerful than Mahalanobis  $r$ MEWMA control charts.

In Chapter 4, a simulation study is conducted in order to compare the in-control and out-of-control performances of  $r$ MEWMA control charts and the parametric MEWMA control charts.

The second part of the thesis is devoted to the introduction and modelling of the drilling process and experimental investigation of the performance of the proposed monitoring strategies. The principles of the drilling process are introduced in Chapter 5. Furthermore, previous experimental investigation conducted in order to study the dynamics of the process and its main results are reviewed.

In Chapter 6, time series analysis is used to provide a modelling approach in order to predict the temporal development of the process. It is used in Chapter 8 to setup the  $r$ MEWMA monitoring procedure. The empirical evidence of the proposed time series model is checked using several data sets.

In Chapter 7, amplitude-dependent exponential autoregressive time series modelling is used to describe the time varying dynamics of the process. The results showed that using this approach, an on-line procedure can be used to answer questions about the time varying dynamics of the process namely fixed points and limit cycles. Furthermore, it provides the basis of  $\text{ExpAr}(p)$  time series based control charts.

Finally, the performances of the proposed  $r$ MEWMA and  $\text{ExpAr}(p)$  time series based control charts are investigated using several data sets in Chapter 8. The results showed that the  $r$ MEWMA control charts quickly detect the start of the transition from stable drilling to chatter vibration. Furthermore, most of the out-of-control signals produced by these control charts are related to known changes in the dynamics of the process (i.e., guiding pads leave the starting bush, the tool is completely in the hole). For the  $\text{ExpAr}(40)$  time series based control charts, the results showed that they are less powerful than  $r$ MEWMA control charts. This is due to the “non-optimal” estimation procedure of the  $\text{ExpAr}(40)$  time series model parameters and the choice of its time lag  $p = 40$ .

## 9.2 Future Work

### 9.2.1 Multiple Frequency Modelling

In Chapter 6, the van der Pol model is used to describe the transition from stable drilling to chatter vibration in one frequency. Therefore, the amplitudes of the relevant frequencies are modelled separately. As noted by Weinert *et al.* (2004), the van der Pol model accounts for a subset of experimental results, especially when only one frequency dominates chatter vibration. Naturally, the model fails to capture all aspects of the process when this assumption becomes invalid. It is always the case when chatter vibration at the beginning of the drilling process is observed. Indeed, two or three frequencies dominate the process and they affect each other either by excitatory or inhibitory interaction. Therefore a more complicated model that include the interactions between the relevant frequencies is needed. In this case a multivariate time series model can be used instead to calculate the residuals. The proposed  $r$ MEWMA control chart can be easily used to monitor such residuals.

### 9.2.2 Integration of Process Monitoring and Adjustment

The objective of this work is to provide on-line monitoring strategies to detect chatter vibration as early as possible in order to adjust the process and suppress chatter vibration. Hence, a procedure to integrate process monitoring and adjustment is needed. A possible procedure can be summarized in the following steps:

1. Employ a control chart on-line to detect any possible process change.
2. Once the control chart has produced a signal, estimate the shift magnitude, identify the time point at which the shift has occurred and interpret the out-of-control signal.
3. Using the information of step 2 adjust the process based on a control scheme.

Future research should focus on step 2. If the control chart react to process change and produce an out-of-control signal, a procedure to estimate the shift magnitude, to identify the time point at which the shift has occurred and to interpret the out-of-control signal are needed.

Firstly, the estimation of the amount of shift in the process may help the process engineers to distinguish between out-of-control signals. Moreover, it provides a basis for the adequate corrective action in order to adjust the process. Secondly, the identification of the time point at which the shift has occurred may help the process engineers to adjust the process. Finally, the out-of-control interpretation is basic for the adjustment of the process. In fact, when the control chart indicates an out-of-control condition, it is important to determine which frequency, or combination of frequencies, of the multivariate process caused the process to go out-of-control. In practice, the identification of the type of chatter (i.e., chatter at the beginning of the drilling process, low-high frequency chatter) will usually make it easier for engineers to adjust the process.

This page intentionally left blank

Appendix **A**

**Tables on the Performance of  $r$  MEWMA  
and  $p$  MEWMA Control Charts**

**Table A.1:** In-control ( $\delta = 0$ ) and out-of-control ( $\delta \neq 0$ ) run length properties of Mahalanobis  $r$ MEWMA control charts with  $\lambda = 0.05$  and  $h = -0.169$  based on reference samples of size  $m$

$m$		Shift Magnitude $\delta$						
		0.0	0.5	1.0	1.5	2.0	2.5	3.0
10	ARL	766.26	764.05	756.17	744.60	729.75	714.32	699.50
	SDRL	762.02	761.96	761.61	760.86	760.45	758.67	757.25
	$Q(.10)$	83	81	73	61	47	34	25
	$Q(.50)$	533	530	522	510	494	479	462
	$Q(.90)$	1762	1759	1750	1737	1723	1705	1690
47	ARL	200.45	191.11	153.92	83.93	27.99	8.62	5.60
	SDRL	189.63	189.31	182.54	148.26	82.08	26.82	8.65
	$Q(.10)$	28	20	10	6	5	5	4
	$Q(.50)$	144	134	89	16	8	6	5
	$Q(.90)$	447	437	393	262	28	10	7
100	ARL	171.96	153.33	85.10	21.77	7.93	5.72	4.83
	SDRL	152.16	150.68	125.51	51.72	8.40	1.59	0.92
	$Q(.10)$	26	18	9	6	5	4	4
	$Q(.50)$	130	110	28	11	7	5	5
	$Q(.90)$	370	351	245	29	12	8	6
200	ARL	175.27	137.96	46.27	12.07	7.14	5.43	4.65
	StErr	151.49	145.27	80.76	11.26	2.61	1.34	0.81
	$Q(.10)$	26	16	8	6	5	4	4
	$Q(.50)$	136	82	21	10	6	5	4
	$Q(.90)$	376	334	91	20	10	7	6
500	ARL	189.77	116.08	26.19	10.79	6.85	5.30	4.56
	StErr	170.64	135.97	26.38	5.42	2.31	1.25	0.76
	$Q(.10)$	26	16	8	6	5	4	4
	$Q(.50)$	140	66	19	9	6	5	4
	$Q(.90)$	425	287	50	18	10	7	6
1000	ARL	196.66	98.58	23.73	10.52	6.76	5.25	4.53
	StErr	184.50	113.12	17.91	5.04	2.23	1.21	0.74
	$Q(.10)$	26	16	8	6	5	4	4
	$Q(.50)$	140	62	19	9	6	5	4
	$Q(.90)$	445	222	45	17	10	7	5
$\infty$	ARL	200.03	81.88	22.32	10.29	6.68	5.22	4.51
	SDRL	194.77	75.05	15.10	4.76	2.17	1.19	0.73
	$Q(.10)$	26	16	8	6	5	4	4
	$Q(.50)$	140	59	18	9	6	5	4
	$Q(.90)$	453	179	42	17	10	7	5

NOTE: ARL = average run length  
SDRL = standard deviation of run length distribution  
 $Q(q)$  =  $q$ th percentile of run length distribution

**Table A.2:** In-control ( $\delta = 0$ ) and out-of-control ( $\delta \neq 0$ ) run length properties of Mahalanobis  $r$ MEWMA control charts with  $\lambda = 0.1$  and  $h = -0.279$  based on reference samples of size  $m$

$m$		Shift Magnitude $\delta$						
		0.0	0.5	1.0	1.5	2.0	2.5	3.0
10	ARL	647.29	645.62	640.58	631.54	619.95	605.50	590.84
	SDRL	641.19	641.28	641.02	640.92	640.54	639.29	637.40
	$Q(.10)$	70	68	63	53	41	27	17
	$Q(.50)$	450	448	444	435	424	408	393
	$Q(.90)$	1489	1488	1482	1473	1461	1446	1428
41	ARL	199.30	193.05	165.56	106.89	44.33	13.44	5.79
	SDRL	191.38	191.55	188.45	166.97	112.75	52.17	17.12
	$Q(.10)$	27	20	9	6	4	4	4
	$Q(.50)$	141	134	104	19	8	5	4
	$Q(.90)$	449	443	413	322	132	11	7
100	ARL	178.39	161.66	97.71	26.64	7.53	5.15	4.41
	SDRL	163.13	161.73	141.74	68.24	12.04	1.58	0.79
	$Q(.10)$	26	16	8	5	4	4	4
	$Q(.50)$	132	114	29	10	6	5	4
	$Q(.90)$	389	372	283	33	11	7	5
200	ARL	181.27	146.76	55.55	12.10	6.54	4.93	4.30
	SDRL	162.45	156.65	98.90	17.06	2.75	1.30	0.65
	$Q(.10)$	26	15	7	5	4	4	4
	$Q(.50)$	137	89	22	9	6	4	4
	$Q(.90)$	394	356	144	21	10	7	5
500	ARL	192.08	124.75	28.74	10.31	6.27	4.82	4.26
	SDRL	175.87	146.12	38.36	6.00	2.39	1.18	0.60
	$Q(.10)$	26	15	7	5	4	4	4
	$Q(.50)$	140	71	19	9	6	4	4
	$Q(.90)$	431	312	56	18	9	6	5
1000	ARL	197.41	106.28	24.79	10.03	6.17	4.78	4.25
	SDRL	186.51	123.53	21.41	5.52	2.29	1.13	0.58
	$Q(.10)$	25	15	7	5	4	4	4
	$Q(.50)$	141	66	18	9	6	4	4
	$Q(.90)$	446	243	50	17	9	6	5
$\infty$	ARL	201.16	87.90	22.97	9.77	6.12	4.76	4.23
	SDRL	196.13	84.10	17.29	5.16	2.23	1.11	0.56
	$Q(.10)$	25	14	7	5	4	4	4
	$Q(.50)$	141	62	18	8	6	4	4
	$Q(.90)$	456	195	46	16	9	6	5

NOTE: ARL = average run length  
 SDRL = standard deviation of run length distribution  
 $Q(q)$  =  $q$ th percentile of run length distribution

**Table A.3:** In-control ( $\delta = 0$ ) and out-of-control ( $\delta \neq 0$ ) run length properties of Mahalanobis  $r$ MEWMA control charts with  $\lambda = 0.2$  and  $h = -0.435$  based on reference samples of size  $m$

$m$		Shift Magnitude $\delta$						
		0.0	0.5	1.0	1.5	2.0	2.5	3.0
10	ARL	427.12	426.15	422.95	416.50	406.57	394.16	380.78
	SDRL	424.32	424.29	424.26	423.72	423.00	421.94	420.50
	$Q(.10)$	46	45	42	36	26	14	6
	$Q(.50)$	296	295	292	286	275	262	248
	$Q(.90)$	985	984	981	975	964	952	937
31	ARL	200.54	196.66	179.91	141.45	86.38	39.88	15.14
	SDRL	194.34	194.18	192.76	184.71	156.57	110.59	63.81
	$Q(.10)$	26	21	9	5	4	3	3
	$Q(.50)$	141	137	120	71	9	5	4
	$Q(.90)$	454	451	433	382	281	119	8
100	ARL	181.87	166.66	109.11	34.99	7.90	4.48	3.63
	SDRL	170.94	169.89	153.88	89.21	22.27	2.73	0.93
	$Q(.10)$	24	15	7	4	3	3	3
	$Q(.50)$	132	115	34	9	5	4	3
	$Q(.90)$	404	388	309	64	11	7	5
200	ARL	184.55	155.20	67.11	13.38	5.96	4.22	3.51
	SDRL	171.25	167.85	118.04	28.35	3.80	1.44	0.81
	$Q(.10)$	24	14	6	4	3	3	3
	$Q(.50)$	136	95	23	8	5	4	3
	$Q(.90)$	409	376	202	23	10	6	5
500	ARL	193.26	132.92	33.56	10.16	5.65	4.11	3.45
	SDRL	182.22	157.14	52.13	7.24	2.64	1.32	0.75
	$Q(.10)$	25	14	6	4	3	3	3
	$Q(.50)$	139	76	20	8	5	4	3
	$Q(.90)$	436	336	68	19	9	6	4
1000	ARL	197.22	114.21	27.09	9.78	5.56	4.08	3.43
	SDRL	189.28	133.08	27.25	6.46	2.54	1.29	0.73
	$Q(.10)$	24	14	6	4	3	3	3
	$Q(.50)$	139	70	19	8	5	4	3
	$Q(.90)$	449	266	57	18	9	6	4
$\infty$	ARL	199.74	94.81	24.55	9.46	5.49	4.04	3.42
	SDRL	196.10	93.09	20.62	5.94	2.42	1.26	0.71
	$Q(.10)$	24	13	6	4	3	3	3
	$Q(.50)$	139	65	18	8	5	4	3
	$Q(.90)$	454	215	51	17	9	6	4

NOTE: ARL = average run length  
SDRL = standard deviation of run length distribution  
 $Q(q)$  =  $q$ th percentile of run length distribution



**Table A.4:** In-control ( $\delta = 0$ ) and out-of-control ( $\delta \neq 0$ ) run length properties of Mahalanobis  $r$ MEWMA control charts with  $\lambda = 0.3$  and  $h = -0.551$  based on reference samples of size  $m$

$m$		Shift Magnitude $\delta$						
		0.0	0.5	1.0	1.5	2.0	2.5	3.0
10	ARL	342.18	341.42	339.42	334.52	326.63	316.80	306.92
	SDRL	338.74	338.62	338.77	338.89	338.54	337.80	337.35
	$Q(.10)$	38	37	35	30	22	12	5
	$Q(.50)$	238	237	236	230	222	212	201
	$Q(.90)$	786	785	784	779	771	759	749
28	ARL	199.77	196.56	183.44	151.96	105.25	59.10	28.04
	SDRL	193.98	193.91	193.13	187.73	169.44	133.97	93.43
	$Q(.10)$	25	21	9	5	3	3	3
	$Q(.50)$	140	137	124	86	12	5	4
	$Q(.90)$	456	452	438	399	325	205	44
100	ARL	185.15	170.90	118.21	43.15	9.17	4.32	3.47
	SDRL	176.11	175.05	162.56	104.09	31.47	4.67	0.91
	$Q(.10)$	24	15	6	4	3	3	3
	$Q(.50)$	133	118	40	10	5	4	3
	$Q(.90)$	414	398	329	124	12	6	5
200	ARL	188.05	160.85	76.68	15.85	5.88	4.02	3.36
	SDRL	177.44	173.60	131.29	40.39	4.87	1.49	0.75
	$Q(.10)$	23	14	6	4	3	3	3
	$Q(.50)$	138	99	25	8	5	3	3
	$Q(.90)$	420	389	234	26	10	6	4
500	ARL	196.22	138.36	38.11	10.40	5.47	3.92	3.32
	SDRL	185.11	163.28	63.83	8.37	2.85	1.34	0.69
	$Q(.10)$	24	14	6	4	3	3	3
	$Q(.50)$	141	79	21	8	5	3	3
	$Q(.90)$	445	350	78	20	9	6	4
1000	ARL	199.35	119.63	29.83	9.91	5.38	3.88	3.31
	SDRL	192.86	140.93	32.33	7.28	2.73	1.31	0.67
	$Q(.10)$	24	13	6	4	3	3	3
	$Q(.50)$	141	73	20	8	5	3	3
	$Q(.90)$	455	280	65	19	9	6	4
$\infty$	ARL	201.00	99.02	26.16	9.58	5.29	3.85	3.29
	SDRL	197.71	98.23	23.12	6.66	2.61	1.26	0.65
	$Q(.10)$	24	13	6	4	3	3	3
	$Q(.50)$	141	68	19	8	5	3	3
	$Q(.90)$	459	223	56	18	9	5	4

NOTE: ARL = average run length  
 SDRL = standard deviation of run length distribution  
 $Q(q)$  =  $q$ th percentile of run length distribution

**Table A.5:** In-control ( $\delta = 0$ ) and out-of-control ( $\delta \neq 0$ ) run length properties of simplicial  $r$ MEWMA control charts with  $\lambda = 0.05$  and  $h = -0.169$  based on reference samples of size  $m$

$m$		Shift Magnitude $\delta$						
		0.0	0.5	1.0	1.5	2.0	2.5	3.0
100	ARL	172.81	153.57	92.25	26.66	9.20	6.39	5.54
	SDRL	152.84	152.08	133.61	61.88	15.95	1.87	1.05
	$Q(.10)$	27	18	9	6	5	5	5
	$Q(.50)$	130	110	29	12	7	6	5
	$Q(.90)$	375	355	266	35	13	9	7
200	ARL	175.79	140.26	48.23	12.49	7.51	5.81	5.04
	SDRL	152.35	148.52	83.26	10.32	2.78	1.42	0.83
	$Q(.10)$	26	17	9	6	5	4	4
	$Q(.50)$	137	84	22	10	7	5	5
	$Q(.90)$	378	340	97	21	11	8	6

NOTE: ARL = average run length  
 SDRL = standard deviation of run length distribution  
 $Q(q)$  =  $q$ th percentile of run length distribution

**Table A.6:** In-control ( $\delta = 0$ ) and out-of-control ( $\delta \neq 0$ ) run length properties of simplicial  $r$ MEWMA control charts with  $\lambda = 0.1$  and  $h = -0.279$  based on reference samples of size  $m$

$m$		Shift Magnitude $\delta$						
		0.0	0.5	1.0	1.5	2.0	2.5	3.0
100	ARL	181.56	162.46	105.28	33.88	9.28	5.76	4.86
	SDRL	165.62	163.62	146.44	82.07	19.13	2.03	1.11
	$Q(.10)$	26	16	8	5	4	4	4
	$Q(.50)$	135	114	32	11	7	5	5
	$Q(.90)$	398	375	302	52	13	8	6
200	ARL	181.66	150.83	60.65	13.25	6.91	5.16	4.49
	SDRL	163.66	161.99	107.64	26.04	3.04	1.42	0.82
	$Q(.10)$	26	16	8	5	4	4	4
	$Q(.50)$	140	91	23	9	6	5	4
	$Q(.90)$	391	360	170	22	11	7	6

NOTE: ARL = average run length  
 SDRL = standard deviation of run length distribution  
 $Q(q)$  =  $q$ th percentile of run length distribution

**Table A.7:** In-control ( $\delta = 0$ ) and out-of-control ( $\delta \neq 0$ ) run length properties of simplicial  $r$ MEWMA control charts with  $\lambda = 0.2$  and  $h = -0.435$  based on reference samples of size  $m$

$m$		Shift Magnitude $\delta$						
		0.0	0.5	1.0	1.5	2.0	2.5	3.0
100	ARL	186.39	169.38	118.15	46.50	11.92	5.51	4.26
	SDRL	176.97	174.44	161.38	106.30	38.02	9.82	1.30
	$Q(.10)$	25	16	7	4	4	3	3
	$Q(.50)$	133	116	40	11	6	4	4
	$Q(.90)$	415	399	330	135	14	8	6
200	ARL	186.55	158.92	73.79	15.34	6.43	4.56	3.81
	SDRL	176.87	173.57	127.70	34.09	3.80	1.60	0.95
	$Q(.10)$	24	15	7	4	3	3	3
	$Q(.50)$	137	96	24	9	5	4	4
	$Q(.90)$	413	377	221	25	11	7	5

NOTE: ARL = average run length  
 SDRL = standard deviation of run length distribution  
 $Q(q)$  =  $q$ th percentile of run length distribution

**Table A.8:** In-control ( $\delta = 0$ ) and out-of-control ( $\delta \neq 0$ ) run length properties of simplicial  $r$ MEWMA control charts with  $\lambda = 0.3$  and  $h = -0.551$  based on reference samples of size  $m$

$m$		Shift Magnitude $\delta$						
		0.0	0.5	1.0	1.5	2.0	2.5	3.0
100	ARL	193.06	177.47	129.83	59.24	17.23	5.92	4.12
	SDRL	186.12	185.20	174.97	127.57	61.12	17.08	5.30
	$Q(.10)$	24	15	7	4	3	3	3
	$Q(.50)$	138	122	50	11	6	4	4
	$Q(.90)$	431	415	352	191	18	8	6
200	ARL	191.00	167.77	86.78	20.30	6.58	4.31	3.58
	SDRL	184.23	183.79	145.91	57.37	9.46	1.75	0.98
	$Q(.10)$	24	15	6	4	3	3	3
	$Q(.50)$	138	104	28	9	5	4	3
	$Q(.90)$	426	405	260	31	11	6	5

NOTE: ARL = average run length  
 SDRL = standard deviation of run length distribution  
 $Q(q)$  =  $q$ th percentile of run length distribution

**Table A.9:** In-control ( $\delta = 0$ ) and out-of-control ( $\delta \neq 0$ ) run length properties of Mahalanobis  $r$ MEWMA and  $p$ MEWMA control charts with bivariate normal observations. Reference samples of size  $m = 200$  are used. The control limits are selected using simulation in order to achieve an in-control ARL of 200

$\delta$		$p$ MEWMA		$r$ MEWMA			
				$\lambda$			
				0.05	0.10	0.20	0.30
0.0	ARL <sub>0</sub>	201.56	202.94	198.95	199.48	198.77	
	SDRL <sub>0</sub>	190.14	177.94	180.68	186.97	190.36	
	$Q_0(.10)$	32	30	27	25	24	
	$Q_0(.50)$	143	158	150	146	145	
	$Q_0(.90)$	451	438	432	444	447	
0.5	ARL <sub>1</sub>	33.32	163.26	163.80	170.90	173.85	
	SDRL <sub>1</sub>	35.95	175.13	176.26	186.05	190.73	
	$Q_1(.10)$	12	18	17	15	15	
	$Q_1(.50)$	25	98	99	105	106	
	$Q_1(.90)$	59	390	392	413	422	
1.0	ARL <sub>1</sub>	11.86	54.23	61.91	74.85	85.10	
	SDRL <sub>1</sub>	4.7	98.73	112.34	133.22	145.42	
	$Q_1(.10)$	7	9	8	7	6	
	$Q_1(.50)$	11	23	23	24	26	
	$Q_1(.90)$	18	115	173	225	259	
1.5	ARL <sub>1</sub>	7.51	12.55	12.72	14.16	16.05	
	SDRL <sub>1</sub>	2.21	10.84	19.45	36.26	40.44	
	$Q_1(.10)$	5	6	5	4	4	
	$Q_1(.50)$	7	10	9	9	8	
	$Q_1(.90)$	10	21	21	23	25	
2.0	ARL <sub>1</sub>	5.57	7.51	6.70	6.09	6.09	
	SDRL <sub>1</sub>	1.35	2.74	2.86	3.19	8.82	
	$Q_1(.10)$	4	5	4	3	3	
	$Q_1(.50)$	5	7	6	5	5	
	$Q_1(.90)$	7	11	10	10	10	
2.5	ARL <sub>1</sub>	4.44	5.73	5.00	4.30	4.07	
	SDRL <sub>1</sub>	0.93	1.39	1.33	1.51	1.52	
	$Q_1(.10)$	3	4	4	3	3	
	$Q_1(.50)$	4	5	5	4	4	
	$Q_1(.90)$	6	8	7	6	6	
3.0	ARL <sub>1</sub>	3.78	4.90	4.35	3.55	3.39	
	SDRL <sub>1</sub>	0.72	0.84	0.70	0.84	0.80	
	$Q_1(.10)$	3	4	4	3	3	
	$Q_1(.50)$	4	5	4	3	3	
	$Q_1(.90)$	5	6	5	5	4	

NOTE: ARL = average run length  
 SDRL = standard deviation of run length distribution  
 $Q(q)$  =  $q$ th percentile of run length distribution

**Table A.10:** In-control ( $\delta = 0$ ) and out-of-control ( $\delta \neq 0$ ) run length properties of Mahalanobis  $r$ MEWMA and  $p$ MEWMA control charts with bivariate  $t(3)$  observations. Reference samples of size  $m = 200$  are used. The control limits are selected using simulation in order to achieve an in-control ARL of 200

$\delta$		$p$ MEWMA	$r$ MEWMA			
			$\lambda$			
			0.05	0.10	0.20	0.30
0.0	ARL <sub>0</sub>	153.67	200.14	197.14	199.62	199.73
	SDRL <sub>0</sub>	139.45	173.66	176.54	186.79	189.14
	$Q_0(.10)$	24	30	28	27	26
	$Q_0(.50)$	114	156	149	146	146
	$Q_0(.90)$	337	429	426	438	437
0.5	ARL <sub>1</sub>	33.00	119.62	129.16	149.83	163.62
	SDRL <sub>1</sub>	40.20	151.53	158.89	175.92	185.20
	$Q_1(.10)$	11	14	13	12	13
	$Q_1(.50)$	24	52	59	78	95
	$Q_1(.90)$	58	325	344	384	406
1.0	ARL <sub>1</sub>	11.42	18.07	20.35	31.34	47.55
	SDRL <sub>1</sub>	6.99	34.83	46.74	78.52	104.88
	$Q_1(.10)$	6	7	6	5	5
	$Q_1(.50)$	10	12	12	12	14
	$Q_1(.90)$	17	26	30	46	104
1.5	ARL <sub>1</sub>	7.16	7.62	6.89	6.89	8.10
	SDRL <sub>1</sub>	3.34	2.51	2.77	8.92	20.76
	$Q_1(.10)$	5	5	5	4	4
	$Q_1(.50)$	7	7	6	6	6
	$Q_1(.90)$	10	10	10	10	12
2.0	ARL <sub>1</sub>	5.29	5.81	5.07	5.54	4.30
	SDRL <sub>1</sub>	1.59	1.11	1.16	1.74	1.57
	$Q_1(.10)$	4	5	4	4	3
	$Q_1(.50)$	5	6	5	4	4
	$Q_1(.90)$	7	7	6	6	6
2.5	ARL <sub>1</sub>	4.26	5.17	4.36	3.83	3.46
	SDRL <sub>1</sub>	1.11	0.55	0.64	0.77	1.01
	$Q_1(.10)$	3	5	4	3	3
	$Q_1(.50)$	4	5	4	4	4
	$Q_1(.90)$	5	6	5	5	
3.0	ARL <sub>1</sub>	3.61	4.93	4.11	3.40	3.15
	SDRL <sub>1</sub>	0.88	0.45	0.36	0.57	0.46
	$Q_1(.10)$	3	4	4	3	3
	$Q_1(.50)$	3	5	4	3	3
	$Q_1(.90)$	5	5	4	4	4

NOTE: ARL = average run length  
 SDRL = standard deviation of run length distribution  
 $Q(q)$  =  $q$ th percentile of run length distribution

**Table A.11:** In-control ( $\delta = 0$ ) and out-of-control ( $\delta \neq 0$ ) run length properties of Mahalanobis  $r$ MEWMA and  $p$ MEWMA control charts with bivariate  $G(1, 1)$  observations. Reference samples of size  $m = 200$  are used. The control limits are selected using simulation in order to achieve an in-control ARL of 200

$\delta$		$p$ MEWMA		$r$ MEWMA			
				$\lambda$			
				0.05	0.10	0.20	0.30
0.0	ARL <sub>0</sub>	192.90	203.20	200.34	198.98	200.38	
	SDRL <sub>0</sub>	177.97	179.22	182.15	185.14	189.18	
	$Q_0(.10)$	30	30	28	26	26	
	$Q_0(.50)$	140	157	150	146	146	
	$Q_0(.90)$	429	439	437	442	449	
0.5	ARL <sub>1</sub>	33.39	163.88	154.79	153.36	160.24	
	SDRL <sub>1</sub>	37.82	196.73	191.18	186.00	187.41	
	$Q_1(.10)$	12	12	11	10	11	
	$Q_1(.50)$	25	55	57	69	87	
	$Q_1(.90)$	58	440	418	403	407	
1.0	ARL <sub>1</sub>	11.89	93.73	88.80	77.36	75.87	
	SDRL <sub>1</sub>	4.81	170.64	166.19	150.81	145.58	
	$Q_1(.10)$	7	7	6	5	5	
	$Q_1(.50)$	11	15	13	14	16	
	$Q_1(.90)$	18	346	321	277	255	
1.5	ARL <sub>1</sub>	7.42	21.59	17.65	18.75	19.11	
	SDRL <sub>1</sub>	2.25	72.57	61.82	67.39	64.84	
	$Q_1(.10)$	5	5	5	4	4	
	$Q_1(.50)$	7	8	7	6	6	
	$Q_1(.90)$	10	19	18	19	21	
2.0	ARL <sub>1</sub>	5.48	6.54	5.82	5.50	5.17	
	SDRL <sub>1</sub>	1.35	7.07	7.16	12.61	9.19	
	$Q_1(.10)$	4	5	4	4	3	
	$Q_1(.50)$	5	6	5	4	4	
	$Q_1(.90)$	7	8	8	7	8	
2.5	ARL <sub>1</sub>	4.42	5.33	4.56	4.06	3.69	
	SDRL <sub>1</sub>	0.96	0.73	0.83	0.87	0.96	
	$Q_1(.10)$	3	5	4	3	3	
	$Q_1(.50)$	4	5	4	4	3	
	$Q_1(.90)$	6	6	5	5	5	
3.0	ARL <sub>1</sub>	3.74	5.03	4.18	3.58	3.26	
	SDRL <sub>1</sub>	0.76	0.48	0.50	0.64	0.58	
	$Q_1(.10)$	3	5	4	3	3	
	$Q_1(.50)$	4	5	4	4	3	
	$Q_1(.90)$	5	5	5	4	4	

NOTE: ARL = average run length  
SDRL = standard deviation of run length distribution  
 $Q(q)$  =  $q$ th percentile of run length distribution

**Table A.12:** In-control ( $\delta = 0$ ) and out-of-control ( $\delta \neq 0$ ) run length properties of Mahalanobis  $r$ MEWMA and  $p$ MEWMA control charts with bivariate normal observations. Reference samples of size  $m = 10000$  are used.

$\delta$		$p$ MEWMA		$r$ MEWMA			
				$\lambda$			
				0.05	0.10	0.20	0.30
0.0	ARL <sub>0</sub>	199.10	201.93	203.44	201.36	202.37	
	SDRL <sub>0</sub>	182.71	196.04	198.04	195.38	202.05	
	$Q_0(.10)$	34	27	26	25	24	
	$Q_0(.50)$	145	140	144	140	138	
	$Q_0(.90)$	445	467	451	459	465	
0.5	ARL <sub>1</sub>	26.78	82.82	88.10	94.39	99.62	
	SDRL <sub>1</sub>	15.18	77.13	85.18	92.37	99.04	
	$Q_1(.10)$	12	16	15	14	13	
	$Q_1(.50)$	23	58	62	66	68	
	$Q_1(.90)$	47	182	194	213	226	
1.0	ARL <sub>1</sub>	11.19	22.41	23.15	24.93	26.31	
	SDRL <sub>1</sub>	4.07	15.34	17.33	20.96	23.01	
	$Q_1(.10)$	7	8	7	6	6	
	$Q_1(.50)$	11	18	18	19	19	
	$Q_1(.90)$	17	42	47	52	57	
1.5	ARL <sub>1</sub>	7.17	10.31	9.76	9.46	9.59	
	SDRL <sub>1</sub>	2.07	4.78	5.13	6.05	6.64	
	$Q_1(.10)$	5	6	5	4	4	
	$Q_1(.50)$	7	9	8	8	8	
	$Q_1(.90)$	10	17	16	17	18	
2.0	ARL <sub>1</sub>	5.28	6.64	6.12	5.50	5.33	
	SDRL <sub>1</sub>	1.29	2.13	2.23	2.45	2.59	
	$Q_1(.10)$	4	5	4	3	3	
	$Q_1(.50)$	5	6	6	5	5	
	$Q_1(.90)$	7	9	9	9	9	
2.5	ARL <sub>1</sub>	4.24	5.23	4.77	4.03	3.87	
	SDRL <sub>1</sub>	0.90	1.19	1.12	1.24	1.27	
	$Q_1(.10)$	3	4	4	3	3	
	$Q_1(.50)$	4	5	4	4	3	
	$Q_1(.90)$	5	7	6	6	6	
3.0	ARL <sub>1</sub>	3.55	4.51	4.23	3.42	3.29	
	SDRL <sub>1</sub>	0.69	0.74	0.56	0.72	0.63	
	$Q_1(.10)$	3	4	4	3	3	
	$Q_1(.50)$	3	4	4	3	3	
	$Q_1(.90)$	4	5	5	4	4	

NOTE: ARL = average run length  
 SDRL = standard deviation of run length distribution  
 $Q(q)$  =  $q$ th percentile of run length distribution

**Table A.13:** In-control ( $\delta = 0$ ) and out-of-control ( $\delta \neq 0$ ) run length properties of Mahalanobis  $r$ MEWMA and  $p$ MEWMA control charts with bivariate  $t(3)$  observations. Reference samples of size  $m = 10000$  are used.

$\delta$		$p$ MEWMA		$r$ MEWMA			
				$\lambda$			
				0.05	0.10	0.20	0.30
0.0	ARL <sub>0</sub>	194.95	199.17	206.00	198.36	200.70	
	SDRL <sub>0</sub>	189.54	195.12	203.44	193.40	198.41	
	$Q_0(.10)$	28	27	26	24	24	
	$Q_0(.50)$	137	140	144	138	141	
	$Q_0(.90)$	440	452	467	446	461	
0.5	ARL <sub>1</sub>	28.25	44.98	51.56	64.97	77.98	
	SDRL <sub>1</sub>	18.07	36.01	45.10	61.21	75.98	
	$Q_1(.10)$	12	13	12	11	12	
	$Q_1(.50)$	25	34	38	46	54	
	$Q_1(.90)$	48	91	108	143	175	
1.0	ARL <sub>1</sub>	11.31	11.69	11.55	12.68	14.71	
	SDRL <sub>1</sub>	4.44	5.00	5.89	7.96	10.96	
	$Q_1(.10)$	7	7	6	5	5	
	$Q_1(.50)$	11	11	10	11	11	
	$Q_1(.90)$	16	18	19	23	29	
1.5	ARL <sub>1</sub>	7.06	6.76	6.19	5.80	5.82	
	SDRL <sub>1</sub>	2.06	1.67	1.76	2.16	2.55	
	$Q_1(.10)$	5	5	4	4	4	
	$Q_1(.50)$	7	6	6	5	5	
	$Q_1(.90)$	9	9	9	8	9	
2.0	ARL <sub>1</sub>	5.23	5.36	4.71	4.25	3.92	
	SDRL <sub>1</sub>	1.24	0.78	0.90	0.96	1.11	
	$Q_1(.10)$	4	5	4	3	3	
	$Q_1(.50)$	5	5	5	4	4	
	$Q_1(.90)$	7	6	6	5	5	
2.5	ARL <sub>1</sub>	4.19	4.79	4.18	3.56	3.27	
	SDRL <sub>1</sub>	0.89	0.60	0.46	0.65	0.58	
	$Q_1(.10)$	3	4	4	3	3	
	$Q_1(.50)$	4	5	4	3	3	
	$Q_1(.90)$	5	5	5	4	4	
3.0	ARL <sub>1</sub>	3.51	4.29	4.05	3.19	3.07	
	SDRL <sub>1</sub>	0.70	0.50	0.26	0.45	0.33	
	$Q_1(.10)$	3	4	4	3	3	
	$Q_1(.50)$	3	4	4	3	3	
	$Q_1(.90)$	4	5	4	4	3	

NOTE: ARL = average run length  
SDRL = standard deviation of run length distribution  
 $Q(q)$  =  $q$ th percentile of run length distribution



**Table A.14:** In-control ( $\delta = 0$ ) and out-of-control ( $\delta \neq 0$ ) run length properties of Mahalanobis  $r$ MEWMA and  $p$ MEWMA control charts with bivariate  $G(1, 1)$  distributions. Reference samples of size  $m = 10000$  are used.

$\delta$		$p$ MEWMA		$r$ MEWMA			
				$\lambda$			
				0.05	0.10	0.20	0.30
0.0	ARL <sub>0</sub>	196.60	200.54	200.77	199.52	201.65	
	SDRL <sub>0</sub>	191.07	192.59	195.76	195.85	198.02	
	$Q_0(.10)$	30	25	25	24	23	
	$Q_0(.50)$	136	140	142	140	140	
	$Q_0(.90)$	441	465	453	450	458	
0.5	ARL <sub>1</sub>	26.87	280.41	169.13	114.92	101.73	
	SDRL <sub>1</sub>	15.25	677.57	337.32	193.47	147.18	
	$Q_1(.10)$	12	10	9	9	10	
	$Q_1(.50)$	23	36	37	42	49	
	$Q_1(.90)$	47	782	486	314	253	
1.0	ARL <sub>1</sub>	11.28	30.14	27.64	24.52	25.19	
	SDRL <sub>1</sub>	4.13	53.67	43.71	34.57	34.50	
	$Q_1(.10)$	7	6	6	5	5	
	$Q_1(.50)$	11	12	12	12	13	
	$Q_1(.90)$	17	69	69	60	60	
1.5	ARL <sub>1</sub>	7.16	8.74	8.19	7.83	7.84	
	SDRL <sub>1</sub>	2.02	4.76	5.14	5.68	6.18	
	$Q_1(.10)$	5	5	5	4	4	
	$Q_1(.50)$	7	7	7	6	6	
	$Q_1(.90)$	10	14	14	14	14	
2.0	ARL <sub>1</sub>	5.26	5.82	5.17	4.69	4.42	
	SDRL <sub>1</sub>	1.24	1.24	1.32	1.41	1.61	
	$Q_1(.10)$	4	5	4	4	3	
	$Q_1(.50)$	5	5	5	4	4	
	$Q_1(.90)$	7	7	7	6	6	
2.5	ARL <sub>1</sub>	4.21	5.01	4.36	3.81	3.50	
	SDRL <sub>1</sub>	0.89	0.70	0.71	0.76	0.78	
	$Q_1(.10)$	3	4	4	3	3	
	$Q_1(.50)$	4	5	4	4	3	
	$Q_1(.90)$	5	6	5	4	4	
3.0	ARL <sub>1</sub>	3.53	4.56	4.09	3.38	3.15	
	SDRL <sub>1</sub>	0.68	0.63	0.38	0.58	0.46	
	$Q_1(.10)$	3	4	4	3	3	
	$Q_1(.50)$	3	5	4	3	3	
	$Q_1(.90)$	4	5	4	4	4	

NOTE: ARL = average run length  
 SDRL = standard deviation of run length distribution  
 $Q(q)$  =  $q$ th percentile of run length distribution

**Table A.15:** In-control ( $\delta = 0$ ) and out-of-control ( $\delta \neq 0$ ) run length properties of simplicial  $r$ MEWMA control charts with bivariate normal observations. Reference samples of size  $m = 200$  are used. The control limits are selected using simulation in order to achieve an in-control ARL of 200

		$r$ MEWMA			
		$\lambda$			
$\delta$		0.05	0.10	0.20	0.30
0.0	ARL <sub>0</sub>	206.39	201.61	202.39	200.48
	SDRL <sub>0</sub>	183.34	179.83	193.32	192.14
	$Q_0(.10)$	29	29	28	27
	$Q_0(.50)$	158	153	146	145
	$Q_0(.90)$	444	439	443	438
0.5	ARL <sub>1</sub>	165.43	165.29	174.43	182.31
	SDRL <sub>1</sub>	172.56	169.86	189.19	196.39
	$Q_1(.10)$	19	17	17	16
	$Q_1(.50)$	102	102	107	118
	$Q_1(.90)$	394	396	415	436
1.0	ARL <sub>1</sub>	57.06	74.83	86.97	97.64
	SDRL <sub>1</sub>	102.64	132.46	144.88	158.13
	$Q_1(.10)$	9	8	7	7
	$Q_1(.50)$	24	24	27	31
	$Q_1(.90)$	134	224	264	286
1.5	ARL <sub>1</sub>	14.65	13.80	17.06	22.27
	SDRL <sub>1</sub>	25.59	29.54	42.69	58.84
	$Q_1(.10)$	6	5	4	4
	$Q_1(.50)$	11	10	9	10
	$Q_1(.90)$	23	23	27	34
2.0	ARL <sub>1</sub>	7.98	7.00	6.76	6.79
	SDRL <sub>1</sub>	2.98	2.96	3.79	9.67
	$Q_1(.10)$	5	4	4	3
	$Q_1(.50)$	7	6	6	5
	$Q_1(.90)$	12	11	11	11
2.5	ARL <sub>1</sub>	6.11	5.25	4.62	4.41
	SDRL <sub>1</sub>	1.43	1.45	1.62	1.85
	$Q_1(.10)$	5	4	3	3
	$Q_1(.50)$	6	5	4	4
	$Q_1(.90)$	8	7	7	7
3.0	ARL <sub>1</sub>	5.29	4.57	3.86	3.60
	SDRL <sub>1</sub>	0.74	0.85	0.96	0.97
	$Q_1(.10)$	5	4	3	3
	$Q_1(.50)$	5	4	4	3
	$Q_1(.90)$	6	6	5	5

NOTE: ARL = average run length  
SDRL = standard deviation of run length distribution  
 $Q(q)$  =  $q$ th percentile of run length distribution

**Table A.16:** In-control ( $\delta = 0$ ) and out-of-control ( $\delta \neq 0$ ) run length properties of simplicial  $r$ MEWMA control charts with bivariate  $t(3)$  observations. Reference samples of size  $m = 200$  are used. The control limits are selected using simulation in order to achieve an in-control ARL of 200

		$r$ MEWMA			
		$\lambda$			
$\delta$		0.05	0.10	0.20	0.30
0.0	ARL <sub>0</sub>	197.97	189.90	191.20	202.48
	SDRL <sub>0</sub>	178.79	174.42	178.28	190.18
	$Q_0(.10)$	31	26	27	27
	$Q_0(.50)$	144	138	137	148
	$Q_0(.90)$	438	413	418	451
0.5	ARL <sub>1</sub>	126.13	129.56	146.84	156.12
	SDRL <sub>1</sub>	160.42	160.86	169.37	180.99
	$Q_1(.10)$	14	12	12	12
	$Q_1(.50)$	56	60	79	86
	$Q_1(.90)$	340	343	368	401
1.0	ARL <sub>1</sub>	18.50	20.91	36.16	56.45
	SDRL <sub>1</sub>	42.81	44.91	85.58	122.68
	$Q_1(.10)$	7	6	6	5
	$Q_1(.50)$	13	12	13	15
	$Q_1(.90)$	28	31	56	159
1.5	ARL <sub>1</sub>	7.87	7.05	6.86	10.16
	SDRL <sub>1</sub>	2.40	2.64	3.85	33.95
	$Q_1(.10)$	6	5	4	4
	$Q_1(.50)$	7	6	6	6
	$Q_1(.90)$	11	10	11	14
2.0	ARL <sub>1</sub>	6.00	5.25	4.71	4.63
	SDRL <sub>1</sub>	1.12	1.26	1.38	1.83
	$Q_1(.10)$	5	4	4	3
	$Q_1(.50)$	6	5	4	4
	$Q_1(.90)$	8	7	6	7
2.5	ARL <sub>1</sub>	5.36	4.57	3.99	3.68
	SDRL <sub>1</sub>	0.69	0.74	0.77	0.89
	$Q_1(.10)$	5	4	3	3
	$Q_1(.50)$	5	4	4	3
	$Q_1(.90)$	6	5	5	5
3.0	ARL <sub>1</sub>	5.05	4.25	3.68	3.35
	SDRL <sub>1</sub>	0.48	0.49	0.64	0.64
	$Q_1(.10)$	5	4	3	3
	$Q_1(.50)$	5	4	4	3
	$Q_1(.90)$	6	5	4	4

NOTE: ARL = average run length  
 SDRL = standard deviation of run length distribution  
 $Q(q)$  =  $q$ th percentile of run length distribution

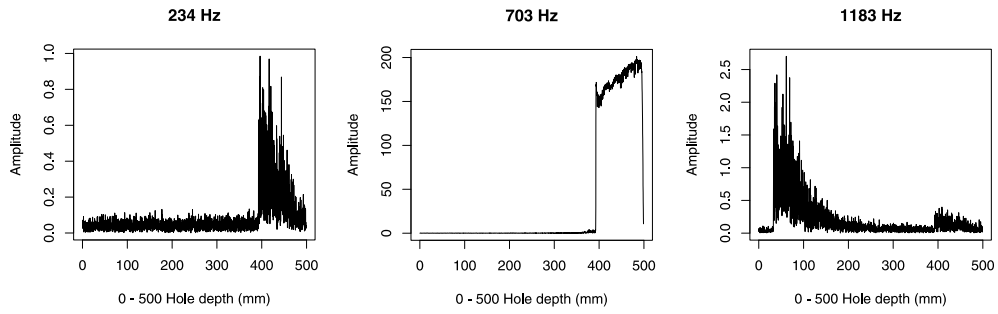
**Table A.17:** In-control ( $\delta = 0$ ) and out-of-control ( $\delta \neq 0$ ) run length properties of simplicial  $r$ MEWMA control charts with bivariate  $G(1, 1)$  distributions. Reference samples of size  $m = 200$  are used. The control limits are selected using simulation in order to achieve an in-control ARL of 200

		$r$ MEWMA			
		$\lambda$			
$\delta$		0.05	0.10	0.20	0.30
0.0	ARL <sub>0</sub>	201.53	197.23	205.15	202.85
	SDRL <sub>0</sub>	171.20	179.05	191.49	186.99
	$Q_0(.10)$	31	27	26	27
	$Q_0(.50)$	157	147	149	153
	$Q_0(.90)$	421	427	459	441
0.5	ARL <sub>1</sub>	155.72	154.13	150.76	140.30
	SDRL <sub>1</sub>	202.24	204.45	208.87	197.62
	$Q_1(.10)$	7	6	4	4
	$Q_1(.50)$	29	26	26	24
	$Q_1(.90)$	431	434	443	412
1.0	ARL <sub>1</sub>	117.92	115.43	112.33	111.38
	SDRL <sub>1</sub>	193.78	194.84	193.13	192.28
	$Q_1(.10)$	5	4	3	3
	$Q_1(.50)$	11	10	9	9
	$Q_1(.90)$	404	407	396	377
1.5	ARL <sub>1</sub>	73.62	75.91	84.93	83.94
	SDRL <sub>1</sub>	157.23	161.28	180.15	169.89
	$Q_1(.10)$	5	4	3	3
	$Q_1(.50)$	7	7	6	6
	$Q_1(.90)$	307	324	349	328
2.0	ARL <sub>1</sub>	14.59	21.47	33.54	40.79
	SDRL <sub>1</sub>	51.66	78.74	113	120.20
	$Q_1(.10)$	4	4	3	3
	$Q_1(.50)$	6	5	5	4
	$Q_1(.90)$	15	15	22	43
2.5	ARL <sub>1</sub>	6.48	5.81	8.35	11.50
	SDRL <sub>1</sub>	12.33	9.55	39.78	50.72
	$Q_1(.10)$	4	4	3	3
	$Q_1(.50)$	5	5	4	3
	$Q_1(.90)$	9	8	8	9
3.0	ARL <sub>1</sub>	5.44	4.74	4.12	4.59
	SDRL <sub>1</sub>	1.24	1.17	1.61	11.71
	$Q_1(.10)$	4	4	3	3
	$Q_1(.50)$	5	4	4	3
	$Q_1(.90)$	7	6	6	6

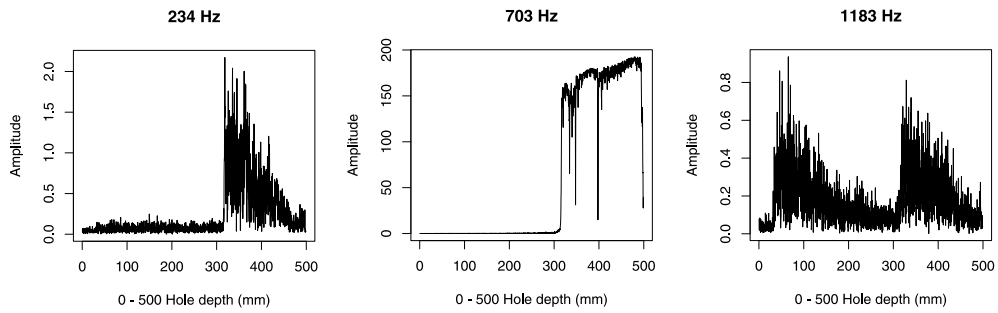
NOTE: ARL = average run length  
SDRL = standard deviation of run length distribution  
 $Q(q)$  =  $q$ th percentile of run length distribution

# Appendix B

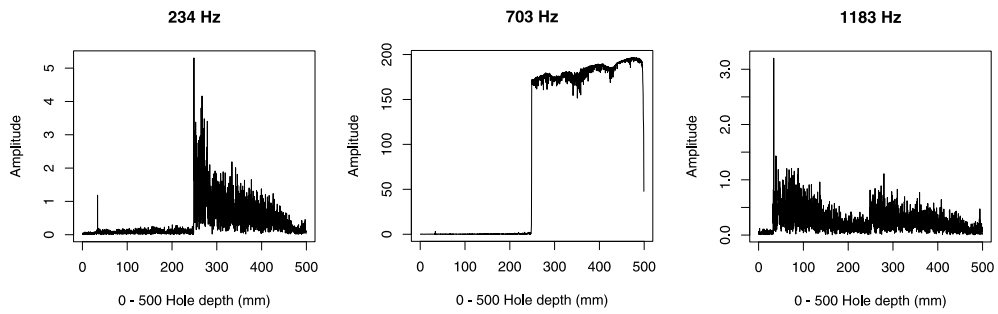
## **Plots of the Amplitudes of Frequencies 234, 703 and 1183 Hz**



(a) Experiment #5

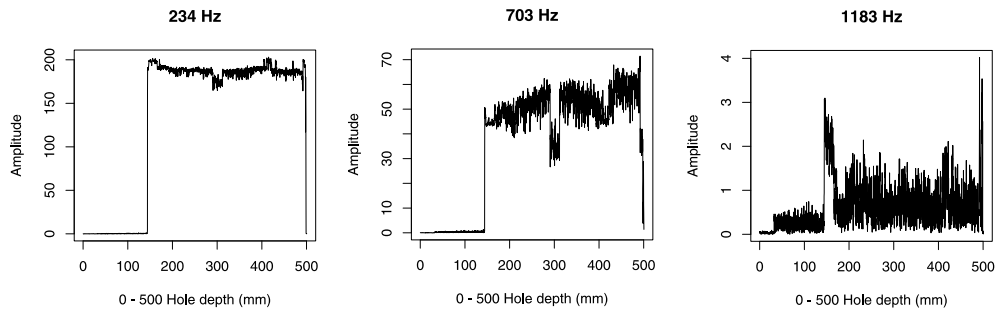


(b) Experiment #7

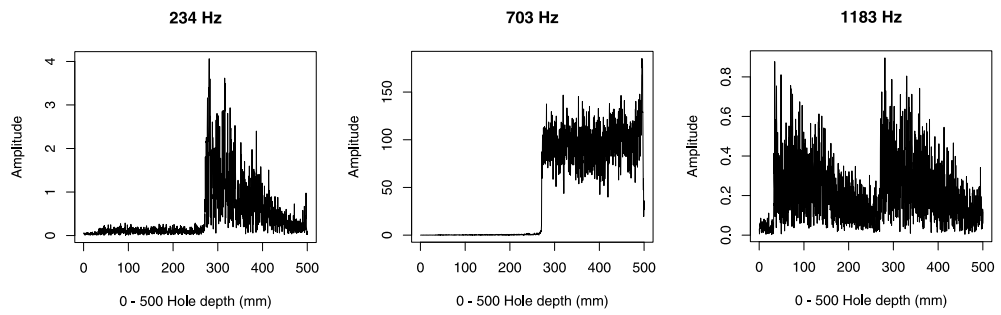


(c) Experiment #9

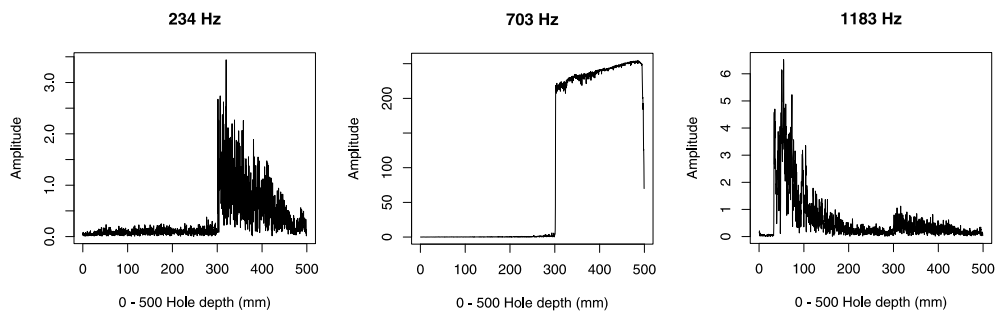
**Figure B.1:** Amplitudes of frequencies 234, 703 and 1183 Hz in experiments (a) #5, (b) #7 and (c) #9



(d) Experiment #11



(e) Experiment #15



(f) Experiment #21

**Figure B.1:** Amplitudes of frequencies 234, 703 and 1183 Hz in experiments (d) #11, (e) #15 and (f) #21 (Continued)

This page intentionally left blank



Appendix **C**

**Tables on the Time Series Analysis of  
the Amplitudes of the Relevant  
Frequencies**

**Table C.1:** Test statistics and p-values for Ljung-Box tests (Experiment #5)

Hole depth (mm)	Observation number	234 Hz		703 Hz		1183 Hz	
		test statistic	p-value	test statistic	p-value	test statistic	p-value
0-39	1-200	0.03	0.86	0.19	0.66	128.67	0.00**
39-78	201-400	0.11	0.74	0.00	0.96	1.44	0.23
78-117	401-600	1.12	0.29	1.42	0.23	10.53	0.00**
117-156	601-800	1.10	0.29	0.01	0.93	1.80	0.18
156-195	801-1000	1.61	0.20	1.26	0.26	0.41	0.52
195-234	1001-1200	2.43	0.12	1.39	0.24	0.85	0.35
234-273	1201-1400	0.59	0.44	0.24	0.62	3.00	0.08*
273-312	1401-1600	0.60	0.44	1.55	0.21	0.00	0.97
312-351	1601-1800	1.03	0.31	0.69	0.40	3.27	0.07*
351-390	1801-2000	2.49	0.11	88.62	0.00**	0.90	0.34
390-429	2001-2200	6.70	0.00**	186.02	0.00**	5.26	0.02**
429-468	2201-2400	11.20	0.00**	119.02	0.00**	3.97	0.04**

NOTES: - \*\* and \* denote significant values at the 5% and 10 % confidence level, respectively.  
- The shaded lines refer to chatter vibration.

**Table C.2:** Test statistics and p-values for Ljung-Box tests (Experiment #7)

Hole depth (mm)	Observation number	234 Hz		703 Hz		1183 Hz	
		test statistic	p-value	test statistic	p-value	test statistic	p-value
0-57	1-200	4.21	0.04**	5.38	0.02**	59.38	0.00**
57-115	201-400	0.12	0.72	1.03	0.31	0.10	0.75
115-172	401-600	1.70	0.19	1.13	0.29	0.03	0.86
172-229	601-800	0.80	0.37	2.65	0.10*	0.02	0.90
229-287	801-1000	0.35	0.55	26.89	0.00**	0.13	0.72
287-344	1001-1200	110	0.00**	197.55	0.00**	40.26	0.00**
344-401	1201-1400	40.34	0.00**	125.03	0.00**	0.08	0.78
401-459	1401-1600	31.35	0.00**	103.26	0.00**	2.60	0.10*

NOTES: - \*\* and \* denote significant values at the 5% and 10 % confidence level, respectively.  
 - The shaded lines refer to chatter vibration.

**Table C.3:** Test statistics and p-values for Ljung-Box tests (Experiment #9)

Hole depth (mm)	Observation number	234 Hz		703 Hz		1183 Hz	
		test statistic	p-value	test statistic	p-value	test statistic	p-value
0-35	1-200	2.37	0.12	1.42	0.23	33.51	0.00**
35-70	201-400	5.42	0.02**	6.15	0.01**	4.15	0.04**
70-104	401-600	3.47	0.06*	2.05	0.15	4.40	0.04**
104-139	601-800	4.47	0.03**	2.69	0.10	0.29	0.59
139-174	801-1000	1.87	0.17	0.06	0.80	0.40	0.53
174-209	1001-1200	5.51	0.02**	7.67	0.00**	2.86	0.09*
209-244	1201-1400	2.13	0.14	34.4	0.00**	0.88	0.35
244-279	1401-1600	77.9	0.00**	193.5	0.00**	2.73	0.10*
279-313	1601-1800	12.17	0.00**	40.44	0.00**	0.58	0.45
313-348	1801-2000	1.52	0.22	56.84	0.00**	0.60	0.44
348-383	2001-2200	0.10	0.75	98.50	0.00**	0.07	0.80
383-418	2201-2400	0.50	0.48	30.08	0.00**	1.58	0.21
418-453	2401-2600	4.08	0.04**	151.85	0.00**	0.02	0.90
453-487	2601-2800	4.10	0.04**	29.30	0.00**	1.01	0.31

NOTES: - \*\* and \* denote significant values at the 5% and 10 % confidence level, respectively.

- The shaded lines refer to chatter vibration.

**Table C.4:** Test statistics and p-values for Ljung-Box tests (Experiment #11)

Hole depth (mm)	Observation number	234 Hz		703 Hz		1183 Hz	
		test statistic	p-value	test statistic	p-value	test statistic	p-value
0-40	1-200	107.1	0.00**	95.20	0.00**	108.23	0.00**
40-81	201-400	16.94	0.00**	0.47	0.49	0.31	0.58
81-121	401-600	21.95	0.00**	0.32	0.57	0.29	0.59
121-161	601-800	198.12	0.00**	197.97	0.00**	186.60	0.00**
161-201	801-1000	150.18	0.00**	90.77	0.00**	108.06	0.00**
201-242	1001-1200	27.25	0.00**	60.79	0.00**	39.05	0.00**
242-282	1201-1400	30.57	0.00**	30.49	0.00**	33.35	0.00**
282-322	1401-1600	130.04	0.00**	167.30	0.00**	2.80	0.09*
322-362	1601-1800	1.04	0.30	22.82	0.00**	18.12	0.00**
362-403	1801-2000	16.59	0.00**	30.18	0.00**	6.32	0.01**
403-443	2001-2200	158.15	0.00*	153.93	0.00**	76.50	0.00**
443-483	2201-2400	24.20	0.00**	62.66	0.00**	12.41	0.00**

NOTES: - \*\* and \* denote significant values at the 5% and 10 % confidence level, respectively.  
- The shaded lines refer to chatter vibration.

**Table C.5:** Test statistics and p-values for Ljung-Box tests (Experiment #15)

Hole depth (mm)	Observation number	234 Hz		703 Hz		1183 Hz	
		test statistic	p-value	test statistic	p-value	test statistic	p-value
0-57	1-200	4.89	0.00**	41.61	0.00**	57.01	0.00**
57-115	201-400	2.08	0.15	12.20	0.00**	0.10	0.76
115-172	401-600	5.17	0.02**	6.77	0.01**	0.00	0.99
172-229	601-800	4.18	0.04**	5.40	0.02**	1.80	0.18
229-287	801-1000	138.6	0.00**	188.91	0.00**	50.56	0.00**
287-344	1001-1200	41.44	0.00**	7.90	0.00**	1.83	0.17
344-401	1201-1400	22.88	0.00**	14.42	0.00**	0.04	0.85
401-459	1401-1600	39.69	0.00**	25.90	0.00**	1.90	0.17

NOTES: - \*\* and \* denote significant values at the 5% and 10 % confidence level, respectively.  
- The shaded lines refer to chatter vibration.

**Table C.6:** Test statistics and p-values for Ljung-Box tests (Experiment #21)

Hole depth (mm)	Observation number	234 Hz		703 Hz		1183 Hz	
		test statistic	p-value	test statistic	p-value	test statistic	p-value
0-60	1-200	9.16	0.00**	37.41	0.00**	176.99	0.00**
60-120	201-400	0.78	0.38	0.09	0.76	113.44	0.00**
120-180	401-600	1.80	0.18	5.09	0.03**	49.27	0.00**
180-240	601-800	0.29	0.59	6.05	0.01**	19.15	0.00**
240-300	801-1000	0.12	0.73	68.54	0.00**	0.39	0.53
300-360	1001-1200	4.60	0.03**	118.02	0.00**	0.42	0.51
360-420	1201-1400	1.48	0.22	132.31	0.00**	0.66	0.42
420-480	1401-1600	19.3	0.00**	162.77	0.00**	18.46	0.00**

NOTES: - \*\* and \* denote significant values at the 5% and 10 % confidence level, respectively.  
- The shaded lines refer to chatter vibration.

**Table C.7:** Test statistics and p-values for Teräsvirta-Lin-Granger (TLG), Shapiro-Wilks and Ljung-Box tests (experiment #5, frequency 703 Hz)

Hole depth (mm)	Observation number	TLG test		Shapiro-Wilks test		Ljung-Box test	
		test statistic	p-value	test statistic	p-value	test statistic	p-value
0-39	1-200	0.73	0.69	0.97	0.00**	0.01	0.90
39-78	201-400	0.38	0.83	0.96	0.00**	0.00	0.96
78-117	401-600	0.54	0.76	0.95	0.00**	0.27	0.61
117-156	601-800	0.55	0.76	0.99	0.03**	0.90	0.34
156-195	801-1000	1.41	0.49	0.95	0.00**	2.49	0.11
195-234	1001-1200	1.05	0.59	0.98	0.00**	0.16	0.69
234-273	1201-1400	1.16	0.56	0.96	0.00**	0.06	0.80
273-312	1401-1600	8.41	0.01**	0.97	0.00**	0.78	0.38
312-351	1601-1800	0.40	0.82	0.97	0.00**	0.16	0.69
351-390	1801-2000	2.55	0.28	0.95	0.00**	1.45	0.23

NOTE: \*\* and \* denote significant values at the 5% and 10 % confidence level, respectively.



**Table C.8:** Test statistics and p-values for Teräsvirta-Lin-Granger (TLG), Shapiro-Wilks and Ljung-Box tests (experiment #7, frequency 703 Hz)

Hole depth (mm)	Observation number	TLG test		Shapiro-Wilks test		Ljung-Box test	
		test statistic	p-value	test statistic	p-value	test statistic	p-value
0-57	1-200	0.57	0.75	0.95	0.00**	6.00	0.01*
57-115	201-400	4.54	0.10*	0.97	0.00**	1.11	0.29
115-172	401-600	0.20	0.90	0.98	0.00**	0.05	0.82
172-229	601-800	0.32	0.85	0.97	0.00**	0.02	0.89
229-287	801-1000	0.40	0.82	0.97	0.00**	0.10	0.75
287-344	1001-1200	2.43	0.29	0.76	0.00**	7.10	0.01**

NOTE: \*\* and \* denote significant values at the 5% and 10 % confidence level, respectively.

**Table C.9:** Test statistics and p-values for Teräsvirta-Lin-Granger (TLG), Shapiro-Wilks and Ljung-Box tests (experiment #9, frequency 703 Hz)

Hole depth (mm)	Observation number	TLG test		Shapiro-Wilks test		Ljung-Box test	
		test statistic	p-value	test statistic	p-value	test statistic	p-value
0-35	1-200	9.50	0.01**	0.19	0.00**	37.84	0.00**
35-70	201-400	0.41	0.81	0.98	0.01**	3.02	0.08*
70-104	401-600	0.53	0.77	0.98	0.01**	0.07	0.79
104-139	601-800	0.11	0.94	0.95	0.00**	0.00	0.94
139-174	801-1000	4.87	0.09*	0.95	0.00**	0.16	0.69
174-209	1001-1200	2.41	0.30	0.92	0.00**	0.39	0.53
209-244	1201-1400	2.70	0.26	0.97	0.00**	1.73	0.19

NOTE: \*\* and \* denote significant values at the 5% and 10 % confidence level, respectively.

**Table C.10:** Test statistics and p-values for Teräsvirta-Lin-Granger (TLG), Shapiro-Wilks and Ljung-Box tests (experiment #11, frequency 234 Hz)

Hole depth (mm)	Observation number	TLG test		Shapiro-Wilks test		Ljung-Box test	
		test statistic	p-value	test statistic	p-value	test statistic	p-value
0-40	1-200	20.91	0.00**	0.81	0.00**	0.05	0.83
40-81	201-400	0.11	0.95	0.95	0.00**	0.08	0.80
81-121	401-600	2.43	0.30	0.98	0.00**	1.00	0.31
121-161	601-800	6.23	0.04**	0.05	0.00**	0.17	0.68

NOTE: \*\* and \* denote significant values at the 5% and 10 % confidence level, respectively.

**Table C.11:** Test statistics and p-values for Teräsvirta-Lin-Granger (TLG), Shapiro-Wilks and Ljung-Box tests (experiment #15, frequency 703 Hz)

Hole depth (mm)	Observation number	TLG test		Shapiro-Wilks test		Ljung-Box test	
		test statistic	p-value	test statistic	p-value	test statistic	p-value
0-57	1-200	12.70	0.00**	0.90	0.00**	20.63	0.00**
57-115	201-400	0.83	0.66	0.98	0.04**	0.38	0.54
115-172	401-600	1.89	0.40	0.97	0.00**	0.63	0.43
172-229	601-800	1.20	0.55	0.97	0.00**	0.09	0.77
229-287	801-1000	52.78	0.00**	0.69	0.00**	1.25	0.26

NOTE: \*\* and \* denote significant values at the 5% and 10 % confidence level, respectively.

**Table C.12:** Test statistics and p-values for Teräsvirta-Lin-Granger (TLG), Shapiro-Wilks and Ljung-Box tests (experiment #21, frequency 703 Hz)

Hole depth (mm)	Observation number	TLG test		Shapiro-Wilks test		Ljung-Box test	
		test statistic	p-value	test statistic	p-value	test statistic	p-value
0-60	1-200	20.46	0.00**	0.89	0.00**	6.20	0.01**
60-120	201-300	5.87	0.05**	0.97	0.00**	0.16	0.68
120-180	301-400	0.16	0.92	0.97	0.00**	0.34	0.56
180-240	401-500	4.70	0.09*	0.95	0.00**	0.27	0.60
240-300	501-600	0.27	0.87	0.85	0.00**	2.40	0.12

NOTE: \*\* and \* denote significant values at the 5% and 10 % confidence level, respectively.

This page intentionally left blank



## Bibliography

- ALWAN, L. C. and ROBERTS, H. V. (1988). Time Series Modeling for Statistical Process Control. *Journal of Business and Economic Statistics* **6**, pp. 87–95.
- BARAGONA, R.; BATTAGLIA, F.; and CUCINA, D. (2002). A Note on Estimating Autoregressive Exponential Models. *Quaderni di Statistica* **4**, pp. 71–88.
- BURR, M. A.; RAFALIN, E.; and SOUVAINE, D. L. (2004). Simplicial Depth: An Improved Definition, Analysis, and Efficiency for the Finite Sample Case. *In: Proceedings of the 16th Canadian Conference on Computational Geometry*, pp. 136–139.
- CALZADA, M. E. and SCARIANO, S. M. (2003). Reconciling the Integral Equation and Markov Chain Approaches for Computing EWMA Average Run Lengths. *Communications in Statistics-Simulation and Computation* **32**, pp. 591–604.
- CHAKRABORTI, S.; VAN DER LAAN, P.; and BAKIR, S. T. (2001). Nonparametric Control Charts: An Overview and Some Results. *Journal of Quality Technology* **33**, pp. 304–315.
- CHAMP, C. W. and JONES-FARMER, L. A. (2005). Properties of Multivariate Control Charts with Estimated Parameters. *Journal of Sequential Analysis*. accepted for publication.
- CHENG, A. Y. and OUYANG, M. (2001). On Algorithms for Simplicial Depth. *In: Proceedings of the 13th Canadian Conference on Computational Geometry*, pp. 53–56.
- CROWDER, S. V. (1987). A Simple Method for Studying Run-length Distributions of Exponentially Weighted Moving Average Charts. *Technometrics* **29**, pp. 401–407.
- GIBBONS, J. D. and CHAKRABORTI, S. (1992). *Nonparametric Statistical Inference*. 3rd ed. Marcel Dekker, New York, NY.

- HACKL, P. and LEDOLTER, J. (1992). A New Nonparametric Quality Control Technique. *Communications in Statistics-Simulation and Computation* **21**, pp. 423–443.
- HAGGAN, V. and OZAKI, T. (1981). Modelling Nonlinear Random Vibrations Using an Amplitude-Dependent Autoregressive Time Series Model. *Biometrika* **68**, pp. 189–196.
- HUETER, I. (1994). The Convex Hull of a Normal Sample. *Advances in Applied Probability* **26**, pp. 855–875.
- JOHNSON, M. E. (1987). *Multivariate Statistical Simulation*. John Wiley & Sons, New York, NY.
- LIU, R. Y. (1990). On a Notion of Data Depth Based on Random Simplices. *The Annals of Statistics* **18**, pp. 405–414.
- LIU, R. Y.; PARELIUS, J. M.; and SINGH, K. (1999). Multivariate Analysis by Data Depth: Descriptive Statistics, Graphics and Inference (with discussion). *The Annals of Statistics* **27**, pp. 783–858.
- LOWRY, C. A.; WOODALL, W. H.; CHAMP, C. W.; and RIGDON, S. E. (1992). A Multivariate Exponentially Weighted Moving Average Control Chart. *Technometrics* **34**, pp. 46–53.
- MESSAOUD, A.; THEIS, W.; WEIHS, C.; and HERING, F. (2004). Monitoring of the BTA Deep Hole Drilling Process Using Residual Control Charts. Technical Report 60/2004 of SFB 475, University of Dortmund.
- MESSAOUD, A.; WEIHS, C.; and HERING, F. (2004). A Nonparametric Multivariate Control Chart Based on Data Depth. Technical Report 61/2004 of SFB 475, University of Dortmund.
- MONTGOMERY, D. C. (2001). *Introduction to Statistical Quality Control*. 4th ed. John Wiley & Sons, New York, NY.
- MONTGOMERY, D. C. and MASTRANGELO, C. M. (1991). Some Statistical Process Control Methods for Autocorrelated Data (with discussion). *Journal of Quality Technology* **23**, pp. 179–204.
- OZAKI, T. (1980). Non-linear Time Series Models for Non-linear Random Vibrations. *Journal of Applied Probability* **17**, pp. 84–93.
- OZAKI, T. (1982). The Statistical Analysis of Perturbed Limit Cycle Processes Using Nonlinear Time Series Models. *Journal of Time Series Analysis* **3**, pp. 29–41.



- OZAKI, T. (1985). Non-linear Time Series Models and Dynamical Systems. *In: HANNAN, E. J.; KRISHNAIAH, P. R.; and RAO, M. M. (Eds.), Handbook of statistics*, pp. 25–83. Elsevier Science Publishers B. V., North Holland.
- OZAKI, T. and ODA, H. (1978). Nonlinear Time Series Model Identification by Akaike's Information Criterion. *In: DUBUISSON, B. (Ed.), Information and Systems*, pp. 83–91. Pergamon Press, Oxford, New York.
- ROUSSEEUW, P. J. and RUTS, I. (1996). AS 307: Bivariate Location Depth. *Applied Statistics* **45**, pp. 516–526.
- SHI, Z. and AOYAMA, H. (1997). Estimation of the Exponential Autoregressive Time Series Model by Using the Genetic Algorithm. *Journal of Sound and Vibration* **205**, pp. 309–321.
- SHI, Z.; TAMURA, Y.; and OZAKI, T. (1998). A Study on Real-time Detecting of Machine Tool Chatter. *International Journal of the Japan Society for Precision Engineering* **32**, pp. 178–182.
- SHI, Z.; TAMURA, Y.; and OZAKI, T. (2001). Monitoring the Stability of BWR Oscillation by Nonlinear Time Series Modeling. *Annals of Nuclear Energy* **28**, pp. 953–966.
- STOUMBOS, Z. G. and JONES, L. A. (2000). On the Properties and Design of Individuals Control Charts Based on Simplicial Depth. *Nonlinear Studies* **7**, pp. 147–178.
- STOUMBOS, Z. G. and SULLIVAN, J. H. (2002). Robustness to Non-Normality of the Multivariate EWMA Control Chart. *Journal of Quality Technology* **34**, pp. 260–276.
- TERÄSVIRTA, T.; LIN, C.-F.; and GRANGER, C. W. J. (1993). Power of the Neural Network Linearity Test. *Journal of Time Series Analysis* **14**, pp. 209–220.
- TESTIK, M. C.; RUNGER, G. C.; and BORROR, C. M. (2003). Robustness Properties of Multivariate EWMA Control Charts. *Quality and Reliability Engineering International* **19**, pp. 31–38.
- THEIS, W. (2004). Modelling Varying Amplitudes. Ph.D. dissertation, Department of Statistics, University of Dortmund. <http://eldorado.uni-dortmund.de:8080/FB5/lis7/forschung/2004/Theis>.
- TOBIAS, S. A. (1965). *Machine Tool Vibration*. Blackie and Sons Ltd, London.
- TONG, H. (1990). *Non-linear Time Series: A Dynamical Systems Approach*. Clarendon Press, Oxford.

- WEINERT, K.; WEBBER, O.; GEPPERTH, A.; ZHANG, Y.; and THEIS, W. (2004). Time Varying Dynamics in BTA Deep Hole Drilling. *In: TETI, R. (Ed.), Proceedings of the 4th CIRP International Seminar on Intelligent Computation in Manufacturing Engineering*, pp. 419–424. ICME 2004, R. Sorrenti, Naples, Italy.
- WEINERT, K.; WEBBER, O.; HÜSKEN, M.; MEHNEN, J.; and THEIS, W. (2002). Analysis and Prediction of Dynamic Disturbances of the BTA Deep Hole Drilling Process. *In: TETI, R. (Ed.), Proceedings of the 3rd CIRP International Seminar on Intelligent Computation in Manufacturing Engineering*, pp. 297–302. ICME 2002, Ischia, Italy.
- WEINERT, K.; WEBBER, O.; and PETERS, C. (2005). On the Influence of Drilling Depth Dependent Modal Damping on Chatter Vibration in BTA Deep Hole Drilling. *In: Annals of the CIRP - Manufacturing Technology*, pp. 363–366.
- WOODALL, W. H. (2000). Controversies and Contradictions in Statistical Process Control (with discussion). *Journal of Quality Technology* **32**, pp. 341–378.